Low Loss Polysilicon Waveguides for Silicon Photonics

by

Ling Liao

B.S., Materials Science and Engineering
Massachusetts Institute of Technology, 1995

Submitted to the Department of Materials Science and Engineering
in Partial Fulfillment of the Requirements for the Degree of

Master of Science in Materials Science and Engineering

at the
Massachusetts Institute of Technology

June 1997

© 1997 Massachusetts Institute of Technology
All rights reserved

Signature of Author ....
Department of Materials Science and Engineering
May 9, 1997

Certified by ....
Lionel C. Kimerling
Thomas Lord Professor of Materials Science and Engineering
Thesis Supervisor

Accepted by ....
Linn W. Hobbs
John F. Elliot Professor of Materials
Chairman, Departmental Committee on Graduate Students

OF TECHNOLOGY

DEC 24 1997 ARCHIVES

LIBRARIES

Low Loss Polysilicon Waveguides for Silicon Photonics

by

Ling Liao

Submitted to the Department of Materials Science and Engineering
on May 9, 1997 in Partial Fulfillment of the
Requirements for the Degree of
Master of Science in Materials Science and Engineering

ABSTRACT

Silicon-based optoelectronic integrated circuits for future generations of microprocessors require optical interconnects compatible with silicon very large scale integrated technology. Waveguides consisting of polysilicon (polySi) clad with SiO_2 offer excellent optical confinement and ease of fabrication that are ideal for such interconnect applications. One major challenge with using this material system, however, is the high optical transmission loss of polySi. Most of this loss can be attributed to scattering at rough surfaces and absorption at dangling bond sites in the material bulk. A previous work reduced surface scattering by improving the film surface morphology; it achieved a transmission loss of 35dB/cm at λ=1.55μm[1]. We now report methods for minimizing the bulk loss of polySi. By means of hydrogenation and high temperature anneals, transmission loss can be reduced to 9dB/cm. We also demonstrate that right angle bends with radii of ~1μm can be fabricated with loss less than 1dB. This level of performance is the first to meet the requirements of on chip optical clock distribution.

Thesis Supervisor: Lionel C. Kimerling
Title: Thomas Lord Professor of Materials Science and Engineering

Acknowledgment

The results in this thesis represent the efforts of many. First, much gratitude is owed to Professor L. C. Kimerling, who has been the source of vision and technical guidance for this project. His advice is deeply appreciated. I am also indebted to Anuradha Agarwal for all the processing work and insightful discussions, to James Foresi for his expertise and development of crucial measurement techniques, and to Xiaoman Duan for her work in the areas of TEM and X-ray diffraction. I am also grateful to Desmond Lim and Marcie Black, whose pioneering research paved the way for this thesis work. A special thanks also goes to Thomas Chen, who has graciously allowed me to use this thesis template. Last but not least, I would like to give my deepest appreciation to DeWang Li and my family for their support and understanding.

Contents

1. Introduction **10**

1.1 Motivation 10

1.2 Objective 12

1.3 Organization 12

2. Background **14**

2.1 Waveguide Fundamentals 14

2.1.1 Guided-Wave Optics 15

2.1.2 Definition of Waveguide Loss 22

2.2 Waveguide Material Selection 23

2.2.1 Bond and Etch Back Silicon on Insulator 25

2.2.2 Separation by Implantation of Oxygen 26

2.2.3 Doped Silicon 27

2.2.4 PolySi-SiO_2 27

2.3 Mechanisms of Waveguide Loss 28

2.3.1 Surface Roughness 30

2.3.2 Grain Boundaries 31

2.3.3 Amorphous Silicon 34

2.3.4 Intra-grain Defects 36

2.3.5 Lattice Strain 36

2.4 Physical Properties of PolySi Thin Films 37

2.4.1 Surface Morphology 37

2.4.2 Grain Size 38
2.4.3 Hydrogenation 41

3. Experimental Details **44**
3.1 Standard Fabrication Recipe 44
3.2 Processing Experiments 46
3.2.1 Deposition Experiments 46
3.2.2 Annealing Experiments 46
3.2.3 Chemical-Mechanical Polish 47
3.2.4 Etching Experiment 48
3.2.5 Hydrogenation 48
3.2.6 Doping Experiment 50
3.3 Material Characterization 50
3.3.1 Transmission Loss Determination 50
3.3.2 Transmission Electron Microscopy 53
3.3.3 X-ray Diffraction 54
3.3.4 Atomic Force Microscopy 57
3.3.5 Secondary Ion Mass Spectrometry 58
3.3.6 Determination of the Index of Refraction 58
3.4 Bending Loss Determination 59

4. Results **61**
4.1 Cutback Power Loss Measurement 61
4.2 Transmission Electron Microscopy 65
4.3 X-ray Diffraction 70
4.4 Atomic Force Microscopy 74
4.5 Secondary Ion Mass Spectrometry 78
4.6 Determination of Index of Refraction 81
4.7 Bending Loss Determination 81

5. Discussion **82**

5.1 Deposition Conditions 82
5.1.1 Grain structure and Grain Size 82
5.1.2 Surface Roughness and Transmission Loss 83
5.2 Doped Polycrystalline Silicon 84
5.3 Waveguide Thickness 85
5.4 Sidewall Scattering 87
5.5 Bulk Absorption and Scattering 88
5.5.1 Amorphous Silicon - Temperature Treatments 89
5.5.2 Dangling Bonds - Hydrogenation 90
5.6 Bending Loss 92
5.7 Loss vs. Wavelength 93
5.8 Residual Loss 94
5.8.1 Grain Boundary absorption 95
5.8.2 Grain Boundary Scattering 96
5.8.3 Surface Scattering 97

6. Conclusion **98**

7. Future Work **100**

7.1 Dangling Bond Passivation 100
7.2 Surface Planarization 102
7.3 Performance Characterization 102
7.4 Process Integration 103

List of Figures

Figure 2.1: Three commonly used waveguide schemes: a) slab, b) strip, c) fiber. 14

Figure 2.2: Schematic of the polySi/SiO_2 strip waveguide. 15

Figure 2.3: A ray crossing the interface between two media of different refractive indices experiences both reflection and refraction. 16

Figure 2.4: The process of total internal reflection. a) If $n_1<n_2$, refraction cannot be avoided regardless of the incident angle θ_1. b) If $n_1>n_2$, there is a critical incident angle θ_c, above which incident rays are totally reflected... 17

Figure 2.5: Schematic of a planar waveguide. n_1, n_2, and n_3 are the indices of refraction for the top cladding, core, and bottom cladding, respectively...................................... 18

Figure 2.6: Schematic profile of field in total internal reflection for 2 incident angles, $\theta_{i2}<\theta_{i1}<(90°-\theta_c)$.. 19

Figure 2.7: Condition for self-consistency: a wave duplicates itself after two reflections............ 20

Figure 2.8: Schematic showing the relationship between h, k, θ, and β. $(kn_2)^2$ is proportional to the total energy of the TE wave, β_m^2 is the energy in the z direction, and h^2 is the energy in the direction of confinement.. 21

Figure 2.9: Simulated bending loss for Si/SiO_2 strip waveguides 24

Figure 2.10: BESOI fabrication process... 25

Figure 2.11: SIMOX fabrication process. 26

Figure 2.12: Sketches of the optimal local coordinations of a Si atom in a) the ground state configuration and b) the neutral singly-occupied dangling bond configuration. The bond angle α=109.5° 32

Figure 2.13: Electron excitation due to absorption of photons.. 32

Figure 2.14: Absorption coefficient of as-grown and annealed (900°-1000°C) polySi vs. deposition temperature: a) for λ = 514.5nm and b) for λ = 441.4nm...................... 34

Figure 2.15: Indirect gap optical transition requires the participation of the electron, photon, and phonon. 35
Figure 2.16: Pressure dependence of rms surface roughness for silane- and disilane-based processes 38
Figure 2.17: Grain size of polySi as a function of the deposition temperature. a) For $T_d <$ 580°C, grain size increases with decreasing deposition temperature. b) For $T_d >$ 580°C, grain size increases with increasing deposition temperature 40
Figure 2.18: Residual saturation value of the spin density as a function of hydrogenation temperature 42
Figure 2.19: Deuterium concentration profiles in polySi films with different thicknesses of protective oxide 43
Figure 3.1: The cross-sectional view of the strip waveguide structure used to measure transmission loss in polySi. 45
Figure 3.2: The measurement setup used to determine waveguide transmission. 52
Figure 3.3: Diffraction of x-rays by a crystal. Incident rays 1 and 2 are scattered by atoms A and B, respectively; two of the scattered rays are denoted as 1' and 2' 55
Figure 3.4: Effect of lattice strain on the position and shape of a diffraction peak. 56
Figure 3.5: X-ray scattering characteristics of crystalline and amorphous solids. 57
Figure 3.6: Schematic of the two-level waveguide structure. 60
Figure 4.1: XTEM images of a) 625 polySi and b) 560polySi, both annealed with an O_2 furnace leak. 66
Figure 4.2: High resolution TEM image of 560(O_2) polySi 66
Figure 4.3: XTEM image of 560 polySi, annealed for an additional 100 hours at 600°C (O_2). .. 67
Figure 4.4: XTEM image of 560 polySi, annealed for an additional 16 hours at 1100°C (O_2). .. 68
Figure 4.5: XTEM images of 0.2μm-560 polySi, annealed for 16 hours at 600°C a) with an O_2 furnace leak and b) in a pure N_2 ambient 68
Figure 4.6: XTEM images of 0.2μm-560 polySi, annealed for an additional 16 hours at 1100°C (N_2) 69
Figure 4.7: Plan-view TEM images of a) 470°C disilane polySi and b) 700°C fine grain polySi. 70

Figure 4.8: X-ray diffraction curves for standard annealed 625(O_2) and 560(O_2). The broad peaks near 2θ=30° indicate the presence of amorphous silicon, and the sharp peaks identify the preferred grain orientations. 71
Figure 4.9: X-ray diffraction curves for 560(O_2) and 560/100°C(O_2).......... 72
Figure 4.10: X-ray diffraction curves of the 0.2μm-560(O_2) and 0.2μm-560(N_2) standard annealed samples.......... 73
Figure 4.11: X-ray diffraction curve of the 0.2μm-560(N_2) film annealed at 1100°C.......... 74
Figure 4.12: Three-dimensional AFM plot of 625 polySi film surface, whose rms roughness is ~20nm. 76
Figure 4.13: Three-dimensional AFM plot of 625 polySi film surface after CMP, which has an rms roughness of ~5nm. 76
Figure 4.14: Three-dimensional AFM plot of 560 polySi film surface, whose rms roughness is ~4nm. 77
Figure 4.15: Three-dimensional AFM plot of doped polySi film, the large structural features are macroscopic voids, cracks, and disconnects. 78
Figure 4.16: SIMS depth profiles of 560 and 560ECR. ECR passivation increased hydrogen concentration from $6x10^{18}$ to $3x10^{19}$ atoms/cm^3.......... 79
Figure 4.17: SIMS depth profiles of 625 and 625ECR. No appreciable increase in hydrogen level is observed.......... 80
Figure 4.18: SIMS depth profiles of 625CMP and 625CMP+ECR. ECR passivation increased hydrogen concentration from $4x10^{18}$ to $2x10^{19}$ atoms/cm^3.......... 80
Figure 5.1: Temperature dependence of grain size.......... 83
Figure 5.2: Simulated and measured core loss as a function of waveguide thickness.......... 86
Figure 5.3: Simulated sidewall scattering loss as a function of waveguide widths.......... 88
Figure 5.4: Histogram comparing the effectiveness of different hydrogenation techniques. 90
Figure 5.5: Transmission loss at λ = 1.32μm and 1.55μm.......... 93

Chapter 1

Introduction

As chip capabilities continue to increase, interconnect constraints are rapidly becoming the dominant limitation to chip speed. Important among the interconnection problems is high frequency clock distribution, the transmission of the clock signal (the reference timing signal) to all parts of the chip with minimal differential delays. The clock signal synchronizes every subsystem on the chip; it thus determines the rate at which the chip can run.

With clock speeds approaching the GHz level and clock skew on the order of picoseconds, electrical clocking systems will have great difficulties in meeting these challenging performance specifications. For such high speed operation, an electrical system is expected to demand up to 200 watts of power and 2 billion lines/cm^2 of interconnect density [2]. Such enormous power and density requirements will undoubtedly drive silicon VLSI electrical interconnect technology to its physical limits. Not only is such a system challenging to fabricate, issues such as power dissipation, electromigration, and crosstalk will become ever more formidable.

1.1 Motivation

One approach to the high speed challenge is to pursue photonic/electronic integration, such as optoelectronic integrated circuits (OEIC's). In such systems, electrical signals are converted to optical form for transmission. Following reception at the destinations, they are converted back to electrical form for logic operations. The optical interconnection scheme for these systems involve four basic components; they are the light emitter, the waveguide, the modulator, and the detector. OEIC's are an excellent alternative to con-

ventional IC's because, while they maintain the computational capabilities of electronics, they introduce the signal transmission advantages of optics. Electronics is ideal for logic operations because the strong interaction among electrons is desirable when one signal must control another in a logic circuit. Photonics is more suitable for signal transfer because the limited interaction among photons allows low noise and limited crosstalk transmission. Furthermore, since crosstalk determines the minimum distance between adjacent interconnect lines, the limited interference between photonic signals translates to higher interconnection density and extra flexibility of routing. In cases when signal coupling between waveguides is desired, crosstalk can always be increased by modifying interconnect layout.

Some other major advantages of using optical interconnections are high bandwidth, low power consumption, and freedom from certain capacitive loading effects. Furthermore, temporal and wavelength division multiplexing can also increase the volume of data that can be sent down the waveguide. In this case, many signals can be transmitted at different times and wavelengths without data interference. These benefits of OEIC systems can greatly contribute to the minimization of clock skew and, ultimately, lift the limitations on achievable clock speed.

III-V based optoelectronic materials, such as the GaAs/AlGaAs system, actually come closest to accommodating the needs of OEIC technology. However, its integration with silicon is expensive and difficult due to costly alignment problems and the lack of well-defined integration methodology. As a result, the components of OEIC's should be based on, or at least be compatible with, silicon.

For optical interconnection, researchers have studied single crystalline silicon systems and have found transmission loss to be less than 1 dB/cm [3, 4]. Although polySi does not have superior electrical and optical properties, it could be a better alternative to single crystalline silicon. In terms of cost and ease of fabrication, polySi is the material of choice since it can be deposited on a variety of substrates with standard VLSI silicon processing technology. Its use in IC fabrication is already pervasive; some of its applications include the gate electrode in metal-oxide-semiconductor devices, the active layer in thin film transistors, and the high-value resistor in static memory circuits [5, 6]. Finally,

polySi's ease of fabrication also allows it to readily satisfy the important IC requirement of multi-level interconnection, a luxury single crystalline silicon does not have.

1.2 Objective

The objective of this thesis is to investigate the data transmission aspect of a monolithic approach to photonic/electronic integration. The optical interconnect structure studied is a strip waveguide with polysilicon (polySi) core and SiO_2 cladding. The goal is to minimize the transmission loss of this waveguide structure at the standard communication wavelength of 1.55µm. Losses at 1.32µm are also measured for comparison. Various polySi processing procedures are investigated and modified for lowest loss waveguides. The effects of process history on material properties such as grain size, grain quality, and spin density are evaluated. Then the changes in these physical properties are related to the different measured transmission losses.

The polySi/SiO_2 system considered has the tremendously desirable property of a large core/cladding refractive index contrast of 3.5/1.5. Such index contrast enables excellent optical confinement, thus allowing sub-micron interconnect dimensions similar to or even smaller than conventional metallic lines. Such small dimensions, combined with limited crosstalk, can result in very high interconnection density. Furthermore, the superb optical confinement translates to low bending loss, permitting additional routing flexibilities. Passive devices such as out-of-plane bends are also fabricated and tested to verify this theoretical understanding.

1.3 Organization

This document provides a detailed look at the development of polySi waveguides for silicon-compatible photonic integrated circuits. Chapter 2 presents fundamental waveguide theory and other relevant background such as material issues, sources of waveguide loss, and loss measurement technique. These topics are essential to understanding the challenge of reducing transmission loss in polySi. Chapter 3 outlines the general waveguide fabrication procedure, the numerous experimental studies, and material characterization techniques. In Chapter 4, the results of these experiments and analyses are presented. Then

Chapter 5 evaluates the findings and discusses how various material properties influence transmission loss, and how process modifications can be made to achieve the desired properties. Chapter 6 brings together all the important findings and achievements of this research effort. It serves as a comprehensive view of loss reduction in polySi.

Although significant strides have been made in improving transmission performance, the current lowest loss of 9dB/cm is still higher than the 1dB/cm of crystalline silicon. Furthermore, since the ultimate goal is to integrate optical components with electronics, modification of the current fabrication process is necessary to accommodate the various thermal budget and through-put constraints of IC manufacturing. Chapter 7, therefore, outlines some experiments for future polySi waveguide development.

Chapter 2

Background

2.1 Waveguide Fundamentals

In optical waveguides electromagnetic (EM) waves are confined and guided in a medium of one refractive index by a surrounding medium of lower refractive index. The center region through which the optical rays travel is known as the core, and the surrounding material which imbeds the core is known as the cladding. In such a system, waves remain confined to the core without irradiating into the surroundings by multiple internal reflections at the boundaries. The three most commonly used waveguide schemes are illustrated in Figure 2.1; they are slab, strip, and fiber guides.

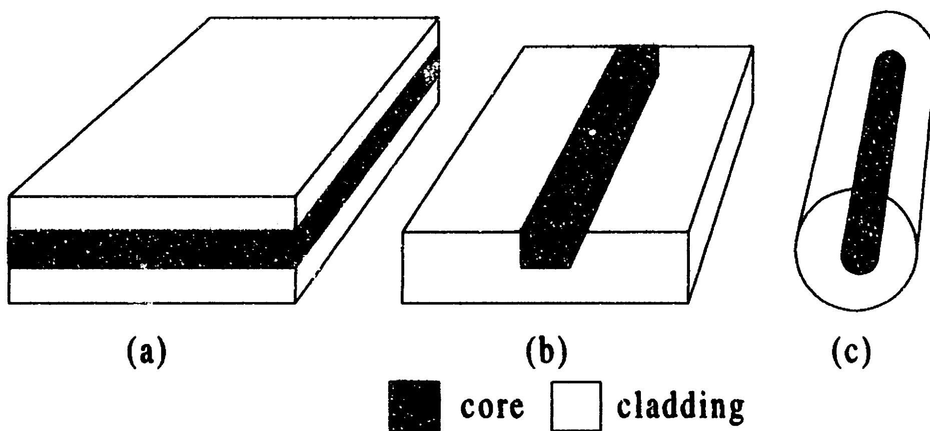

Figure 2.1: Three commonly used waveguide schemes: a) slab, b) strip, c) fiber.

For the purpose of this thesis, rectangular strip waveguides with polySi core and SiO_2 cladding are investigated (see Figure 2.2). Strip guide structures are ideal for IC interconnect applications in that they offer small dimensions, low bending loss, and limited crosstalk. The propagation behavior of EM waves in rectangular strip waveguides is very complicated because light is confined in both horizontal and vertical directions. The analytical calculation of the field distribution and the propagation constants is not possible, apart from a few exceptions. For a fundamental understanding of light guidance, propagation in a simpler structure such as a planar waveguide will therefore be discussed.

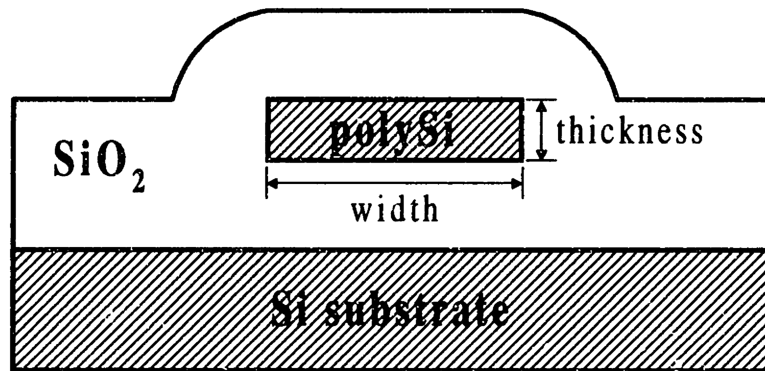

Figure 2.2: Schematic of the polySi/SiO_2 strip waveguide.

2.1.1 Guided-Wave Optics

When light waves propagate through objects whose dimensions are much larger than the wavelength, the wave's behavior can be sufficiently described by rays obeying geometrical rules. Ray optics, therefore, is used here for a fundamental explanation of light guidance. Consider a ray traveling from a medium of refractive index n_1 through a second medium of index n_2 (Figure 2.3). At the interface it experiences both reflection and refraction. The refracted ray obeys the law of refraction or Snell's Law:

$$n_1 \sin\theta_1 = n_2 \sin\theta_2 , \tag{2.1}$$

where θ_1 is the angle of incidence and θ_2 is the angle of refraction.

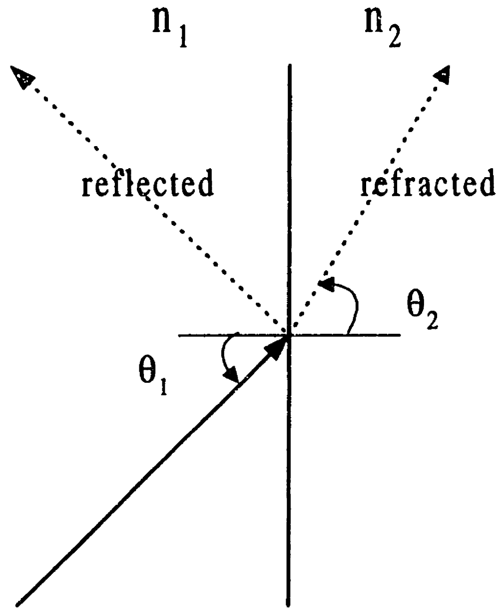

Figure 2.3: A ray crossing the interface between two media of different refractive indices experiences both reflection and refraction.

If $n_1<n_2$, the refracted ray bends away from the boundary, $\theta_2<\theta_1$. Refraction cannot be avoided regardless of the incident angle (see Figure 2.4a). On the other hand, if $n_1>n_2$ the refracted ray bends toward the boundary, $\theta_2>\theta_1$. As θ_1 increases, θ_2 approaches 90° first (see Figure 2.4b). There is a critical incident angle θ_c where θ_2 equals 90°, such that

$$\theta_c = \sin^{-1}\frac{n_2}{n_1}. \qquad (2.2)$$

When $\theta_1>\theta_c$, Snell's Law cannot be satisfied and refraction does not take place. The incident rays are totally reflected at the boundaries without suffering intensity loss due to refraction. For a waveguide, the entire cladding medium (n_2) must have lower index than the core (n_1) for light confinement. Furthermore, the larger the index contrast, the smaller the critical angle, which ultimately translates to better optical confinement. The polySi/SiO_2 waveguide studied in this thesis has n_1=3.5 and n_2=1.5; its critical angle for total reflection is therefore 25°. Silica fibers used for transatlantic communications, on the

other hand, have a much smaller index contrast. Its n_1 of 1.46 and n_2 of 1.445 results in θ_c=81.8° [7].

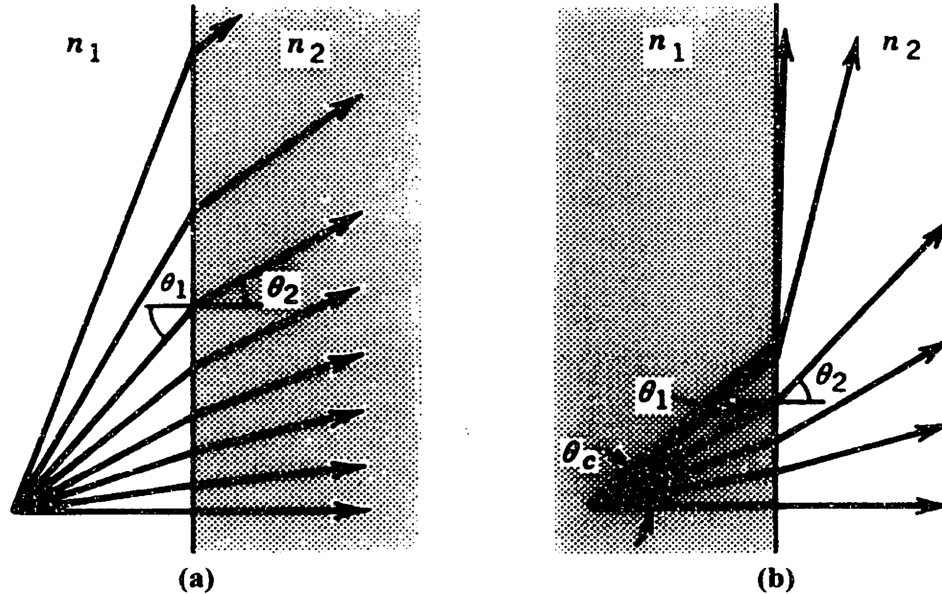

Figure 2.4: The process of total internal reflection. a) If $n_1<n_2$, refraction cannot be avoided regardless of the incident angle θ_1. b) If $n_1>n_2$, there is a critical incident angle θ_c, above which incident rays are totally reflected.

The core and cladding indices also determine the amount of external radiation that can couple into the waveguide. A ray incident from air becomes a guided ray only if upon refraction into the core it satisfies the condition of total internal reflection. As a result, only a cone of external rays are guided by the waveguide. This cone is defined by the maximum accepted angle of incidence θ_a:

$$\theta_a = \sin^{-1} NA, \tag{2.3}$$

where

$$NA = n_1^2 - n_2^2. \tag{2.4}$$

NA is the numerical aperture. It describes the light-gathering capacity of the waveguide. For the polySi/SiO2 system, NA=1. In other words, rays incident from all directions are guided.

Waveguides for IC applications have dimensions on the order of micrometers. For light guidance in such miniature systems, the electromagnetic (EM) wave nature of light must be included for an accurate understanding of propagation. Electromagnetic radiation travels in the form of two mutually coupled vector waves, an electric wave and a magnetic wave. When the two vector waves lie in a plane perpendicular to the direction of propagation, the radiation is called a transverse EM wave. For a simple analysis, each optical ray can be considered as a transverse EM plane wave. The total EM field is the sum of these plane waves.

Consider a planar waveguide in which the light is guided inside the center slab. The top cladding, core, and bottom cladding have refractive indices n_1, n_2, and n_3, respectively. A wave with its wavevector lying in the *x-z* plane makes an angle θ_i with the *z*-axis, the direction of propagation (see Figure 2.5). When $\theta_i<(90°-\theta_c)$ the wave travels by repeatedly reflecting off of the walls of the core. The cladding is not perfectly reflective; the field penetrates, giving a evanescent transmitted wave where no power travels toward or away from the core. This wave decays exponentially in the cladding with a *1/e* decrease in field after a penetration depth of *p*. Figure 2.6 shows the profile of the field in total internal reflection for 2 incident angles, $\theta_{i2}<\theta_{i1}<(90°-\theta_c)$. The larger the angle of incidence, the greater the penetration depth. For $\theta_i=(90°-\theta_c)$, the penetration depth is infinite.

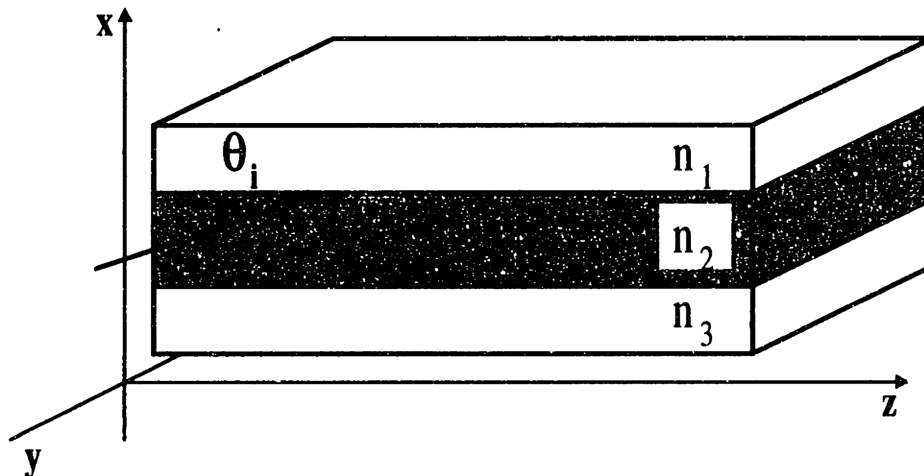

Figure 2.5: Schematic of a planar waveguide. n_1, n_2, and n_3 are the indices of refraction for the top cladding, core, and bottom cladding, respectively.

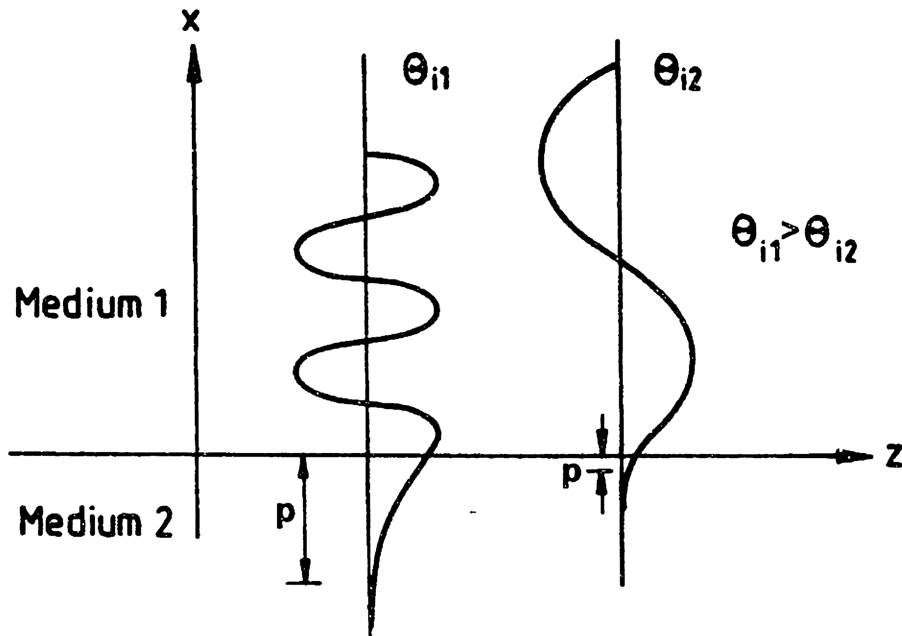

Figure 2.6: Schematic profile of field in total internal reflection for 2 incident angles, $\theta_{i2}<\theta_{i1}<(90°-\theta_c)$ [8]

Of the total field within the limit of total internal reflection, only a limited number of EM plane waves with discreet incident angles are allowed as guided waves of the structure. These waves must meet the self-consistency condition in that they repeat in phase and superimpose upon themselves after every two reflections. This condition is illustrated in Figure 2.7. The allowed waves guarantee that the same transverse field distribution and polarization are maintained at all distances along the waveguide axis. Fields that satisfy both conditions of total internal reflection and self-consistency are called modes of the waveguide. Each allowed incident angle θ_m (m=1,2,3...) corresponds to a field called the m_{th} mode. The m=1 mode is the fundamental mode, it has the smallest θ_m angle. Because the fundamental mode makes the least number of reflections and has the shortest depth of penetration upon reflection, it is also the most energetic mode. As a result, higher order modes generally have higher losses because their fields extend more deeply into the cladding.

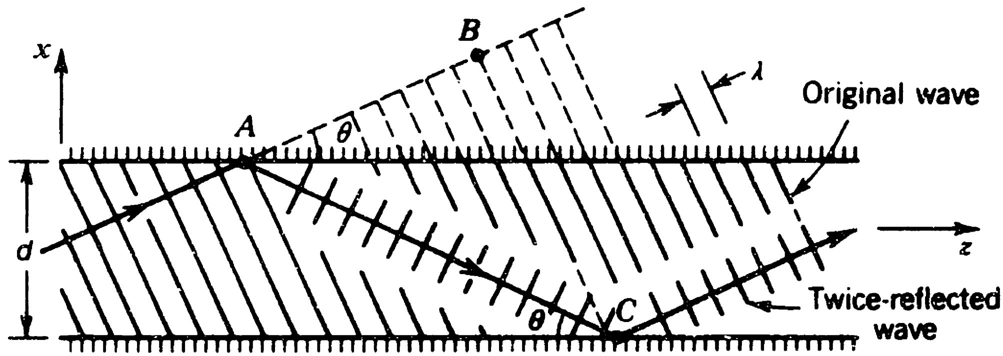

Figure 2.7: Condition for self-consistency: a wave duplicates itself after two reflections [7].

Consider again the planar waveguide illustrated in Figure 2.5. The transverse electric (TE) field distribution in this guide can be written as

$$E_y = \begin{cases} A\exp(-qx) & 0 \le x \le \infty \\ B\left[\cos(hx) - \frac{q}{h}\sin(hx)\right] & -d \le x \le 0 \\ C\exp(p(x+d))\left[\cos(hd) + \frac{q}{h}\sin(hd)\right] & -\infty \le x \le -d, \end{cases} \quad (2.5)$$

where q and p are penetration depths of the top and bottom cladding, d is the thickness of the core, and h is the propagation constant in the direction of confinement. h, q, p are all functions of the propagation constant β and can be determined by solving a set of 4 transcendental equations:

$$\begin{aligned} q &= \sqrt{\beta^2 - n_1^2 k^2} \\ h &= \sqrt{n_2^2 k^2 - \beta^2} \\ p &= \sqrt{\beta^2 - n_3^2 k^2} \\ \tan(hd) &= \frac{p+q}{h\left(1 - pq/h^2\right)}, \end{aligned} \quad (2.6)$$

where $k=\omega/c$ is the wavenumber.

Since the guided TE wave is composed of two plane waves traveling at angles $\pm\theta_i$ with the z-axis, their wavevectors have components $(0, \pm k_x, k_z)$. The sum or difference of these vectors therefore varies with z as $exp(-jk_z z)$. The propagation constant β is $k_z=k\cos\theta$. As a result of θ being quantized, so is β: $\beta_m=k\cos\theta_m$. The solution to the transcendental equations is the set of discrete allowed values β_m. The number of such β_m values is therefore the maximum number of allowed modes M. For a symmetric planar

waveguide (n_1=n_3), another way to determine the value of M is to use the following relationship:

$$M \doteq 2\frac{d}{\lambda_o}\sqrt{n_2^2 - n_1^2} \,. \tag{2.7}$$

Again, n_1 and n_2 are refractive indices of the cladding and core, and d is the thickness of the core layer. The symbol $\doteq$ denotes that the right hand side of the equation is increased to the nearest integer.

There is a relationship between h, k, θ, and β. It is illustrated in Figure 2.8. $(kn_2)^2$ is proportional to the total energy of the TE wave, β_m^2 is the energy in the z direction, and h^2 is the energy in the direction of confinement. Since all the energy in the two directions must sum to equal the total energy, the simple geometric setup of a right triangle is used to enhance understanding. Given the solutions to β_m, one can use this geometric relationship to calculate the set of θ_m values.

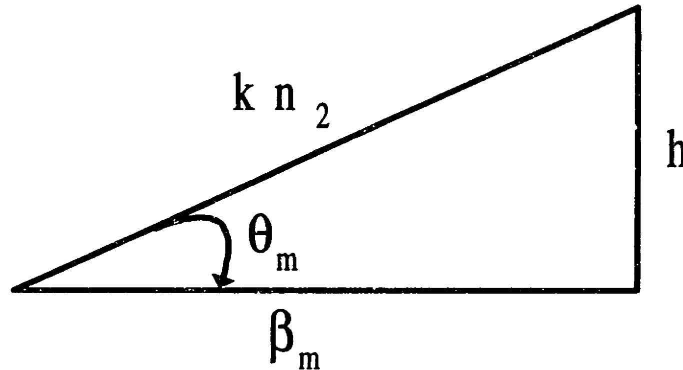

Figure 2.8: Schematic showing the relationship between h, k, θ, and β. $(kn_2)^2$ is proportional to the total energy of the TE wave, β_m^2 is the energy in the z direction, and h^2 is the energy in the direction of confinement.

For λ=1.55μm, a 1μm thick polySi/SiO_2 planar waveguide supports 5 modes. The fundamental mode has propagation constant β=13.93μm^{-1}, confined direction propagation constant h=2.71μm^{-1}, penetration depth p=q=12.53μm^{-1}, and incident angle θ=11°. A

0.2μm thick waveguide supports only the fundamental mode, which has the solution of β=11.38μm^{-1}, h=8.48μm^{-1}, p=q=9.61μm^{-1}, and θ=36.7°.

For λ=1.32μm, assuming the refractive indices remain constant, a 1μm thick waveguide also has 5 allowed modes. The fundamental mode has the solution of β=16.3μm^{-1}, h=2.78μm^{-1}, p=q=14.68μm^{-1}, and θ=9.7°. Again, the 0.2μm thick waveguide supports only the fundamental mode, which has the solution of β=13.78μm^{-1}, h=9.14μm^{-1}, p=q=11.82μm^{-1}, and θ=33.6°.

2.1.2 Definition of Waveguide Loss

Due to optical absorption and scattering, light propagating through a homogeneous waveguide exhibits an exponential power decrease as a function of distance. Power loss or attenuation is the most important figure of merit for waveguide performance because it limits the magnitude of the transmitted power. The attenuation coefficient α is defined in units of decibel per length (dB/length)

$$a = \frac{10}{L}\log_{10}\frac{1}{\mathrm{T}}, \tag{2.8}$$

where $T=P(L)/P(0)$ is the ratio of transmitted power to incident power for a waveguide of length L. For example, a T of 0.01 corresponds to a 20dB attenuation.

For a propagation distance of x centimeters, the waveguide attenuation is αx decibels and the power at point x is

$$\begin{aligned} P(x) &= P(0)10^{-\frac{\alpha x}{10}} \quad \text{or,} \\ p(x) &= P(0)e^{-0.23\alpha x} \end{aligned} \tag{2.9}$$

where P(0) denotes the incident power and α is in dB/cm. Equation 2.8 is useful in determining the intrinsic transmission loss of a waveguide. Equation 2.9 is useful in determining the power output of a waveguide of length x.

2.2 Waveguide Material Selection

The major barrier to the full realization of optoelectronic IC's had been the pursuit of hybrid systems. These designs rely on the integration of standard VLSI electronics and compound semiconductor optoelectronics. The integration of these dissimilar materials had proven unappealing due to costly alignment problems and the lack of well-defined integration methodology. The recent demonstration of the Si:Er LED [9] and SiGe detector on silicon [10] has made possible a monolithic approach to optoelectronic/electronic integration. Since the Si-based LED has a strong emission peak centered at 1.55μm [9] and the detector operates efficiently at 1.3μm [10], the waveguide materials must be non-absorbing at both of these wavelengths. Furthermore, since sub-micrometer interconnect dimensions and limited bending loss are required in IC applications, large core-cladding refractive index contrast is a must to ensure excellent optical confinement. While selecting the waveguide material system, other attributes to look for are ease of fabrication and low coupling loss.

At the wavelengths of 1.3 and 1.55μm, the SiO_2 system has demonstrated exceptionally low loss of a fraction of a decibel per kilometer for long-haul communications. One would be inclined to believe that if this material is used for integrated waveguides, transmission loss would be a non-issue. Nonetheless, since the silicon substrate has a very high refractive index of 3.5 at 1.55μm, a natural concern is the radiation of optical power out of the waveguide into this substrate. One can reduce this effect by raising the index contrast with additional doping and increasing the cladding thickness. This solution requires a cladding thickness of at least 8-10μm. The long deposition time of such thick SiO_2 layer is prohibitive in standard processing. Furthermore, the small index contrast of a SiO_2 system requires large bending radii to limit bending loss.

If Si is used as the waveguide core, both Si_3N_4 and SiO_2 have significantly lower indices to offer excellent optical confinement as the cladding material. It turns out that SiO_2 is better than Si_3N_4 both because its index of 1.5 is lower than Si_3N_4's 2.5 and it has a faster deposition rate. Depending on the waveguide structure, the requirement of cladding thickness in a Si/SiO_2 system can be as low as 200-700nm without significant power radi-

ating into the substrate [11]. Furthermore, the Si waveguide structure is preferred because it can be integrated with Si-based emitter and detector without excess optical coupling loss.

A rectangular strip structure is investigated in this work because it more tightly confines the field laterally than other waveguide designs. This tight lateral confinement, combined with the large Si/SiO_2 index difference, leads to very low bending losses. As the simulation plot in Figure 2.9 suggests, the Si/SiO_2 strip structure can have bending radii on the order of micrometers without suffering noticeable loss. Furthermore, this waveguide's superior confinement allows optical interconnect dimensions on the order of, or even smaller than, conventional interconnects. Lim [11] showed simulations of single mode strip guides as small as 0.2μm by 0.5μm. Nonetheless, there are challenges associated with using the strip design. Most significant is the strong interaction between the confined field and the waveguide surfaces. This interaction can result in significant scattering loss in the event of rough surfaces.

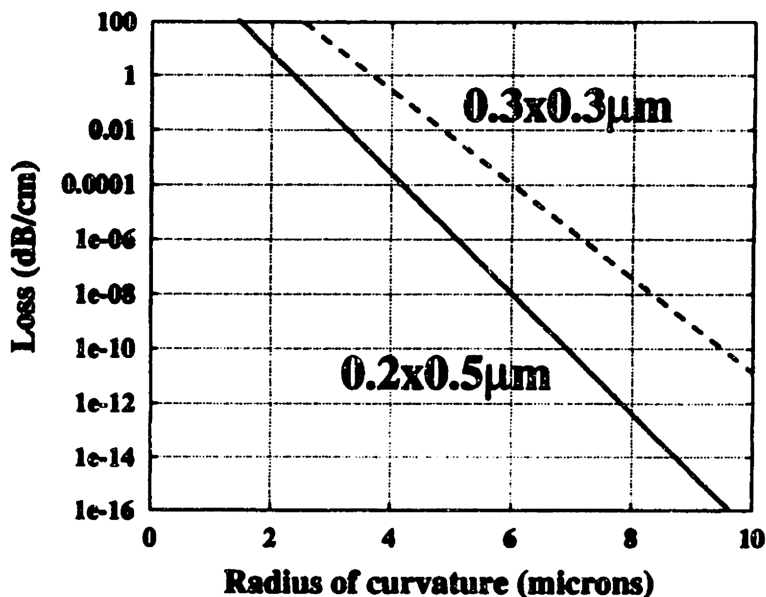

Figure 2.9: Simulated bending loss for Si/SiO_2 strip waveguides [11].

Other research groups have investigated the functionality of Si/SiO_2 waveguides for 1.55μm and 1.3μm operation [12, 13]. They all have limited their studies to crystalline

silicon (c-silicon) systems, three of which are described below. The polySi system gained recognition only recently. Its advantages and disadvantages are described for comparison.

2.2.1 Bond and Etch Back Silicon on Insulator

Bond and Etch back Silicon On Insulator (BESOI) is a technique by which a Si-SiO_2-Si structure is formed (see Figure 2.10). Two Si wafers, one with a top oxide layer and the other with a buried boron layer, are bonded together by thermal annealing. The wafer with the boron implant is then ground and chemically etched back to form the thin top silicon layer. The buried boron region acts as an etch stop to control the thickness of the silicon layer.

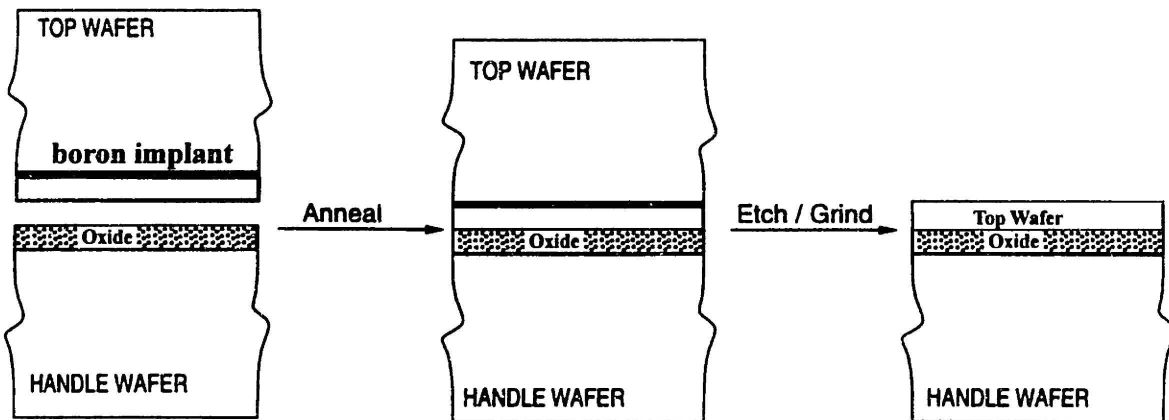

Figure 2.10: BESOI fabrication process.

The advantage of this process is the formation of high quality oxide and silicon. BESOI waveguides have low defect crystalline cores and have demonstrated losses less than 1 dB/cm. Unfortunately, BESOI fabrication is expensive and time consuming due to the numerous process steps involved. Furthermore, since the final top Si thickness is only about 0.1% of the original wafer thickness, it is hard to attain highly uniform layers. Presently, the best thickness uniformity achievable is ±10nm for a thickness of no less than 0.2μm [14]. Another important limitation of BESOI is that fabrication of multiple levels is

difficult. As a result, waveguides are often required to use the precious active areas of silicon.

2.2.2 Separation by Implantation of Oxygen

As the name suggests, Separation by IMplantation of OXygen (SIMOX) is a technique that forms a buried oxide layer beneath a c-silicon region by implanting high doses of oxygen ions into the wafer (see Figure 2.11). A high temperature anneal then follows to form the continuous layer of SiO_2 and to recrystallize the top silicon. Since this Si layer is heavily damaged during implantation, significant amounts of dislocations and stacking faults remain even after anneal [15]. SIMOX waveguides, nonetheless, do not appear to be affected by these defects. Their transmission losses of less than 1dB/cm are similar to those of the BESOI guides. On the other hand, better thickness uniformity can be obtained with SIMOX structures. For a top silicon thickness of 0.2μm, well-controlled implantation can yield a thickness uniformity of ±3nm [14].

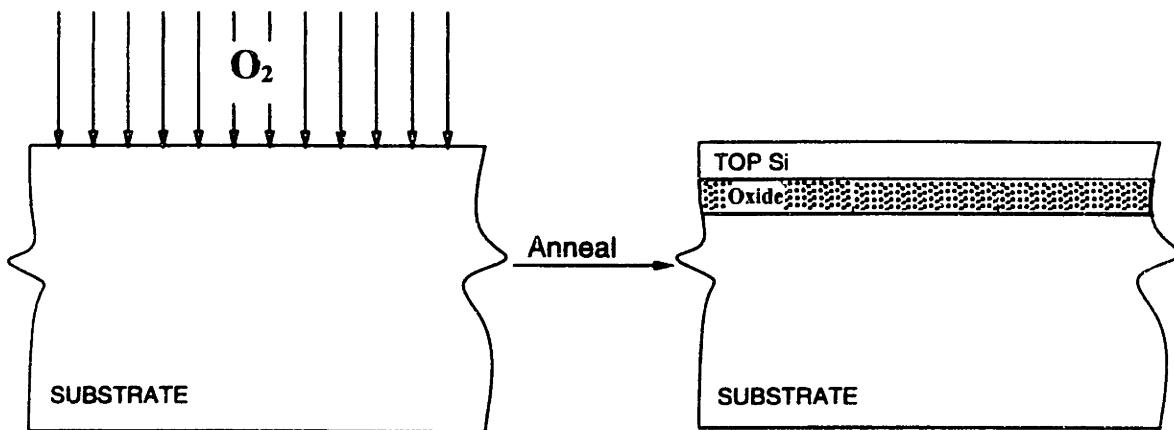

Figure 2.11: SIMOX fabrication process.

One major limitation with using the SIMOX technique for waveguide applications is that it allows only very thin oxide layers, thicknesses that may not prevent radiation losses from the core to the substrate. Other disadvantages of SIMOX waveguides are

similar to those of BESOI guides; they are the fabrication limitation of single level structures, high cost, and utilization of active silicon area.

2.2.3 Doped Silicon

Another silicon-based waveguide scheme utilizes the free carrier refraction effect. In this structure, light guidance is possible because free carriers change the refractive index of silicon. At λ=1.55μm, the change in electron and hole concentrations, ΔN_e and ΔN_h respectively, affect the refractive index in the manner described by the following equations:

$$\Delta n = -3.499 * 10^{-21} (\Delta N_e)^{1.0228} \quad or \quad \Delta n = -5.369 * 10^{-18} (\Delta N_h)^{0.80866} \tag{2.10}$$

Since doped silicon has lower index than undoped silicon, it is used as the cladding. Unfortunately, the index contrast is small even for high free carrier concentration. Optical confinement is poor; therefore, this scheme can lead to high bending loss, large waveguide dimension, and low interconnection density.

2.2.4 PolySi-SiO_2

The PolySi waveguides used for this thesis are similar in structure to BESOI and SIMOX guides. They too have silicon guiding cores and SiO_2 cladding layers. The fabrication of these waveguides, however, is much more straightforward. First, a silicon oxide layer is thermally grown on top of a silicon substrate. Then a polySi layer is deposited using conventional low pressure chemical vapor deposition (LPCVD) technology. To crystallize amorphous silicon regions and to enhance grain growth, thermal annealing generally follows.

In terms of superior index contrast and VLSI compatibility, the polySi waveguide is equivalent to BESOI and SIMOX structures. Its ease of fabrication, however, places it miles ahead of the others for IC interconnect applications. Thermal oxide growth and LPCVD deposition are relatively inexpensive processes widely used in today's VLSI fabrication. CVD technology can deposit PolySi and SiO_2 on a variety of substrates; as a result, this flexibility can enable the realization of multiple levels of interconnection for high

functionality IC's. Waveguides can also be fabricated in three dimensions, thus permitting communication between different interconnection layers.

As mentioned above, one major limitation of c- silicon waveguides is their utilization of precious silicon area dedicated to electronics. The fabrication flexibility of polySi removes this shortcoming and allows interconnects to be placed on elevated layers. Furthermore, polySi waveguide processing has complete control over the critical parameter of film thickness. Layers as thin as several hundred angstroms and as thick as tens of micrometers have been demonstrated. In BESOI fabrication, on the other hand, silicon thickness is limited by the effectiveness of the silicon etch, and uniform layers less than 0.2μm is virtually impossible to attain. In SIMOX fabrication, even the thickest oxide available may not be enough to prevent the field from radiating out of the core. The advantages of low cost, process simplicity, and fabrication flexibility are unique to polySi. They allow designers the type of freedom unimaginable in single-crystalline systems.

Prior to 1994 there had been no attempts to make optical waveguides out of polySi. This neglect of polySi/SiO_2 can be attributed to reports of polySi absorption as high as 1700 dB/cm at λ=1.3μm and 1.55μm [16]. The first polySi waveguide was fabricated in 1994 and its transmission loss at 1.55μm was reported as 80 dB/cm. [1]. This loss corresponds to an output to input power ratio of 10^{-8} after only one centimeter. To further appreciate the enormity of this loss value, one should note that BESOI's 1dB/cm attenuation (which can serve as a theoretical minimum for loss in polySi) translates to a power ratio of almost 0.8.

By 1995 significant progress had been made in reducing loss; Black reported an assuring 35 dB/cm. Before one can attempt to further reduce this attenuation, the obvious question is of course: what factors are contributing to this 35 dB/cm?

2.3 Mechanisms of Waveguide Loss

Attenuation is perhaps the most fundamental determinant of waveguide performance in that it limits the magnitude of the transmitted power. It therefore dictates the output requirement of the emitter and detection limit of the receiver. Optical absorption and scattering are two main sources of loss; they can occur at any point of lattice irregularity along

the length of the waveguide. Another potential source of attenuation is imperfect optical confinement, it can result from poor cladding quality or insufficient thickness.

Optical absorption takes place when photons interact with electrons or with vibrational states of the core. During this interaction the material absorbs photons which have sufficient energy to promote electron excitation. 1.55μm light has an energy of 0.8eV. In a defect-free silicon crystal, whose energy gap is ~1.1eV, this radiation is transmitted without suffering loss. However, any distortion of the crystal lattice order such as random material structure, imperfections, and impurities may give rise to defect states in the energy gap, resulting in possible photon absorption.

Also associated with these lattice distortions are local variations of the refractive index, which can cause optical scattering, the other major mechanism of waveguide loss. Any scattering event can be modeled as an absorption of photon energy followed by its re-emission in all directions. A light wave incident on a sample is absorbed by its atomic or molecular constituents, which then act as dipoles with certain oscillating frequency. The resulting radiation is of course the scattered light. To calculate the optical intensity at any point away from the incident beam, it is necessary to sum the intensity of all waves entering this point. If the sample is homogeneous, the dipoles oscillate relative to one another with fixed phase differences. The sum of their intensities equals zero in all directions; as a result, light scattering does not take place in a homogeneous medium. For an inhomogeneous solid, on the other hand, the disordered atoms oscillate in a more random manner and, consequently, the resulting scattered beams are spatially incoherent and the sum of their intensity is non-zero. For material inhomogeneities that have linear dimensions much smaller than the optical wavelength but contain sufficient number of atoms for statistical analysis, scattering follows the Rayleigh law of $I \propto \lambda^{-4}$. The intensity of Rayleigh scattered light therefore increases as the wavelength of the incident beam decreases. Scattered light that makes an angle with the core surface normal less than the critical angle for total reflection can radiate out of the waveguide. Fortunately, part of its energy remains within the core due to normal reflection. Outlined below are several likely loss mechanisms for polySi/SiO_2 waveguides.

2.3.1 Surface Roughness

A rectangular strip waveguide has four surfaces which interacts with the guided light; they are the top surface, bottom surface, and sidewalls. Rough features on any of these areas can cause significant transmission power loss due to surface scattering. The roughness of the four surfaces are likely to be different and are determined or affected by different processes.

PolySi is deposited on an oxide layer, its bottom surface roughness is therefore a near translation of the oxide surface topography. Since the oxide is an amorphous layer and is thermally grown, its surface is normally quite smooth. PolySi's top surface, on the other hand, can be quite rough due to the nature of the deposition process and the subsequent grain growth during anneal. Sidewall roughness is more difficult to quantify and is primarily determined by the photolithography and etch process.

For the SiO_2/polySi/SiO_2 structure, whose n_{Si}=3.5 and n_{SiO2}=1.5, the critical angle is 25°. Even with such superior index contrast, nearly 90% of the scattered light does not experience total internal reflection. Furthermore, part of the scattered light that does remain in the core is not guided because it does not meet the self-consistency requirement. The rest of the scattered light is distributed in various modes. Higher order modes, having to experience more reflections and more interactions with other scattering sites, are higher loss modes. In some waveguides, these higher order modes are so lossy that they don't persist to the output. In other words, only a very small percentage of the scattered radiation ever propagates the entire length of the waveguide.

Surface roughness is also known to magnify the effect of surface absorption. This absorption is primarily due to surface defects such as impurities and under-coordinated atoms. Because surface area is increased with surface roughness, the amount of such defects is also expected to increase. The result, of course, is further power loss.

For an estimate of the contribution of surface roughness to loss, Tien derived an expression from a understanding of the modal characteristics of the waveguide:

$$\alpha = A^2 \frac{(\cos\theta)^3}{2\sin\theta} \frac{1}{d+\frac{1}{p}+\frac{1}{q}} \qquad (2.11)$$

θ is the incident angle of the EM wave in the waveguide, p and q are the penetration depths of the mode into the top and bottom cladding, and d is the core thickness. A is a measurement of surface roughness; it is given by

$$A=\frac{4\pi}{\lambda}\sqrt{\sigma_{12}^2+\sigma_{23}^2} \tag{2.12}$$

σ_{12} and σ_{23} are the RMS roughness of the top and bottom core/cladding interfaces, and λ is the wavelength in the core material.

The first major breakthrough in polySi waveguide loss reduction was made by cutting down surface roughness. Black was able to achieve a 43 dB/cm transmission loss reduction simply by smoothing the waveguide surface. Her high loss sample had a RMS roughness of 20nm and a loss of 77 dB/cm. After chemical-mechanical polish, the roughness was decreased to 7nm and the corresponding loss was 34dB/cm. This loss reduction of 43 dB/cm was predicted nicely by Tien's analysis, which yielded a slightly higher value of 48dB/cm. This discrepancy can be attributed to the various assumptions made while performing the calculation.

2.3.2 Grain Boundaries

Grain boundaries are essentially arrays of dislocations or even amorphous regions that separate crystalline materials of different orientations. At these boundaries, planes of atoms terminate and fill the wedge shaped regions between the grains. As a result, grain boundaries are a great source of defects in an otherwise ordered crystal lattice. Electron spin resonance (ESR) studies of polySi have identified most of its grain boundary defects to be singly-occupied dangling bonds, or neutral threefold coordinated silicon. Figure 2.12 compares the local coordinations of a silicon atom in the ground state and in the neutral dangling bond configuration. These dangling bonds exist as defect states in the bandgap of silicon. They are estimated to be 0.65±0.15eV below the conduction band minimum [17].

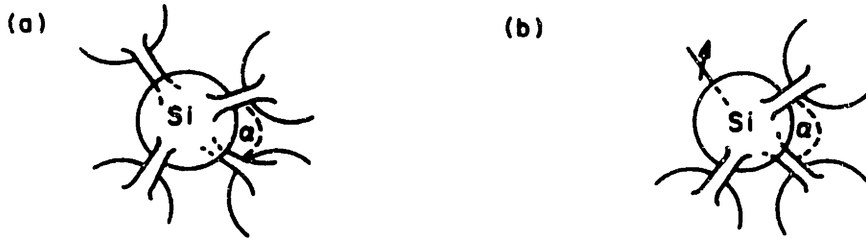

Figure 2.12: Sketches of the optimal local coordinations of a Si atom in a) the ground state configuration and b) the neutral singly-occupied dangling bond configuration. The bond angle α=109.5° [18].

The presence of these dangling bond defect states in the bandgap allows two types of optical absorption. Photons lose their energy as they take part in exciting either valence band electrons to the defect level or electrons at the defect level to the conduction band (see Figure 2.13). The opposite process of photon emission by radiative recombination is possible, but not likely. In the event that it does occur, it will not contribute to waveguide output because the resulting light has different wavelengths than the desired 1.55μm.

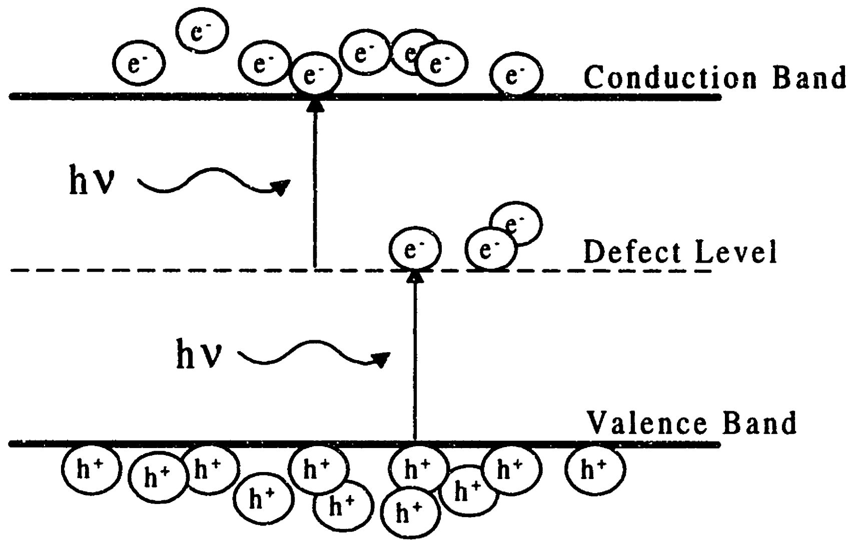

Figure 2.13: Electron excitation due to absorption of photons.

The historic lack of interest in polySi waveguides can be attributed to reports of high absorption, ranging from 450dB/cm [17] to 1700dB/cm [16] at λ=1.55μm. Most of this optical loss was assumed to be inherent absorption by the grain boundaries of the polySi material. Closer examination of the measurement techniques revealed that the re-

ported values incorporated loss due to internal scattering as well. Grain boundary defects are believed to be the main cause of this scattering. These defect states, mostly dangling bonds, trap electrons. They produce accumulation of negatively-charged carriers at the grain boundaries. These aggregate charges give rise to localized increases in potential, which in turn cause changes in the index of refraction.

The notion that grain boundaries have slightly different indices than grains is not unfounded. A study performed by Jackson [17] in 1983 discovered that the bandgap of silicon grain boundary is ~1.0eV, slightly lower than that of crystalline silicon. Since a lower bandgap generally indicates a higher polarizability and higher refractive index, one would expect the index of silicon grain boundary to be slightly greater than that of crystalline silicon. Since a grain boundary, with all its disordered atoms, can be viewed roughly as amorphous, its index should resemble that of the amorphous material. For amorphous silicon, the index is 4, indeed higher than crystalline silicon's 3.5. The end result of the change in refractive index at the grain boundaries is Rayleigh scattering and, ultimately, power loss.

The most obvious way to reduce losses caused by grain boundaries is to reduce the total grain boundary density. This can be achieved by depositing polySi with large grains. A thin film's grain size and structure can be controlled by varying deposition parameters such as temperature, pressure, and process gas. Internal polySi absorption and scattering can also be lowered by thermal treatments such as extended temperature anneals [19]. Figure 2.14 compares the absorption coefficient α of as-grown and annealed polySi. Notice that annealed polySi has a lower α than as-grown polySi regardless of the deposition temperature. Another method to reduce the adverse effects of dangling bonds is the incorporation of monatomic hydrogen. The hydrogen ions bond to the unsatisfied silicon atoms and terminate them as absorption and scattering centers, effectively removing the defect levels in the gap. The details of these loss reduction techniques are discussed later.

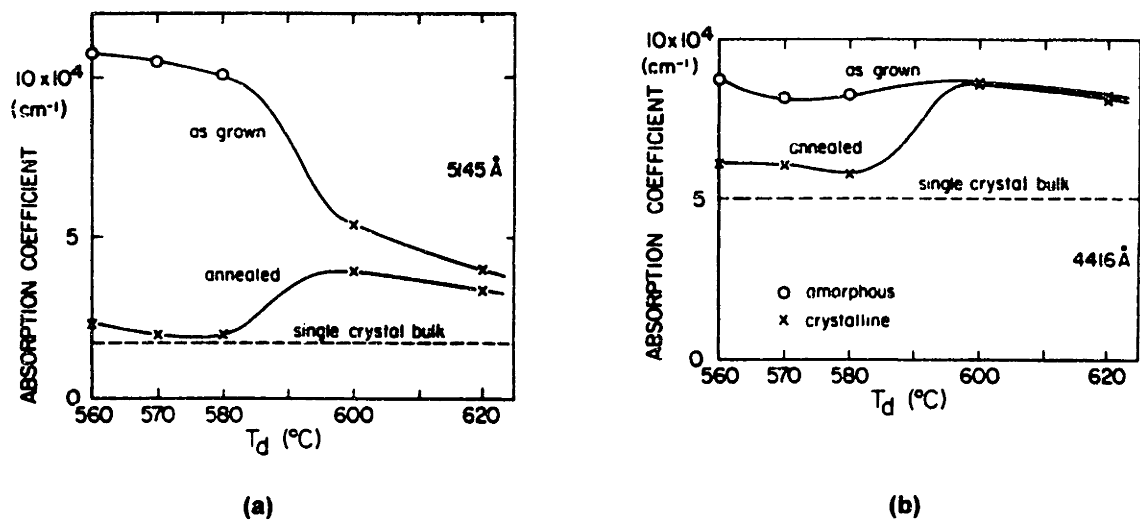

Figure 2.14: Absorption coefficient of as-grown and annealed (900°-1000°C) polySi vs. deposition temperature: a) for $\lambda = 514.5$nm and b) for $\lambda = 441.4$nm [19].

2.3.3 Amorphous Silicon

Due to non-optimal deposition and annealing conditions, most polySi thin films contain regions of amorphous silicon (α-silicon). Unlike crystalline materials, amorphous networks lack long range periodicity. They are characterized by spatial fluctuations of bond angles and perhaps even bond-lengths. Theoretical treatments of non-crystalline solids have shown that either bond stretching or bond bending tends to increase the energies of the valence-band states and decrease the energies of the conduction-band states [20]. As a result, the bonding distortions inherent in amorphous solids can introduce a range of localized states into the energy gap, extending the band edges. In addition to bond distortions, defect centers such as singly-occupied dangling bonds are also abundant in amorphous silicon. As mentioned previously, they also have energy levels in the bandgap. By enabling sub-gap absorption, both bonding distortions and dangling bonds contribute significantly to waveguide loss.

The effects of the above sub-gap absorption on loss may be magnified by the direct gap nature of α-silicon. In semiconductors, optical transitions such as absorption requires the conservation of energy and momentum. For indirect gap materials, namely crystalline silicon, the minimum-energy optical transition across the gap requires an exchange of mo-

mentum that only phonons can accommodate (see Figure 2.15). The occurrence of such three body (electron, photon, and phonon) participation is quite low; therefore, absorption of crystalline silicon rises only slowly with increasing energy. For sub-gap absorption, the same energy and momentum conservation applies. The presence of defect states in the gap determines the possibility of absorption, but it is the momentum of these defect states that determines the likelihood of absorption. On the other hand, for direct gap materials such as α-silicon, crystal momentum is not conserved and all optical transitions are necessarily direct. For this reason, sub-gap absorption in α-silicon can be much more devastating for waveguide transmission.

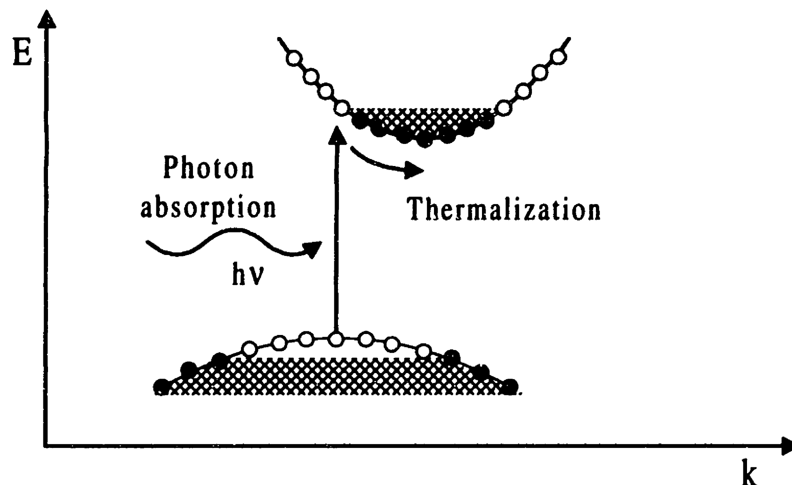

Figure 2.15: Indirect gap optical transition requires the participation of the electron, photon, and phonon.

Scattering loss is another important concern in amorphous silicon. As discussed previously, dangling bonds give rise to localized fluctuations in refractive index by trapping electrons and impurities. The microscopic density inhomogeneities associated with the amorphous state will also cause index changes that act as efficient Rayleigh scattering centers. Furthermore, light traversing the interface between amorphous silicon and polySi can suffer scattering because the two material states have a relatively large refractive index contrast of ~0.5.

The amount of α-silicon in deposited films can be significantly reduced with adequate thermal anneals. The annealing temperatures most commonly used range from 550-700°C [5]. The time needed for crystallization depends on the deposition conditions as well as the selected annealing temperature, it ranges from 5-25 hours.

2.3.4 Intra-grain Defects

After deposition, the silicon film is crystallized with a low temperature anneal. Numerous studies have found defects such as twin boundaries and dislocations in the crystallized grains. As a matter of fact, experimental evidence reveals that crystallization of α-silicon proceeds solely through the formation of micro-twins [21]. These micro-twins are unstable and can be absorbed by larger twins at high temperatures.

Intra-grain defects, like miniature versions of grain boundaries, contain high densities of dangling bonds. With energy levels in the band gap, they can absorb photons in the vicinity. They also give rise to localized index variations, allowing optical scattering.

2.3.5 Lattice Strain

Lattice strain is introduced during deposition, it is dependent on deposition rate and temperature. α-silicon forms the most over-constrained network; it can encompass gross structural features such as cracks and micro-voids as well as local imperfections such as distorted bonds and defect centers. The large structural defects are detrimental to optical transmission; they can cause incredible scattering due to the tremendous index change. The localized bond distortions introduce a range of defect states into the energy gap, allowing optical absorption loss.

Experimental evidence shows that thermal anneals can reduce network strain. One possible explanation is that thermal motions can assist in propagating local strains throughout the material. When local compressive and tensile strains meet, they annihilate each other; thereby reducing the total silicon network strain [22]. When a certain disorder level is achieved, however, there is a free energy barrier for further reduction in strain energy. To surmount this barrier, higher temperature anneals are needed. Once the strain energy reaches a minimum, a steady state is achieved between strain reduction and crea-

tion. Existing strain is distributed in the network according to maximum entropy. Hydrogenation is another way to reduce strain. *H* removes every highly stretched bond through the formation of two *Si:H* bonds.

2.4 Physical Properties of PolySi Thin Films

Only recently has polySi been investigated as a waveguide material, but it has been an integral part of silicon-based microelectronics for many years. Its applications include low-cost solar cells, metal-oxide-semiconductor (MOS) gate technology, and thin film transistor technology. These applications have different material requirements and have prompted many studies of film growth and factors influencing the physical properties of polySi such as surface morphology and grain structure. The results of these studies offer invaluable insight for achieving high quality polySi films and are the first step in making low-loss waveguides.

Currently the most common technique for depositing polySi is low pressure chemical vapor deposition (LPCVD), a process that relies mainly on the pyrolysis of silane or disilane gas. It is an IC manufacturing standard because it offers low cost and high capacity production. All the polySi films investigated in this thesis are deposited in a LPCVD furnace.

2.4.1 Surface Morphology

Studies of silicon deposited on SiO_2 reveal that RMS surface roughness ranges from 1 to 20 nm with some reported data as high as 30nm [23, 24]. These large variations in film roughness are most likely the results of different deposition conditions controlled by temperature, pressure, and process gas. Studies have demonstrated that to obtain very smooth films, one can carry out depositions at temperatures below 580°C. At such temperatures, the final silicon structure is amorphous with RMS surface roughness on the order of 1 nm. To obtain polySi, a crystallization anneal must follow. It is believed that the crystallization process does not contribute to further increase in roughness. An experi-

ment performed by Foresi et. al. demonstrated the effectiveness of the low temperature deposition; they achieved a RMS roughness reduction of 15nm [3].

Deposition pressure is another important determinant of film morphology. It has been shown that the RMS surface roughness of polySi decreases as deposition pressure increases [25]. Figure 2.16 illustrates this trend for two experiments. From this figure, one will notice that the choice of deposition gas also affects the surface roughness of the deposited silicon. It appears that disilane can produce much smoother films even though the process pressures are lower than those used in the silane-based study.

There is also evidence of a strong correlation between surface roughness and film thickness [26]. For a range of thicknesses, thinner films are generally smoother than thicker ones.

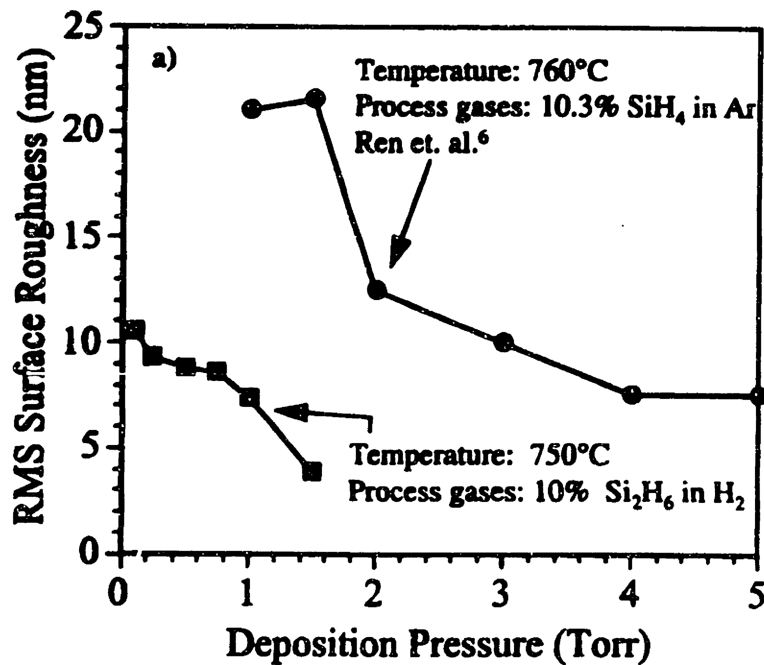

Figure 2.16: Pressure dependence of rms surface roughness for silane- and disilane-based processes [25].

2.4.2 Grain Size

The average grain size of deposited silicon films can vary significantly from 0.05 to 1.3 µm [5, 27]. Like surface morphology, it is greatly dependent on deposition conditions and

film thickness. It is also believed to be a function of high temperature anneal and dopant concentration.

For deposition temperatures T_d below 580°C, the silicon film is amorphous. It contains randomly-distributed nucleation sites for grain formation. These nuclei grow and transform the film into polySi during crystallization anneal. The number of these starting nuclei is strongly dependent on deposition conditions; it is found to decrease with decreasing temperature. As a result, the lower the deposition temperature, the larger the grains. Figure 2.17a illustrates this relationship; notice, however, that there is an optimal temperature which yields the largest average grain size. Although crystallization occurs during thermal treatment, grain size is not found to depend significantly on annealing conditions. For deposition temperatures of 580°C or above, the silicon film is polycrystalline. Nucleation sites are formed at the instant of deposition; grains grow vertically as more material is being added, producing columnar grain structure. The grain size is significantly smaller than that of thermally-crystallized grains, but it does increase with increasing temperature (see Figure 2.17b). This as-deposited film is reasonably stable; there is little structural change during anneal.

Another determinant of grain size is the thickness of the deposited film. Since thicker films allow grains more area to expand, it is not surprising that grain size increases with increasing film thickness.

Studies have shown that grain size is also dependent on high temperature anneals and dopant additions. The grain-growth mechanism of polySi is believed to be controlled by silicon self-diffusion. Growth is accomplished by individual silicon atoms making diffusion jumps across the grain boundaries. In the absence of a driving force, the number of jumps in opposite directions are equal, resulting in no net movement of the boundary. When a driving force exists, the free energy is lowered and atoms migrate from one grain to another, contributing to grain growth. The self-diffusion of silicon is enhanced both by high temperature and heavy doping.

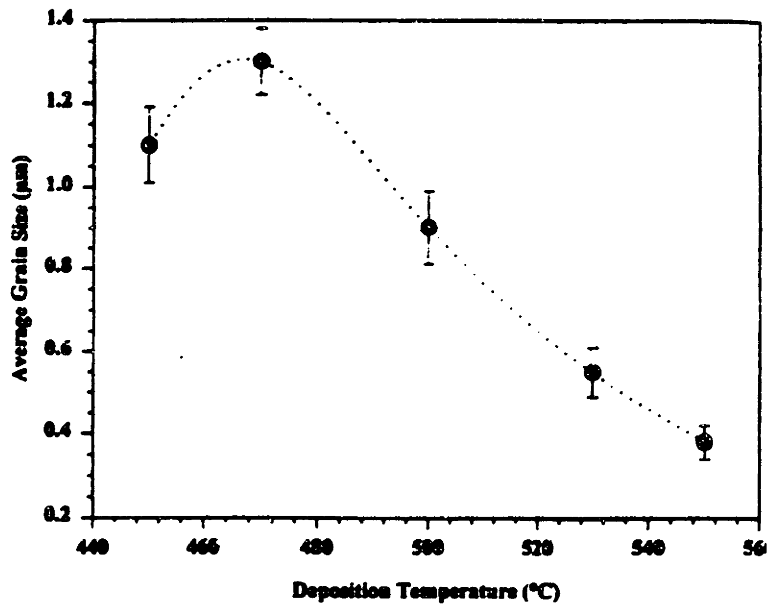

(a)

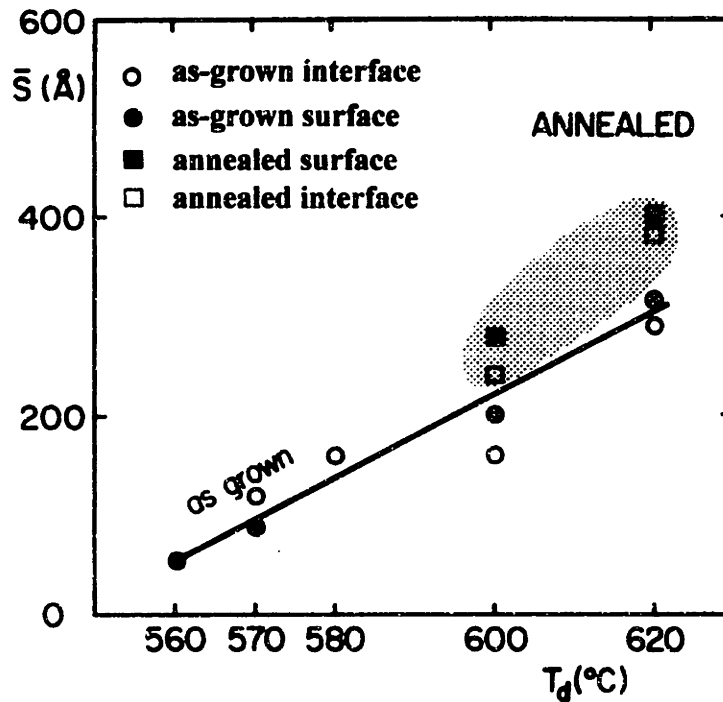

(b)

Figure 2.17: Grain size of polySi as a function of the deposition temperature. a) For T_d < 580°C, grain size increases with decreasing deposition temperature [27]. b) For T_d > 580°C, grain size increases with increasing deposition temperature [19].

2.4.3 Hydrogenation

The optical and electrical performance of polySi is limited by grain boundary and intragranular defects inherent in the polycrystalline structure, as well as interface trap states common to all types of devices. The conventional approach to passivate these defect states is hydrogenation. This technique uses radio frequency or electron cyclotron resonance, and defect passivation occurs as a result of plasma penetration and hydrogen diffusion. The effectiveness of the passivation technique is commonly measured by the reduction of the material's spin density, a parameter easily determined by electron spin resonance (ESR).

Monatomic hydrogen introduced into the polySi film diffuses in the positive charge state, H^+ [28]. It attaches to the dangling bond or defect, annihilating it as an absorption or scattering center. H^+ is also reported to break highly tensile Si-Si bonds to relieve the inherent network strain [18]. In doing so, it eliminates some tail states associated with bonding disorders. Experimental evidence shows that hydrogen passivation decreases the defect concentration to a steady-state value, which is unaffected by additional hydrogen incorporation. As illustrated in Figure 2.18, this residual saturation value, N_{sat}, is strongly dependent on the hydrogenation temperature, T_H [29]. Notice that the lowest value of N_{sat} was obtained at T_H=350°C. The increase of N_{sat} at higher temperatures is likely due to the out-diffusion of hydrogen.

Another positive effect of hydrogen incorporation is that the bandgap of polySi increases with hydrogen content by as much as 0.1eV [17]. Although the change is subtle, it can decrease the likelihood of sub-gap absorption by stretching the bands farther away from the defect levels.

Hydrogenation has been reported to reduce spin density by between a factor of 3 [30] to an order of magnitude [31]. It has also been shown to decrease the sub-gap absorption of fine-grain polySi by approximately 80dB/cm at λ=1.55μm [17].

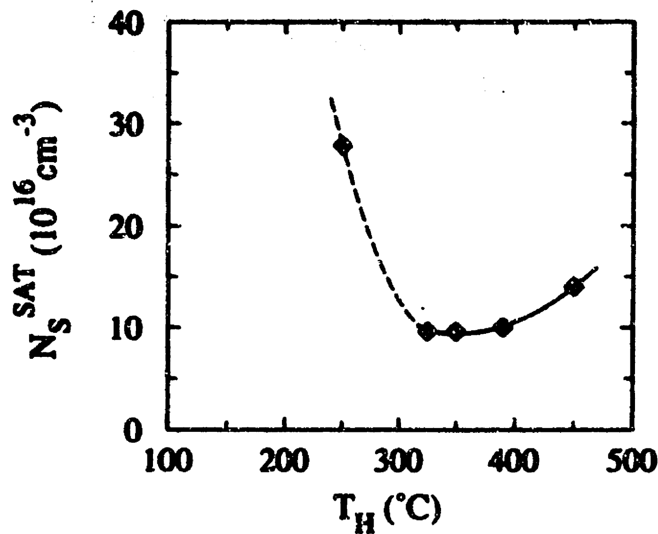

Figure 2.18: Residual saturation value of the spin density as a function of hydrogenation temperature [29].

Nonetheless, there are processing difficulties associated with hydrogen passivation. Studies have shown that the direct exposure of polySi film to the reactive components of a plasma introduces surface damage, which could have the adverse effect of introducing new surface defects [32]. As a result, a protective layer such as SiO_2 is sometimes used during hydrogenation. Unfortunately, the oxide layer strongly attenuates the H^+ flux into the underlying polySi. Depending on the oxide thickness, hydrogen penetration can be reduced by more than 4 orders of magnitude compared to polySi without an oxide layer [28]. Figure 2.19 compares the concentration profiles of deuterium, a readily identifiable isotope which duplicates hydrogen chemistry, in polySi films with different oxide thicknesses. These limitations have prompted the development of remote-source hydrogenation, where the ion velocity is impeded before impact.

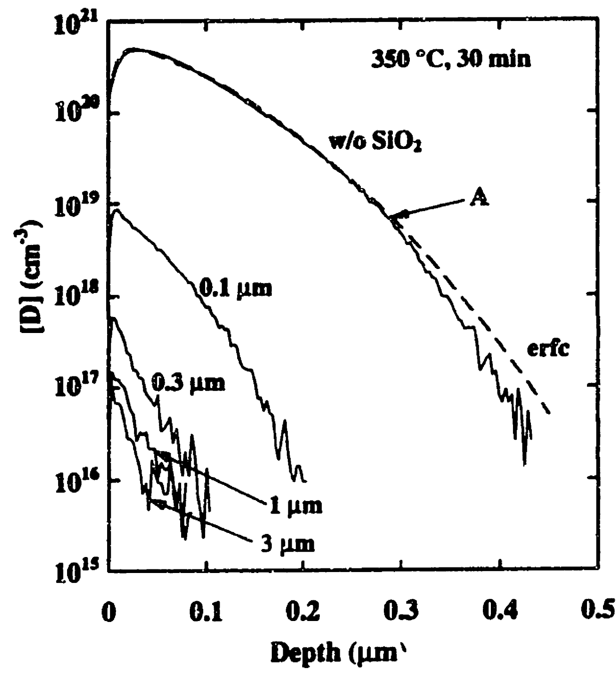

Figure 2.19: Deuterium concentration profiles in polySi films with different thicknesses of protective oxide [28].

Chapter 3

Experimental Details

Even though the fabrication procedure for polySi/SiO_2 waveguides is very straightforward, the exact effects of process parameters on material quality and transmission property are unclear. A systematic investigation of the loss-implications of these parameters, therefore, must be made to achieve high performance waveguides. First, a standard fabrication recipe is used; the resulting waveguide transmission loss and material properties such as grain size, grain structure, and surface roughness are determined. Then process modifications are individually introduced. The subsequent changes in material and transmission characteristics are compared to those of the standard process. In this manner, a better understanding is obtained of the inter-relationship among process, property, and performance. Since small radii waveguide bends with low loss are also crucial for efficient on-chip data distribution, micrometer-size sharp bends are also fabricated and measured. The details of these experiments as well as the characterization techniques are presented below.

3.1 Standard Fabrication Recipe

P-type, <100> silicon wafers are first deposited with 3μm of low pressure chemical vapor deposition (LPCVD) SiO_2, this oxide layer serves as the bottom cladding of the waveguides. Then either 1μm of LPCVD amorphous silicon is deposited at 560°C or 1μm of LPCVD polysilicon is deposited at 625°C. Both of these depositions rely on the pyrolytic decomposition of silane gas at a chamber pressure of ~210 mTorr. To crystallize the amorphous regions in these films into polySi, the wafers are subsequently annealed in

nitrogen for 16 hours at 600°C. Note that one 560°C wafer is intentionally unannealed to allow fabrication of amorphous silicon waveguides for loss comparison. This unannealed amorphous silicon wafer and half of the annealed polySi wafers are patterned into strips with widths of 1, 2, 4, and 8μm and plasma etched with $SF_6/O_2/He$ to obtained the rectangular cores. Finally, a blanket layer of 250nm SiO_2 is deposited to complete the oxide cladding; this SiO_2 layer also serves to protect the waveguide surface during the facet polishing required for transmission loss measurement. Figure 3.1 shows a structure schematic of the resulting strip waveguides, which are referred to according to their deposition temperatures as "560-amorphous", "560" or "625". These structures are used to determine transmission loss as well as etch quality.

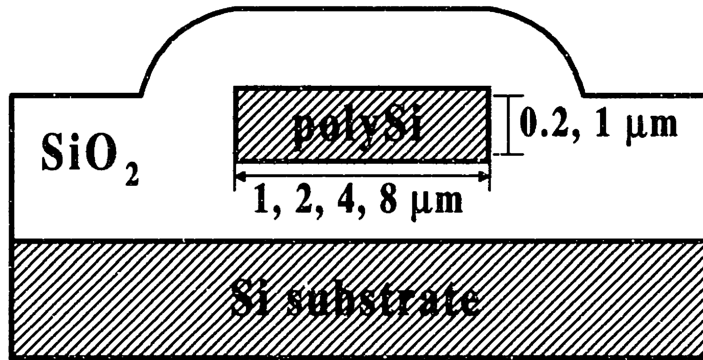

Figure 3.1: The cross-sectional view of the strip waveguide structure used to measure transmission loss in polySi.

The unpatterned wafers, which did not receive the final oxide deposition, are cleaved into sections for material characterization. Relevant material properties examined include grain size, grain structure, surface roughness, and material strain.

Since changes in core dimensions change the waveguide's confinement characteristics and modal distribution, we expected transmission loss to be affected as well. To investigate this possible dependence, thinner waveguides are also fabricated with the standard 560 recipe. The only process modifications include thermal growth of a 1.8μm bottom oxide and deposition of a 0.2μm amorphous silicon. A thinner oxide layer is chosen

because simulation shows that it is sufficient to yield adequate optical confinement. These samples are referred to as "0.2μm-560".

3.2 Processing Experiments

In an effort to lower the transmission loss of the above polySi waveguides and to achieve more desirable material characteristics, experiments are performed involving modifications of the standard fabrication recipe. The details of these experiments are discussed below.

3.2.1 Deposition Experiments

Numerous studies of polySi thin films suggest that deposition conditions are primary determinants of grain size and grain structure [21, 25, 27], of particular importance are deposition temperature, rate, gas, and pressure. To understand the grain size dependence of transmission loss, deposition parameters are varied to obtain both very large and very small polySi grains. Using a disilane process reported by Voutsas et. al. [27], 0.2μm of amorphous silicon is deposited at a temperature of 475°C and pressure of 750mTorr. The wafers are then processed with the same fabrication sequence outlined previously. The grain size after anneal is expected to be greater than 1μm. Since the silicon layer is only 0.2μm thick, the grain structure is likely columnar, traversing the entire thickness of the film.

To obtain very fine grain polySi, high deposition rates are generally used. With help from Applied Materials, 0.2μm of polySi is directly deposited onto the bottom oxide layer at 700°C. To crystallize regions of amorphous silicon that may be present in the film, the standard anneal of 16 hours at 600°C is again used. The expected grain size of this process is between 50-70nm.

3.2.2 Annealing Experiments

Thermal anneal is used after silicon deposition to crystallize the amorphous regions into poly-crystalline form. The conditions of this anneal greatly influence the film's material properties such as degree of crystallinity, grain size, grain quality, and surface roughness. For this thesis three annealing parameters are investigated for the 560 samples; they are

time, temperature, and ambient gas. Suspecting that the standard anneal of 16 hours at 600°C is not sufficient to crystallize the entire 560 silicon film or yield optimal grain quality, the annealed samples are subjected to an additional thermal treatment of either a prolonged anneal or a high temperature anneal. The prolonged heat treatment is carried out in nitrogen ambient at 600°C for 100 hours, whereas the high temperature anneal is carried out at 1100°C for 16 hours. The parameters chosen for these experiments may not be ideal, but they allow clear identification of the determining factor for crystallization: time or temperature.

During the high temperature experiment, it was discovered that the nitrogen annealing ambient is contaminated with a small oxygen leak. In fact, all the heat treatments including that for the standard process are affected. To determine the impact of annealing gas on polySi's optical transmission, the standard 0.2µm-560 waveguides are re-fabricated and annealed in pure nitrogen. Subsequently, the high temperature anneal is also repeated for comparison.

3.2.3 Chemical-Mechanical Polish

Rough features on waveguide surfaces have been found to be a great contributor to optical scattering and absorption. By smoothing the top waveguide surface from a rms roughness of 20nm to 7nm, Black [1] was able to achieve a 43dB/cm reduction in transmission loss. In light of this finding, the relatively rough 625 polySi is chemically-mechanically polished (CMP) prior to patterning. CMP is a widely used method to planarize different material layers in IC fabrication. In this process, the wafer is affixed to a carrier and pressed faced-down on a platen supporting a polishing pad. Both the carrier and platen rotate, and polishing proceeds as an abrasive slurry is dripped onto the pad. A combination of mechanical and chemical actions allow preferential removal of surface material to achieve "global" planarization.

CMP of polySi is performed at Lincoln Laboratory on a WESTECH 372 polisher, which can achieve a thickness uniformity of 1%. A touch down method is used with a polishing time of 30 seconds, pressure of 2psi, and temperature of 30°C. Both the platen

and carrier rotate at a speed of 15rpm. In this thesis, samples which have been polished with this technique are referred to as "625CMP".

3.2.4 Etching Experiment

Since surface roughness is a major contributor to optical scattering and absorption, it was suspected that rough waveguide sidewalls can also result in significant surface loss. To quantitatively measure sidewall roughness, a sample is sawn from a patterned 560 wafer prior to the final oxide deposition; it is then mechanically polished to expose, but not disturb, one waveguide sidewall. Using hot wax, the sample is placed on one sawn edge with the polished side up for atomic force microscopy (AFM), a technique which analyzes surface topography.

Since sidewall roughness is primarily determined by the etch process, two different etch chemistries are investigated. They are $SF_6/O_2/He$, the isotropic plasma etch used for the standard 560 and 625 waveguide processing; and HBr/Cl_2, a preferential anisotropic plasma etch. The waveguides resulting from each of these etch combinations are examined with a scanning electron microscope (SEM), which provides visual information about the sidewall's roughness and shape. The transmission losses of these two types of guides are also measured and compared.

3.2.5 Hydrogenation

To reduce the optical absorption and scattering effects of lattice defects, hydrogenation is used to passivate dangling bonds that reside at grain boundaries, intra-grain defects, and residual amorphous regions. Four passivation techniques are investigated; they are electron cyclotron resonance (ECR) plasma, ultrasound treatment (UST), and plasma ion implantation (PII), and remote-ECR plasma. For ECR hydrogenation [33], 560, 625, 625CMP waveguides and unpatterned samples are immersed in a high density ECR hydrogen plasma. Passivation is performed at 350°C for 40 minutes with 600W power and 0.16mTorr pressure. The concentrations of the incorporated hydrogen as a function of polySi depth are then determined using secondary ion mass spectrometry (SIMS). These

post-hydrogenated samples are referred to as "560ECR", "625ECR", and "625CMP+ECR".

It is known that after ECR passivation, a considerable amount of hydrogen in the polySi film is non-active because its concentration can exceed the number of nonpassivated dangling bonds by as much as two orders of magnitude [29]. Ostapenko et. al. [34] reports that some of these hydrogen atoms do not contribute to passivation because they are weakly bound to one another. The recommended method to promote their separation is low-temperature UST, which is believed to provide the needed activation energy of ~1eV. For the experiment, ultrasound vibrations are applied to the 560ECR waveguides from external circular piezo-ceramic transducers, which are driven to the resonance frequency of their radial and thickness vibrations. This UST is performed at 150°C for 30 minutes with a frequency of 400kHz. To determine the effectiveness of this technique, the transmission losses of these 560ECR waveguides are measured before and after ultrasound treatment.

Another hydrogenation method investigated is PII, developed by Bernstein et. al. [35] In this process, a large negative voltage pulse is applied to the sample immersed in a hydrogen plasma. Hydrogen ions are accelerated by the target potential and implanted into the sample. Like in ECR passivation, the hydrogen reaches the active layer by diffusion. However, due to the large concentration gradient that is created by the high implantation dose, hydrogen incorporation is found to be significantly faster in the PII process. For the experiment, both 560 and 0.2μm-560 waveguides are implanted at 350°C with a dose rate of $2x10^{18}/cm^2$.sec and an energy of 2keV. Again, waveguide loss is measured both before and after processing.

Finally, the technique of remote-source ECR is also investigated. It can minimize possible surface damage by maintaining the sample away from the source so the plasma particles are allowed to slow down before impact. For this experiment, 0.2μm-560(N_2) and 0.2μm-560(1100°C/N_2) waveguides are selected. Hydrogenation exposures of 1 hour are performed at 350°C, 0.33μTorr, and 100W. The resulting transmission losses are measured to determine the effectiveness of this passivation technique. The hydrogen depth profiles will also be acquired and compared using SIMS analysis.

3.2.6 Doping Experiment

Since dangling bonds and refractive index fluctuations at grain boundaries are efficient absorption and scattering centers, the growth of large grain polySi can limit these mechanisms of loss by reducing the density of grain boundaries. One well-documented method of achieving enhanced grain growth is heavy doping, which promotes silicon self-diffusion and allows atoms to migrate from one grain to another [25, 36]. Grain size increases of several orders of magnitude have been reported [37]. Unfortunately, the addition of dopants in the material creates charge carriers, and if its density exceeds 10^{17}carriers /cm^3, free carrier absorption can be detrimental to waveguide transmission [11]. As a result, temperature-assisted grain growth must be accompanied by dopant drive-out.

For the experiment, a gas-phase phosphorous doping technique is used. At 950°C $POCl_3$ gas oxidizes the surface of a patterned 560 wafer while it simultaneously dopes the thin oxide with phosphorous. At this high furnace temperature, dopant drive-in occurs as phosphorous diffuses into the underlying polySi. This process continues for 1½ hours; the final oxide thickness is approximately 120nm. To allow grain growth and dopant out-diffusion, the top oxide is removed and the wafer is subsequently annealed in N_2 at 1000°C for 16 hours. Finally, the transmission characteristics and surface roughness of these waveguides are measured.

3.3 Material Characterization

After each processing modification or experiment, the resulting waveguide material is examined with various characterization tools as described below.

3.3.1 Transmission Loss Determination

3.3.1.1 Sample preparation

First a coat of photoresist is spun onto the patterned wafer to prevent contamination of the waveguide surface during sample preparation. Then the wafer is die sawed, where waveguides of different lengths between 1 and 3mm are cut using a diamond-impregnated

blade saw. Each die contains 4 sets of 20 waveguides of different widths: 1, 2, 4, and 8μm. Both facets of the waveguides are mechanically polished to reduce coupling loss during optical transmission measurement. The polishing technique is adopted from tripod TEM sample preparation. Each die is first mounted onto a sample holder using hot wax. Before the wax hardens, the die is aligned such that the waveguides are exactly perpendicular to the polishing surface and all the facets across the sample edge are evenly polished. Since the diamond saw generally yields very smooth cuts, only 1 and 0.3μm grit alumina-impregnated polishing pads are used. In the event that minor chipping occurred during saw, more coarse media such as 30, 15, and 5μm grit pads are also used. Extreme care is given to ensure consistent facet quality because any variations can lead to differences in coupling losses, creating changes in waveguide output power not indicative of the actual optical transmission. The measured output values for each 20 identical waveguides generally have a standard deviation less than 5%.

After polishing has yielded the desirable facet quality, the die is removed from the sample holder. Any mounting wax that remains on the sample is dislodged by means of a three-step organic solvent clean. The die is first immersed in 1-1-1 trichloroethane (TCA) in an ultrasonic bath for 5 minutes. It is then placed in acetone and finally in methanol with the same ultrasonic agitation. The sequence of TCA, acetone, and methanol is important because TCA is soluble in acetone, acetone is soluble in methanol, and methanol is soluble in water. After the sample is dried, it is immersed in piranha (1:4 H_2O_2:H_2SO_4) for 5 to 10 minutes to dissolve the top coat of photoresist. This resist etch is also very effective in removing any die-saw or polishing residue that may have collected on the sample surface. After the die is rinsed with de-ionized water and dried, an optical microscope is used to determine whether it is adequately polished and sufficiently cleaned. If the two criteria are not met, the above sample preparation process is repeated.

3.3.1.2 Transmission Measurement

Figure 3.2 is a schematic of the setup used to measure both the input and output power of the waveguides. First, light from either a 1.55μm or 1.32μm light emitting diode (LED) is coupled into a single-mode optical fiber. The fiber is then connected to a 90-10 power

splitter. 10% of the light is guided to either a multimeter or an oscilloscope where it is monitored for voltage fluctuations. Throughout the measurement process, this 10% signal is adjusted with the LED current driver to maintain a constant power entering the waveguides. The remaining 90% of the light is guided by an optical fiber with a pointed parabolic tip, which focuses the beam from the 9μm core into a spot size of approximately 4 μm in diameter. This collimated beam is then butt-coupled into the waveguide under test. Optimal alignment is achieved by adjusting the piezoelectric translators to which the optical fiber is attached. The transmitted waveguide output is either qualitatively examined with a CCD camera or quantitatively measured with an infrared detector.

Each die contains 4 sets of 20 waveguides of different widths, but only 1 set is actually used for transmission loss. For the 1μm thick samples, the 8μm wide guides are measured; for the 0.2μm thick samples, the 4μm wide guides are measured. For each 20 waveguides, the power outputs are averaged after excluding some obviously inconsistent data values. This average power is then divided by the input power to obtain the power ratio T. The length of the waveguides L is measured using a calibrated optical microscope.

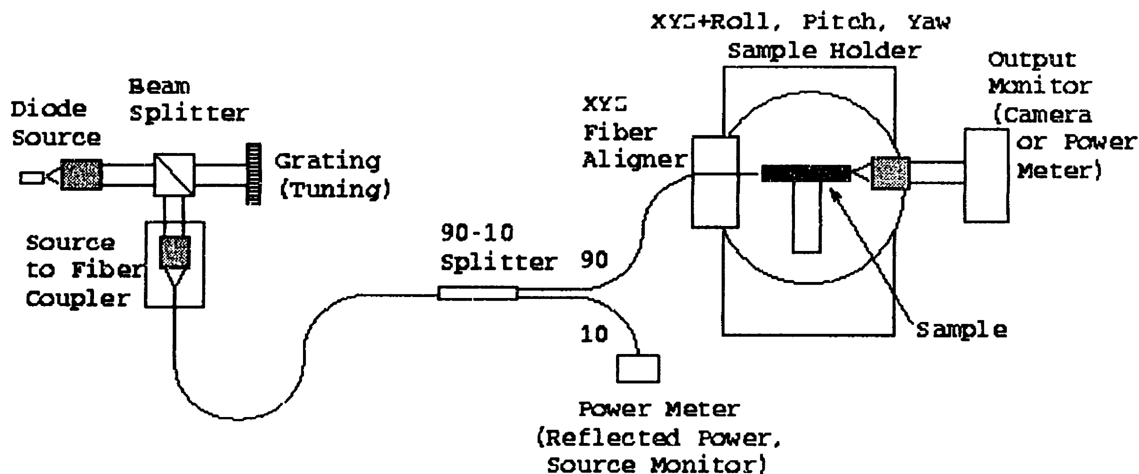

Figure 3.2: The measurement setup used to determine waveguide transmission.

3.3.1.3 Cutback Analysis

Unfortunately, knowledge of both *T* and *L* still does not allow the determination of the attenuation coefficient α because the measured loss encompasses factors other than the actual waveguide loss. It includes reflection and scattering at both the input and output waveguide facets, inefficient collection at the focusing objectives, and imperfect reflection at the optical mirrors. Additionally, since the fiber's output spot is approximately 4μm in diameter and the waveguide is at most 1μm thick, only a fraction of the fiber output is actually collected. In order to factor out these external influences, cutback analysis is used by testing either 40 or 60 waveguides, 20 at each length. The averaged output power is then divided by the input power to identify the ratio T. The cutback technique involves dividing the power ratio T_1 of waveguide length L_1 by the power ratio T_2 of length L_2 to determine α; it is given by

$$\alpha = \frac{dB}{length} = \frac{10}{L_1 - L_2} \log \frac{T_1}{T_2}. \tag{3.1}$$

3.3.2 Transmission Electron Microscopy

The internal microstructure of polySi is visually examined using transmission electron microscopy (TEM), a powerful technique capable of directly observing the complex arrangement of matter at the atomic level. It involves transmitting probe electrons through the specimen of interest; the manner in which these electrons are diffracted yield spatial information about the object, providing at least two-dimensional mapping of internal structural features. For this thesis, a JOEL 200CX-A (LaB_6) TEM is used to analyze both plan-view and cross-section specimens for film crystallinity, grain structure, grain size, and intragrain defects.

The limited penetration power of electrons in polySi restricts the thickness of the TEM specimen to a few hundred nanometers for 50-100kV electrons. Specimen preparation is therefore a delicate and time-consuming task. First the sample is sawn or cleaved into a 3mm x 3mm square of ~500μm thickness. It is then manually thinned to approximately 5μm with silicon carbide grinding paper. To eliminate surface irregularities as a result of the grinding process, the sample is polished with alumina emulsion to a mirror-

like finish. The final nanometer thickness is achieved with ion milling, a process that slowly removes material by ion bombardment.

Using plan-view TEM micrographs, the in-plane grain sizes of the various polySi films are estimated with both a line technique [37] and an area technique [38]. The line technique involves drawing a line on a TEM image and counting the number of grains it crosses. The grain size d is then estimated with the following relationship:

$$d = 1.5\frac{L}{mn}, \tag{3.2}$$

where L is the length of the line, m is the magnification of the image, and n is the number of grains. The area technique is based on a similar principle; it involves counting the number of grains enclosed within a known area:

$$d = \frac{1}{m}\sqrt{\frac{A}{n}}, \tag{3.3}$$

where A is the area. For each sample, both methods are repeated several times to obtain a mean grain size value.

Cross-sectional TEM micrographs are used to evaluate grain dimensions across the thickness of the film. They are also analyzed for grain structure and degree of material crystallinity. Furthermore, high-resolution images are taken to look for lattice imperfections such as intragrain defects.

3.3.3 X-ray Diffraction

Another method used to investigate the internal structure of polySi is x-ray diffraction which, like TEM, is also based on the ability to retrieve spatial information about an object from the manner it diffracts radiation. The probe beam in this case is x-ray, produced from the rapid deceleration of electrons of high kinetic energy.

X-rays impinging on the surface of a specimen are scattered by its different atomic planes. The essential condition for these scattered rays to constructively interfere to form a diffracted beam is given by the Bragg law:

$$n\lambda = 2d\sin\theta, \tag{3.4}$$

where λ is the wavelength of the x-ray, d is the spacing between the particular crystal planes under consideration, θ is the angle between the incident beam and these crystal planes, and n is called the order of reflection which takes on only integral values. The formulation of this diffraction condition is illustrated in Figure 3.3. Consider incident rays 1 and 2; they strike atoms A and B of different atomic planes and are scattered, represented by rays 1' and 2'. The difference in path lengths for rays 1A1' and 2B2' is

$$CB + BD = d \sin\theta + d \sin\theta . \qquad (3.5)$$

For the scattered beams 1' and 2' to be completely in phase and constructively interfere, $CB+BD$ must be either zero or some integral multiple of the wavelength. The resulting relationship is of course the Bragg law of Equation 3.4.

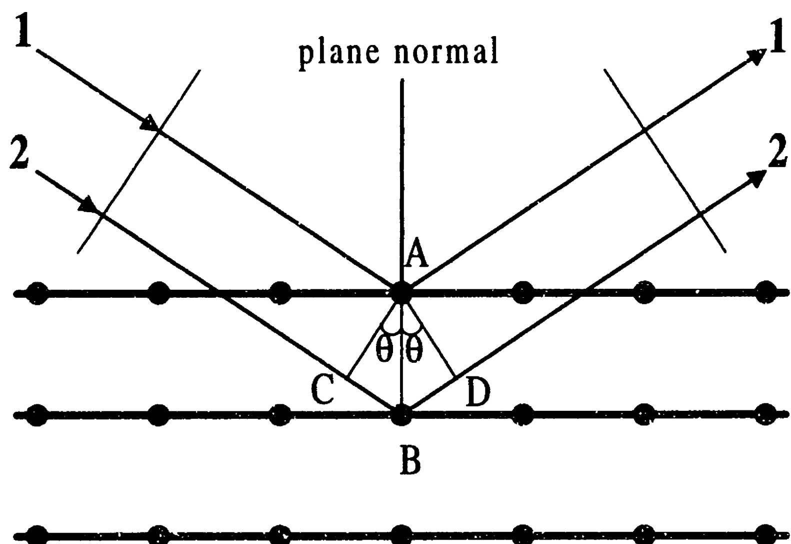

Figure 3.3: Diffraction of x-rays by a crystal. Incident rays 1 and 2 are scattered by atoms A and B, respectively; two of the scattered rays are denoted as 1' and 2'.

For x-ray diffractometry, by using x-rays of known wavelength λ and measuring the incident angle θ, one can determined the spacing d of the various planes in a crystal. By comparing the calculated d with the standard d of a perfect lattice, one can obtain valuable material information such as elastic macro-strain. Furthermore, micro-strain as a result of plastic deformation can also be detected with x-ray diffraction. In this case, the

lattice planes have been distorted in such a way that any interatomic spacing can vary from grain to grain or from one part of the grain to another. This non-uniform micro-strain causes broadening of the corresponding diffraction lines. Figure 3.4 compares the shape and position of a diffraction line for non-strained and strained samples.

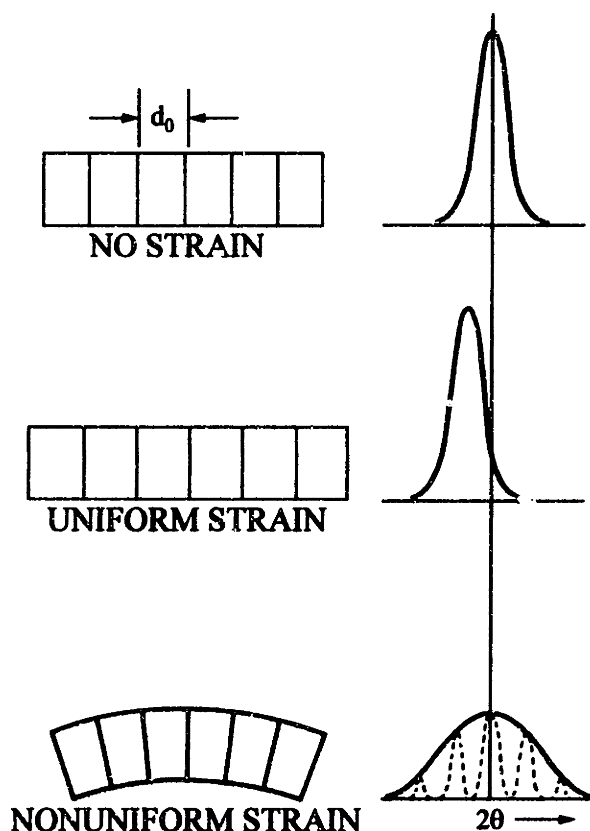

Figure 3.4: Effect of lattice strain on the position and shape of a diffraction peak [39].

X-ray diffraction can also furnish information about a material's degree of crystallinity. For a crystalline solid, the curve of scattered intensity vs. 2θ is almost zero everywhere except at angles where diffraction takes place. For an amorphous solid, on the other hand, the almost complete lack of periodicity results in a scattering curve showing nothing more than one or two broad maxima. These maxima represent the material's statistical preference for these interatomic distances. The diffraction spectra of crystalline and amorphous solids are compared in Figure 3.5. For a polycrystalline solid with amor-

phous regions, both sharp diffraction lines and broad bands are present in its spectrum. To determine this material's volume fraction of grains or degree of crystallinity, the relative integrated intensities of these lines and bands are compared.

Using x-ray diffractometry, various polySi films are analyzed for grain orientation, possible material strain, and degree of crystallinity. Since the polySi films are at most 1μm thick, a small x-ray incident angle is used to ensure that the beam does not penetrate to interact with the underlying oxide layer and give erroneous information.

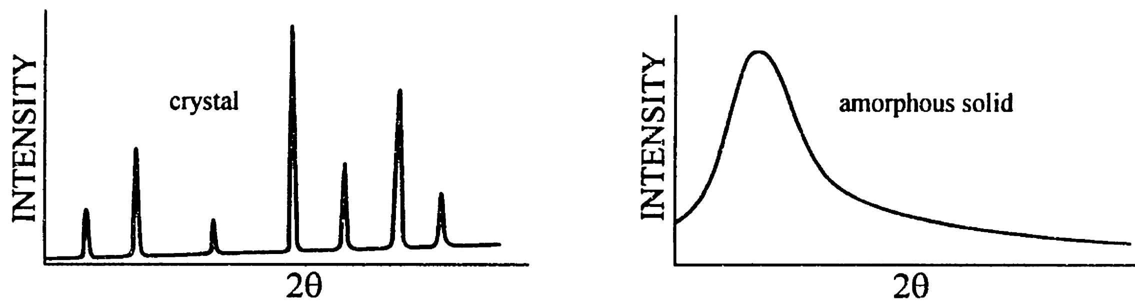

Figure 3.5: X-ray scattering characteristics of crystalline and amorphous solids [40].

3.3.4 Atomic Force Microscopy

The rms surface roughnesses of the polySi films, bottom oxide layer, and waveguide facets are measured using tapping-mode atomic force microscopy (AFM), a high resolution, three-dimensional surface topographic imaging technique. In tapping-mode AFM, a cantilever vibrating near resonance taps the sample while performing raster scans in the x-y plane parallel to the surface. Changes in the amplitude or phase of the cantilever motion as a result of topography are recorded by a sensing and feedback system operating in the z-direction. In this manner, high resolution surface scans are achieved.

In preparation for AFM imaging, the samples are cleaved and then cleaned with organic solvents such as TCA, acetone, and methanol. For measurement of polySi surfaces and waveguide facets, the samples are dipped in buffered oxide etch (7:1 NH_4F:HF) to remove any native oxide that may have accumulated. A Digital Instrument Nanoscope

III with a dimension 3000 stage is used for all analysis. The rms roughness value it provides is a measure of how much feature heights at different locations deviate from the average height. It is calculated with the equation:

$$roughness = \sqrt{\frac{\sum_{i}^{n}(Z_i - Z_{ave})^2}{N}}, \tag{3.6}$$

where Z_i is the feature height at location i, Z_{ave} is the average height, and N is the total number of locations sampled.

3.3.5 Secondary Ion Mass Spectrometry

Before and after each hydrogenation experiment, the concentration of hydrogen as a function of polySi film depth is determined using dynamic secondary ion mass spectrometry (dynamic SIMS). Both waveguides and unpatterned samples are studied to also investigate the effects of a top oxide layer on hydrogen incorporation.

In dynamic SIMS analysis, a high flux of energetic primary particles, in this case $\sim 10^{15}$ argon ions $cm^{-2}sec^{-1}$, is directed at the sample. The result is high-yield ionization and emission of atomic species near the surface. These secondary ions are then collected and analyzed using a quadrupole mass spectrometer . The continual bombardment with the primary beam erodes the material surface very rapidly; therefore, it is possible to monitor changes of elemental composition with depth.

3.3.6 Determination of the Index of Refraction

One of the most important optical parameters of any waveguiding material is its index of refraction. For this thesis, it is estimated to be ~3.5 at λ=1.55μm for all polySi films. This value varies, however, with structural changes such as grain size, grain structure, and degree of crystallinity. To determine the exact refractive index values for the different polySi fabricated, two techniques are considered: spectrophotometry and ellipsometry.

According to a review article by Lubberts et. al. [41], a polysilicon film's refractive index can be determined knowing both the film's extinction coefficient and the transmission behavior of a two layer system consisting of this film on a silica substrate. As a re-

sult, silicon films are deposited at 560°C and 625°C directly onto two silica wafers. After the standard crystallization anneal, these films' transmission spectra are measured using a Cary 5E spectrophotometer. To determine the films' extinction coefficients, photothermal deflection spectroscopy (PDS) is used. In this technique, the above samples are submerged in a liquidous solution whose refractive index has a strong and well-known temperature dependence. A beam of the desired wavelength is dirccted at the sample's surface. As this beam is being absorbed by the polySi layer, the film heats up and causes a temperature rise in the liquidous medium immediately above it. This temperature change in turn results in a change in the liquid's refractive index. A probe beam incident on the sample at a very shallow angle travels through this medium and is deflected. Its deflection behavior varies with the medium's change in index and therefore can be used to calculate the polySi films' absorption.

Ellipsometry is also considered for index determination. In an ellipsometer a monochromatic, linearly polarized, collimated light beam is incident on the material of interest at an oblique angle of incidence. The reflected beam is collected and analyzed to determine the complex number $\rho=r_p/r_s$, where r_p and r_s are the complex Fresnel reflection coefficients at the interface between two optically distinguishable media. The Fresnel coefficients are functions of the angle of incidence, the extinction coefficients and refractive indices of the different layers in the sample, and the various layer thicknesses. As a result, knowledge of the sample's extinction coefficients and layer thicknesses allows determination of the refractive index under consideration.

3.4 Bending Loss Determination

Due to its large refractive index contrast, the Si/SiO_2 strip waveguide structure offers excellent optical confinement. Simulation shows that it can have bending radii on the order of micrometers without suffering noticeable loss [11]. To experimentally verify this theoretical conclusion and also demonstrate the functionality of multiple levels of interconnection, out-of plane micro-bends are fabricated. The process sequence is relatively straightforward. It uses a wafer of completed 560 waveguides as the starting material, upon which another layer of SiO_2 is deposited to ensure absolutely no field penetration. Then

an additional 0.2μm thick amorphous silicon film is deposited at 560°C, followed by the standard crystallization anneal of 16 hours at 600°C. Due to the presence of the underlying waveguides, this silicon film is not flat and has a rippled appearance. Using the same mask, this second silicon layer is patterned into waveguides perpendicular to those underneath. Finally, a blanket oxide is deposited to complete the cladding. A schematic of the resulting two-level structure is illustrated in Figure 3.6.

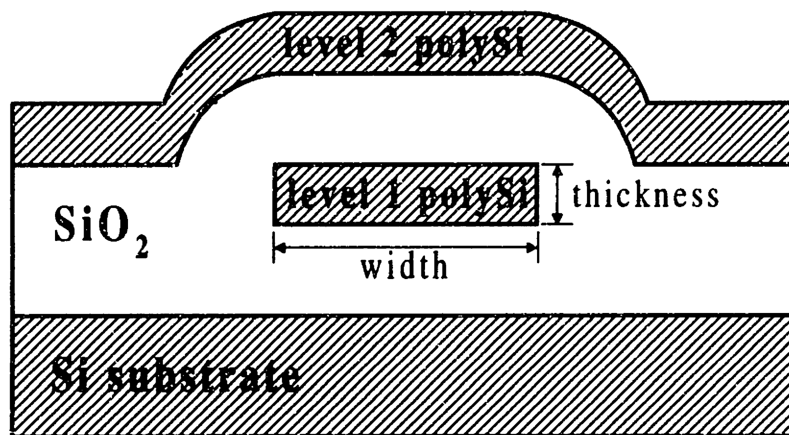

Figure 3.6: Schematic of the two-level waveguide structure.

The transmission loss of these "wavy" structures is determined using the same procedure described previously. First each waveguide's two facets are polished to a mirror-like finish, then its loss is measured with the setup shown in Figure 3.2. 20 such waveguides are analyzed to obtain an average loss value. By also measuring straight waveguides of the same length, the two loss values are compared to determine the contribution from bends.

Chapter 4

Results

4.1 Cutback Power Loss Measurement

Transmission loss is determined in dB/cm for all polySi waveguides using cutback analysis, a technique that factors out extrinsic effects such as coupling losses and measurement setup variations. Two wavelengths of operation are investigated: 1.55μm and 1.32μm. The loss values are displayed in the following tables. Error bars are obtained from measurements of either 40 or 60 samples, 20 at each length. Loss determined with 60 samples are indicated with "*".

For λ=1.55μm, the transmission losses are organized in Tables 4.1 through 4.6 according to the different experiments performed. Values for both 0.2μm and 1μm thick waveguides are included. The thinner guides are identified with the label "0.2μm".

Four deposition temperatures are investigated to fabricate silicon films with different grain sizes and grain structures. The transmission losses of the resulting materials are shown in Table 4.1. Note that all crystalline films presented here are annealed with the standard conditions of 16 hours at 600°C. The 560-amorphous sample has very high loss at 142dB/cm. After crystallization, its transmission improves dramatically and a loss of only 37dB/cm is measured. This value is also much better than that of the 625 sample, which shows a loss of 77dB/cm. Unfortunately, the 700°C fine-grain polySi has very high loss at 164dB/cm. The 470°C disilane waveguides are even worse, they do not even yield enough output power to allow loss determination; it is recorded as having "high loss".

Deposition Temperature (°C)	Transmission Loss (dB/cm)
560-amorphous	142±5
560	37±6
625	77±5
0.2μm-470	164±7
0.2μm-700	high loss

Table 4.1: Cutback loss as a function of deposition temperature.

To determine the annealing conditions needed to completely crystallize the standard 560 films, different thermal treatments are examined. Table 4.2 displays the loss values of these experiments. For waveguides annealed in the low oxygen partial pressure ambient, neither the long-term nor high-temperature treatments improves optical transmission when compared to the standard anneal. In fact, the 1100°C treatment yields such high loss that no output power is detected. Another very interesting observation is that the reduction in waveguide thickness from 1μm to 0.2μm significantly enhances transmission, allowing a loss reduction in the standard annealed sample from 37dB/cm to 25dB/cm. This result can have important implications for future waveguide development because small dimensions are needed for single-mode operation. For waveguides annealed in the pure nitrogen ambient, transmission losses are lower compared to those annealed with the O_2 furnace leak. This effect is most evident for samples treated at 1100°C, where losses are 11dB/cm verses one that is extremely high.

Annealing Sequence	Loss (dB/cm) with O_2 leak -	Loss (dB/cm) - in pure N_2 -
16 hr @ 600°C - standard	37±6	...
16 hr @ 600°C (0.2μm)	25±3	20±1.7*
16 hr @ 600°C / 100 hr @ 600°C	52±1.5*	...
16 hr @ 600°C / 16 hr @1100°C (0.2μm)	high loss	11±2*

Table 4.2: Cutback loss as a function of annealing conditions.

* Loss determined by measuring 60 samples.

The transmission behavior of waveguides having different surface roughnesses are presented in Table 4.3. Notice that the 625 sample has the highest loss of 77dB/cm. After it is planarized with CMP, its loss is significantly reduced to 37dB/cm, comparable to that of the 560 sample.

Waveguide Type	Transmission Loss (dB/cm)
560	37±6
625	77±5
625CMP	37±5*

Table 4.3: Cutback losses before and after chemical mechanical polish.

Different hydrogenation steps are investigated as means to reduce the effects of dangling bond defects and thus, transmission loss. Table 4.4 compares the effectiveness of some of these techniques for 1μm-thick samples annealed in the low oxygen partial pressure ambient. Table 4.5 contains results for 0.2μm-thick samples annealed in pure nitrogen. The losses of 560, 625, 625CMP, and 0.2μm-560 samples are provided for comparison. Notice that the process of ECR passivation yields the best results, allowing loss reductions of approximately 30dB/cm for the 625 waveguides and 20dB/cm for the 560 and 625CMP waveguides. PII is less effective, where only a 7dB/cm decrease is observed. The process of UST, on the other hand, seems to have completely reversed the positive impact of ECR hydrogenation; it brings loss back to approximately 39dB/cm. Remote-source ECR is used to passivate samples annealed in pure nitrogen. Because these materials have low dangling bond densities and good transmission to begin with, the observed decrease in loss as a result of hydrogenation is not as impressive compared to ECR samples. Nonetheless, this remote-source technique, together with the high temperature crystallization treatment, yields the lowest reported polySi waveguide transmission loss of 9dB/cm.

* Loss determined by measuring 60 samples.

Waveguide Types (annealed with O_2 leak)	Transmission Loss (dB/cm)	Waveguide Types (annealed with O_2 leak)	Transmission Loss (dB/cm)
625	77±5	560	37±6
625ECR	47±4	560ECR	15±2.7
625CMP	37±5*	560ECR+UST	39±2.6*
625CMP+ECR	16±1.5	560PII	28±2*

Table 4.4: Cutback losses for waveguides with different hydrogenation methods.

Waveguide Types (annealed in pure N_2)	Loss (dB/cm)
0.2μm-560	20±1.7*
0.2μm-560 (R-ECR)	15±2
0.2μm-560 / 1100°C	11±2*
0.2μm-560 / 1100°C (R-ECR)	9±1.5*

Table 4.5: Cutback losses for waveguides hydrogenated in remote-ECR plasma.

Table 4.6 compares the loss values of 0.2μm-560 waveguides patterned with different etch chemistries. Even though the HBr/Cl_2 anisotropic combination yields much better sidewall quality than $SF_6/O_2/He$, little or no difference in transmission loss is observed. This result implies that scattering due to sidewall roughness is not an important contributor to loss.

Waveguide Type	Transmission Loss
0.2μm-560(O_2) - $SF_6/O_2/He$	25±3
0.2μm-560(O_2) - HBr/Cl_2	26±2.4

Table 4.6: Cutback losses for 0.2μm-560 waveguides patterned with different etch chemistries.

For λ=1.32μm, only a subset of the polySi waveguides are measured for transmission loss. In the following table, these values are compared to those for λ=1.55μm. Notice that for the standard annealed samples, loss is approximately 20dB/cm higher at

---

* Loss determined by measuring 60 samples.

1.32μm than at 1.55μm. This loss difference is significantly reduced, however, when the sample is either subjected to the 1100°C anneal or the ECR hydrogenation.

Waveguide Type	Waveguide Thickness	Transmission Loss (λ=1.55μm)	Transmission Loss (λ=1.32μm)
560(O_2)	0.2μm	26±2*	44±2
560 (N_2)	0.2μm	20±2*	42±3
560 (1100°C N_2)	0.2μm	11±2*	16±3
560ECR	1μm	15±2.7	13±2.6

Table 4.7: Cutback losses at λ=1.55μm and λ=1.32μm.

4.2 Transmission Electron Microscopy

TEM is used to visually examine the different polySi films for grain structure, grain size, degree of crystallinity, and possible intragrain defects. Assuming hydrogenation and etch chemistry have no effect on material structure, microscopy is performed only on samples that have been fabricated with different deposition or annealing conditions. The doped polySi is not examined because it is believed that severe processing conditions have resulted in macroscopic structural defects♦ .

First the standard 1μm 625 and 560 samples (annealed with the oxygen furnace leak) are compared. Figure 4.1 shows the cross-sectional TEM (XTEM) images of these two materials, which have in-plane grain sizes of 0.18 and 0.35μm, respectively. Notice that the 625 polySi, due to surface nucleation at the on-set of deposition, has small, columnar grains that traverse the thickness of the film. The 560 polySi is structurally different, it has larger, non-textured grains as the result of bulk nucleation and thermal grain growth. Also evident from these XTEM micrographs is that the films are not completely crystalline. Not only do they lack distinct grain boundaries, they contain regions of structural disorder indicative of amorphous material.

---

* Loss determined by measuring 60 samples.

♦ See the sub-section on atomic force microscopy.

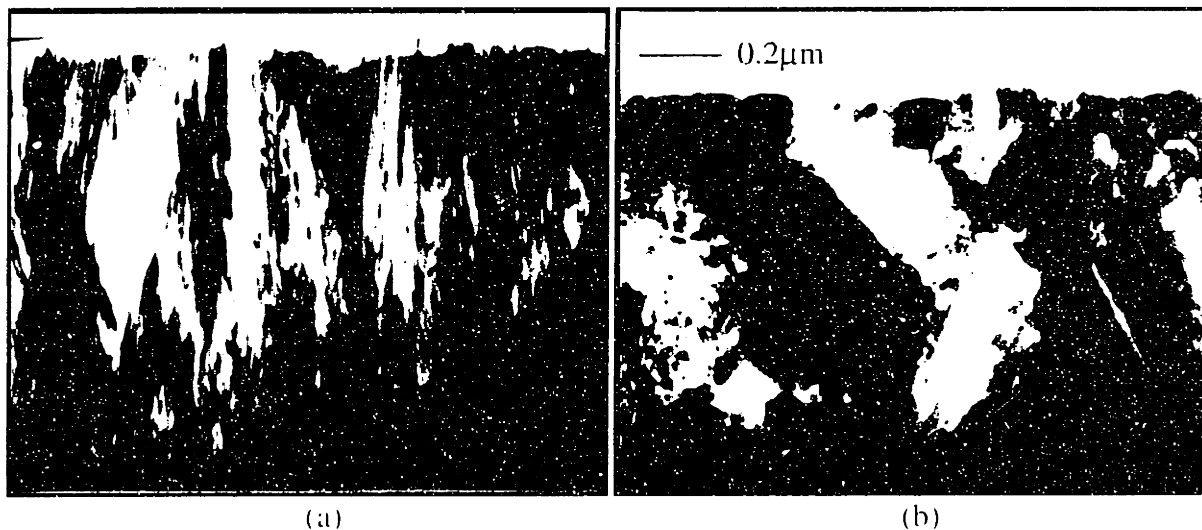

Figure 4.1: XTEM images of a) 625 polySi and b) 560polySi, both annealed with an O_2 furnace leak.

To investigate the finer structural features of polySi, the 560 film is also examined with high resolution TEM (see Figure 4.2). The areas in the lower corners are regions of the bottom SiO_2 layer. Because they are amorphous, they do not exhibit the crystalline order shown by the polySi grains. Notice the directional changes of lattice planes in the central region of the micrograph. Unlike grain boundaries, these features retain their crystalline order; they are intragrain defects known as twin boundaries. Dislocations are also found in these polySi films.

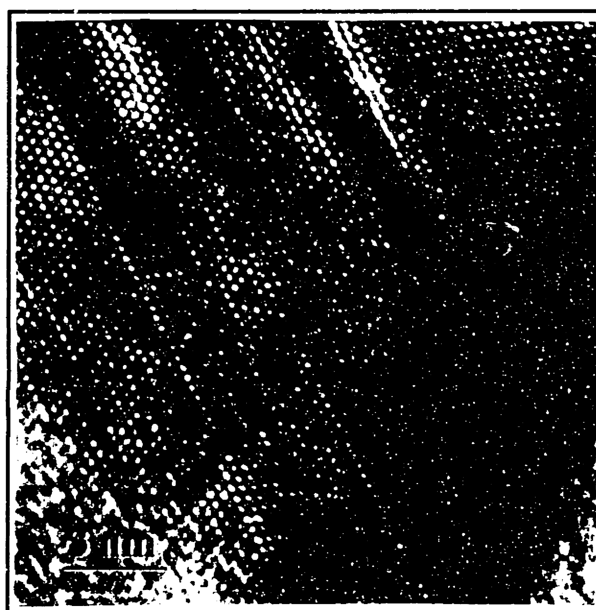

Figure 4.2: High resolution TEM image of 560(O_2) polySi.

The XTEM micrograph of the 560 sample annealed for an additional 100 hours at 600°C is shown in Figure 4.3. Even though it does not substantially change the grain structure, this prolonged heat treatment is effective in crystallizing some of the residual amorphous silicon, as evident from the slightly more distinct grain boundaries. Nonetheless, some amorphous regions remain and no appreciable reduction in intragrain defects is observed. Furthermore, the average grain size stays relatively unchanged at 0.32μm.

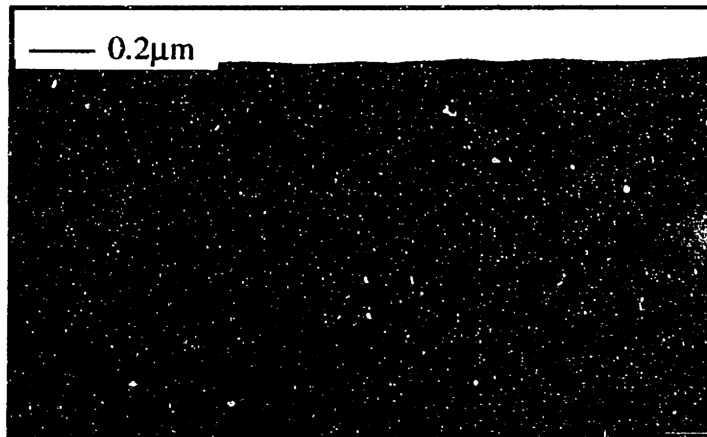

Figure 4.3: XTEM image of 560 polySi, annealed for an additional 100 hours at 600°C (O_2).

The high temperature anneal at 1100°C, on the other hand, shows very dramatic improvement in film crystallinity (see Figure 4.4). There is no evidence of the type of structural disorder associated with amorphous silicon, and the grains and grain boundaries are much more defined. Furthermore, the average grain size increases to more than 0.5μm. The most surprising result of this experiment, however, is the appearance of a thin amorphous layer on top of the polycrystalline film. Since no SiO_2 is deposited after silicon deposition and the polySi film thickness is less than the expected 1μm, the only explanation is that the silicon surface has oxidized during thermal crystallization. After examination of the annealing furnace, an oxygen leak is indeed detected.

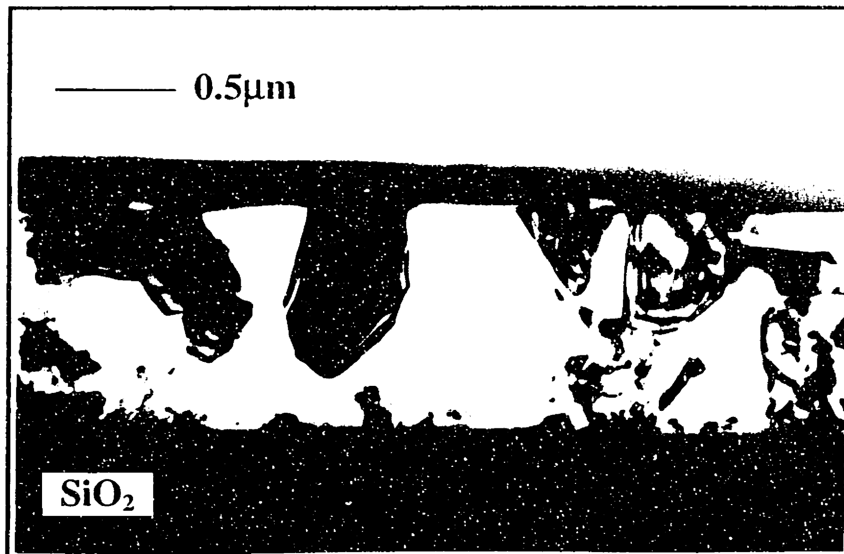

Figure 4.4: XTEM image of 560 polySi, annealed for an additional 16 hours at 1100°C (O_2).

To determine the impact of annealing ambient on waveguide transmission, 0.2μm-560 films are deposited and crystallized in a pure N_2 ambient with both the standard 600°C anneal and high temperature 1100°C anneal. Figure 4.5 compares XTEM images of 0.2μm-560(O_2) and 0.2μm-560(N_2) standard annealed samples. The reduction in film thickness results in columnar grain structure for both materials. It also restricts grain growth in the plane of the films, allowing average grain sizes of only 0.2μm. The most noticeable difference between the two samples is their degree of crystallinity; the pure N_2 annealing ambient undeniably gives more distinct grains and grain boundaries.

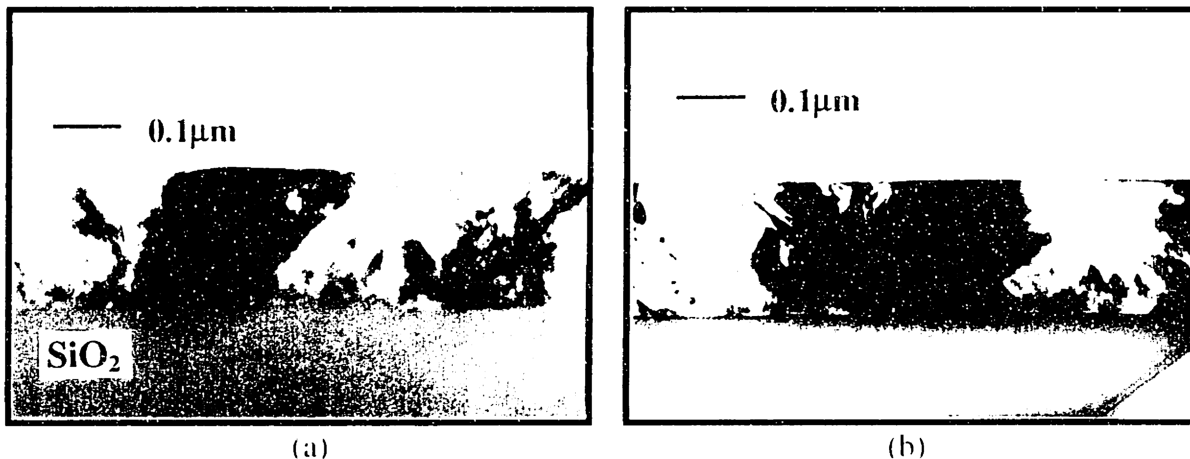

Figure 4.5: XTEM images of 0.2μm-560 polySi, annealed for 16 hours at 600°C a) with an O_2 furnace leak and b) in a pure N_2 ambient.

Figure 4.6 shows the XTEM image of the 0.2μm-560(N_2) sample annealed at 1100°C. Like the standard N_2 annealed polySi of Figure 4.5, this film also has columnar grain structure. However, an increase in grain size to 0.28μm indicates subsequent lateral grain growth despite the thickness restriction. Furthermore, the grains in this material are more crystalline and have smoother boundaries. Even though intragrain defects are still present, as far as one can tell their concentration is slightly reduced. TEM is not performed for the 1100°C annealed 0.2μm-560(O_2) sample because most of the polySi is expected to be oxidized.

Figure 4.6: XTEM images of 0.2μm-560 polySi, annealed for an additional 16 hours at 1100°C (N_2).

The 470°C disilane polySi and 700°C fine grain polySi are also analyzed with TEM. As evident from its plan-view image in Figure 4.7a, the disilane film does not appear very crystalline even after the standard anneal of 16 hours at 600°C. Although the barely distinguishable grain boundaries indicate grain formation, most of the intragrain material appears amorphous. Its average grain size of 0.66μm is also smaller than expected. The fine grain silicon is much better in terms of crystallinity, but regions of amorphous silicon are also present(see Figure 4.7b). The mean grain size is approximately 0.1μm.

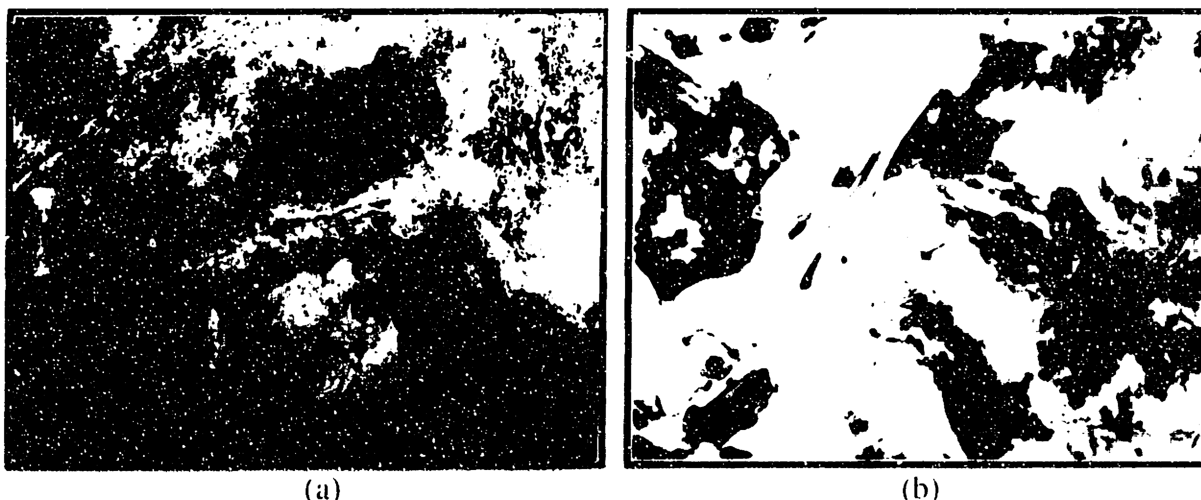

Figure 4.7: Plan-view TEM images of a) 470°C disilane polySi and b) 700°C fine grain polySi.

4.3 X-ray Diffraction

X-ray diffraction is used to determine the degree of crystallinity, dominant grain orientations, and film stress of different polySi films. Figure 4.8 compares the diffraction curves of the standard annealed 625(O_2) and 560(O_2) samples. Notice the broad peak near $2\theta=18°$ for the 560 material, it indicates the presence of amorphous silicon in this film. The same peak is absent for the 625 sample, declaring it as completely crystalline. Various sharp peaks are present in the diffraction curves, they identify the preferred grain orientations. For 625 polySi there are only two dominant peaks: (220) and (400); this is expected since its XTEM image shows largely columnar grain structure. The width of the (400) peak is rather broad, it is probably due to non-uniform stress. The 560 polySi is semi-crystalline, the only noticeable orientation is (111).

Careful examination of the curves also shows a shift of all diffraction peaks to the right of the ideal diffraction locations, a clear signature of uniform material strain. For the 625 polySi this shift translates to a strain of -0.34%. For 560 polySi the shift translates to a strain of -0.36%. To calculate the in-plane film stress from these strain values, the following relationship is used:

$$\sigma = -\frac{E}{\nu}\left(\frac{d_n - d_o}{d_o}\right), \tag{4.1}$$

where σ is the film stress, E is Young's modulus, ν is Poisson's ratio, d_o is the lattice plane spacing in the absence of stress, and d_n is the measured plane spacing. The stress is tensile and is found to be 0.53GPa for the 625 polySi and 0.57GPa for the 560 polySi.

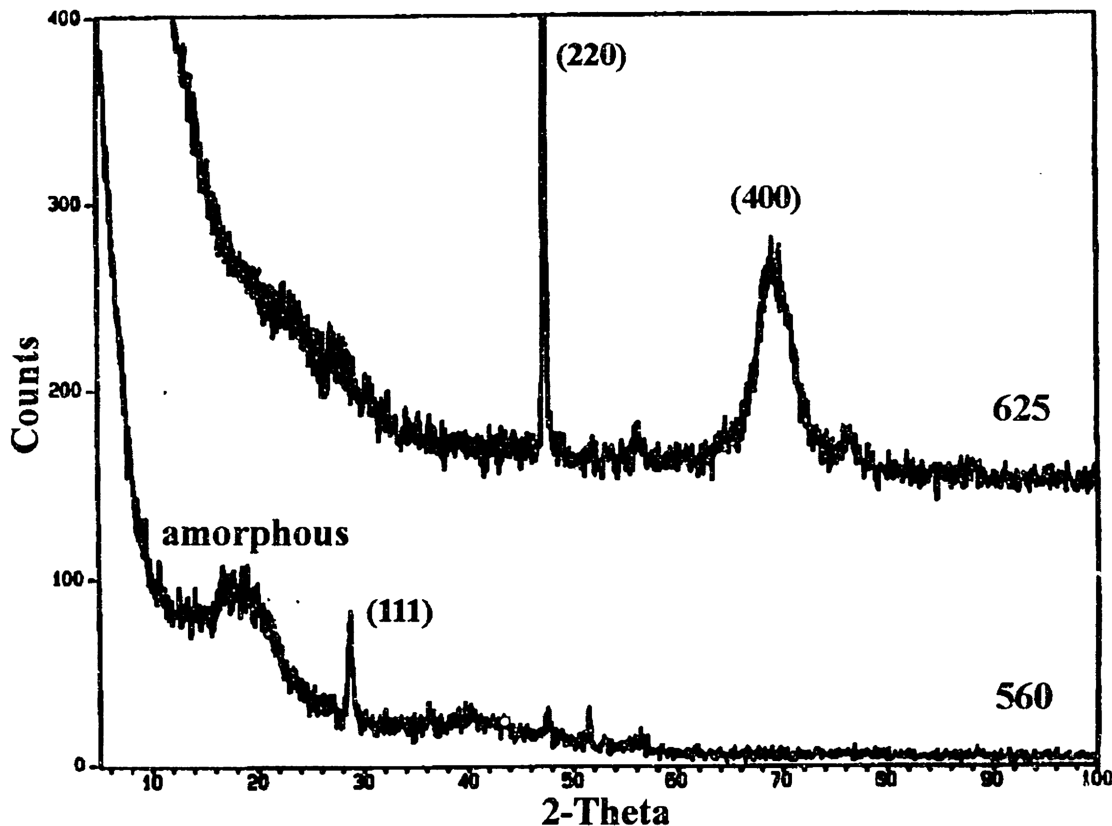

Figure 4.8: X-ray diffraction curves for standard annealed 625(O_2) and 560(O_2). The broad peaks near 2θ=30° indicate the presence of amorphous silicon, and the sharp peaks identify the preferred grain orientations.

The 560 sample annealed for an additional 100 hours at 600°C is also analyzed with X-ray diffraction. Its curve is compared to that of the standard 560 polySi in Figure 4.9. The most noticeable difference between these two materials is a reduction in the intensity of the amorphous peak after further anneal. As a result of this increase in crystal-

linity, other dominant grain orientations are also detected. They are (220), (311), (400), (331), (422), and (511).

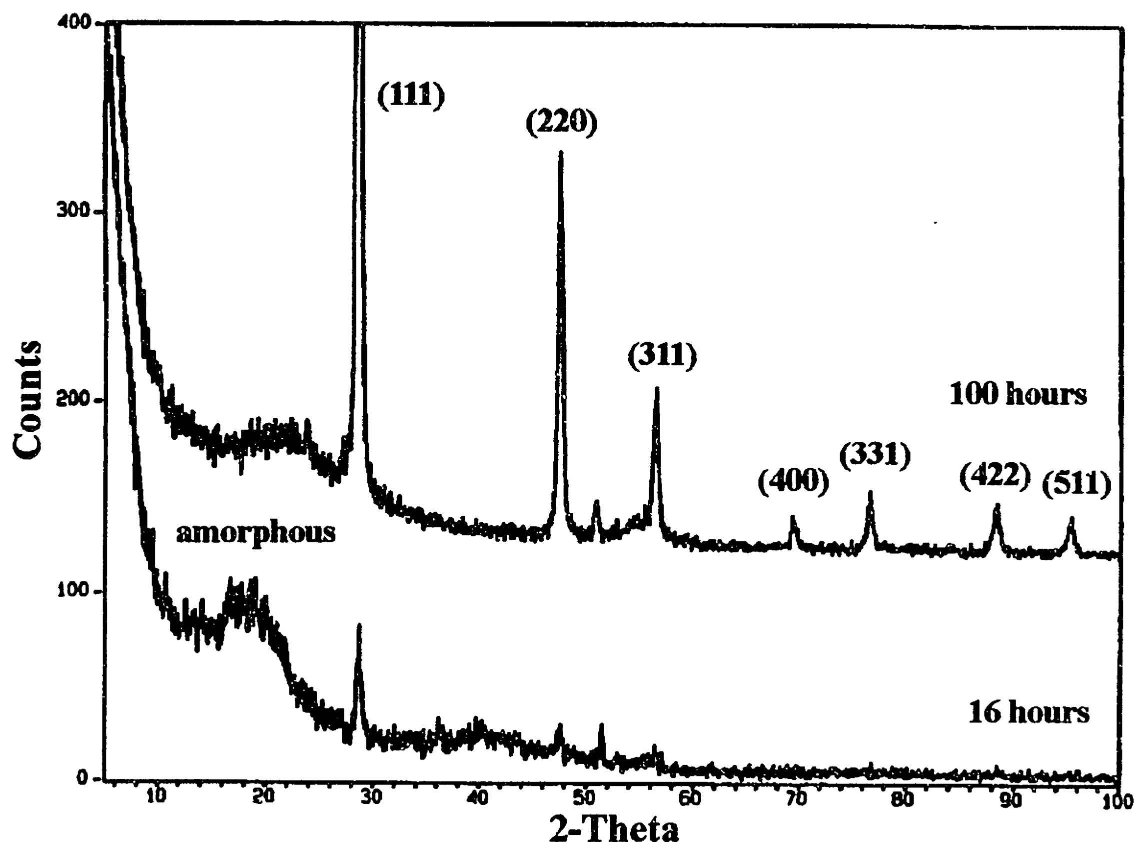

Figure 4.9: X-ray diffraction curves for $560(O_2)$ and $560/100°C(O_2)$.

To determine how different annealing gases affect the silicon film's material structure and amorphous content, Figure 4.10 compares the diffraction curves of the 0.2μm-$560(O_2)$ and 0.2μm-$560(N_2)$ standard annealed samples. The difference is clear: the nitrogen-annealed material is more crystalline with a much less prominent amorphous peak. This conclusion is in agreement with that drawn with TEM imaging, which shows that the presence of the small oxygen partial pressure resulted in less distinct grains and boundaries. Otherwise, the two samples are similar in terms of preferred grain orientation and film stress.

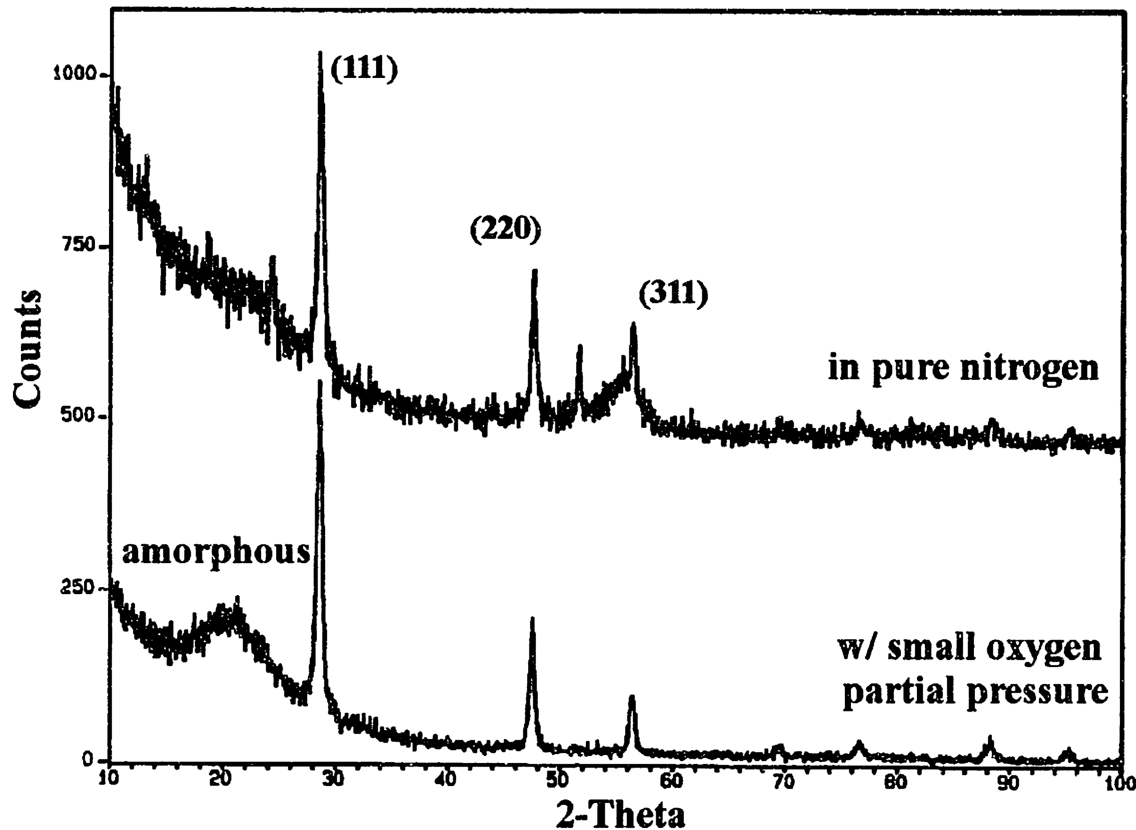

Figure 4.10: X-ray diffraction curves of the 0.2μm-560(O_2) and 0.2μm-560(N_2) standard annealed samples.

The x-ray diffraction result of the 0.2μm-560(N_2) film annealed at 1100°C is shown in Figure 4.11. This curve looks similar to that of the 0.2μm-560(N_2) sample prior to this high temperature step (see Figure 4.10). These two materials have the same dominant orientations, but the additional anneal yields a slightly more crystalline film and a higher percentage of (111) grains. Again, these results agree with those of TEM imaging, which also show a slight improvement in crystallinity as a result of the 1100°C treatment. X-ray diffraction is not performed to analyze the disilane and fine grain polySi because they are found to have exceptionally high loss and non-ideal material structure.

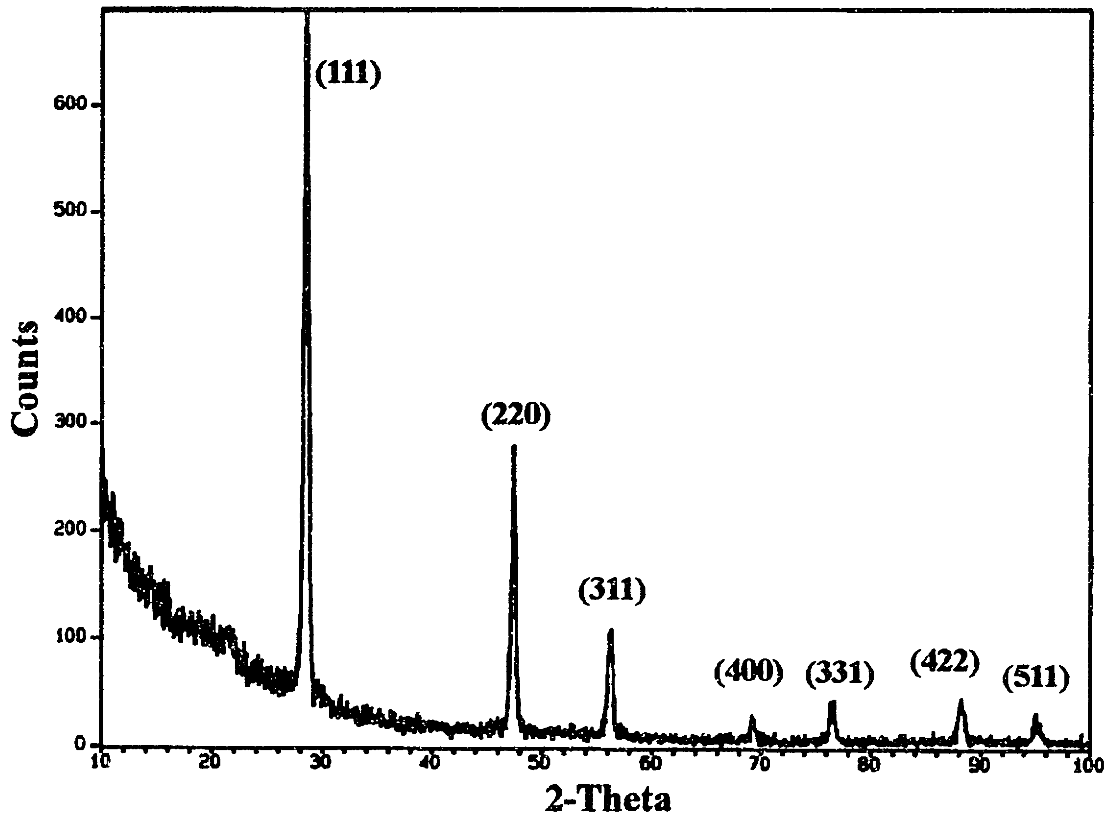

Figure 4.11: X-ray diffraction curve of the 0.2μm-560(N_2) film annealed at 1100°C.

4.4 Atomic Force Microscopy

AFM is used to determine the rms surface roughness of the different polySi films, the bottom oxide cladding, polished waveguide facets, and waveguide sidewalls. Table 4.8 displays some of these measured values.

Sample	rms Roughness (nm)
625	18-20
625CMP	4-5
560-amorphous	2-3
560	3-4
560/100 hours	3-4
560/1100°C(O_2)	10-11
560/1100°C(N_2)	unsuccessful
Doped polySi	47-50
700°C (Fine Grain)	4-5
470°C (Disilane)	2-3
Bottom Oxide	1-2
Waveguide Facet	0.3-2
Waveguide Sidewall	unsuccessful

Table 4.8: rms surface roughness measured with AFM.

The 625 film has the roughest surface of all the polySi investigated, but after CMP its 20nm rms value is reduced to approximately 4nm. Figure 4.12 and Figure 4.13 show the three-dimensional AFM images of these 625 and 625CMP samples, respectively. The crystallized 560 film is relatively smooth (see Figure 4.14); even the additional heat treatment of 100 hours does not appear to have affected its surface topography. The impact of the high temperature anneal is more dramatic, a 10nm rms value is found for the sample annealed with the oxygen furnace leak. This increase in roughness is most likely the result of secondary grain growth and preferential oxidation of certain crystallographic orientations. Unfortunately, the same sample annealed in pure nitrogen cannot be measured because an oxide layer must be grown or deposited on top of the wafer to prevent sublimation of silicon at 1100°C. AFM is performed for other samples annealed in pure nitrogen or after ECR hydrogenation; however, no noticeable change in surface topography is observed.

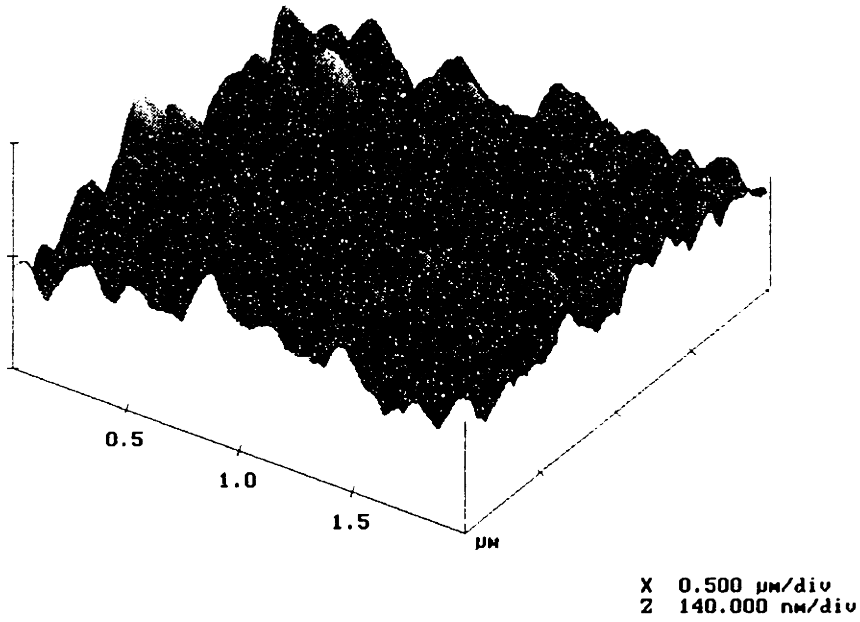

Figure 4.12: Three-dimensional AFM plot of 625 polySi film surface, whose rms roughness is ~20nm.

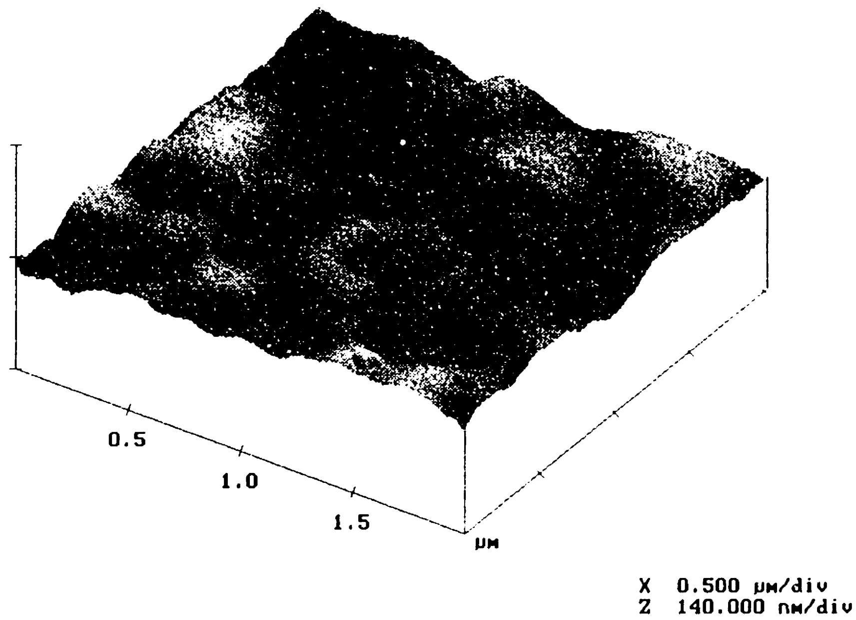

Figure 4.13: Three-dimensional AFM plot of 625 polySi film surface after CMP, which has an rms roughness of ~5nm.

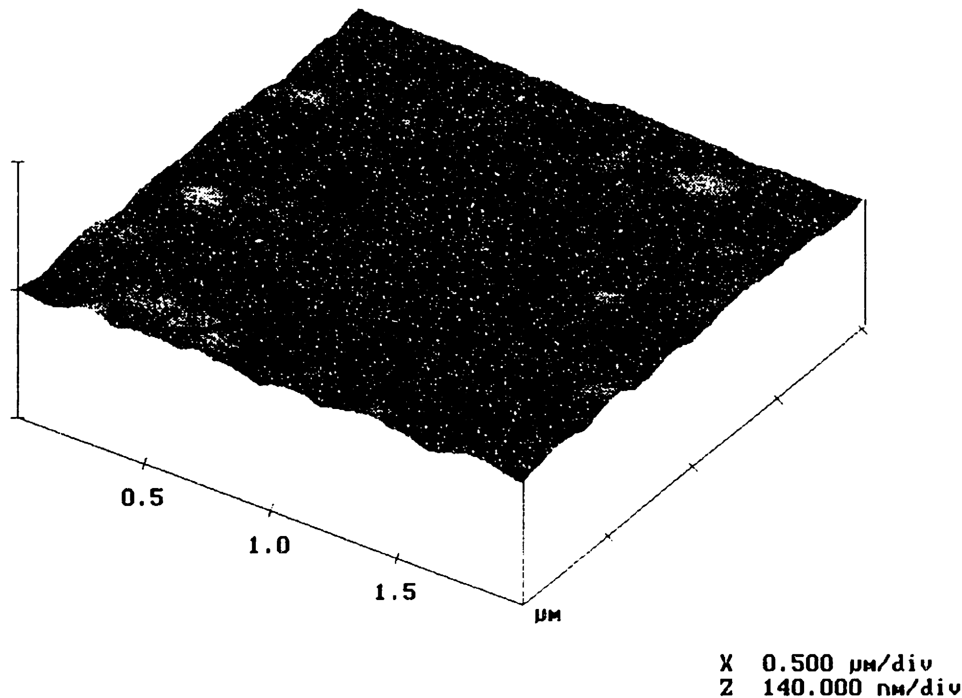

Figure 4.14: Three-dimensional AFM plot of 560 polySi film surface, whose rms roughness is ~4nm.

The doped polySi is found to have an rms roughness of 50nm (see Figure 4.15). Its surface is then examined with an optical microscope. Visible even at low magnifications are voids, cracks, and disconnects, most likely the result of processing related surface damage. The AFM value, therefore, is not representative of this material's true roughness, but rather of these macroscopic features.

Fine-grain and disilane films, on the other hand, have relatively smooth surfaces measuring 3-5nm. The bottom oxide cladding roughness is also examined to obtain topographic information about the bottom surface of the polySi films. It is found to be exceptionally smooth with an rms value of ~1nm. Additionally, the waveguide facets are examined and in most cases have roughness less than 1nm, validating the effectiveness of the current polishing technique. Unfortunately, due to various difficulties involved with positioning the samples on their sides, AFM of waveguide sidewalls is unsuccessful.

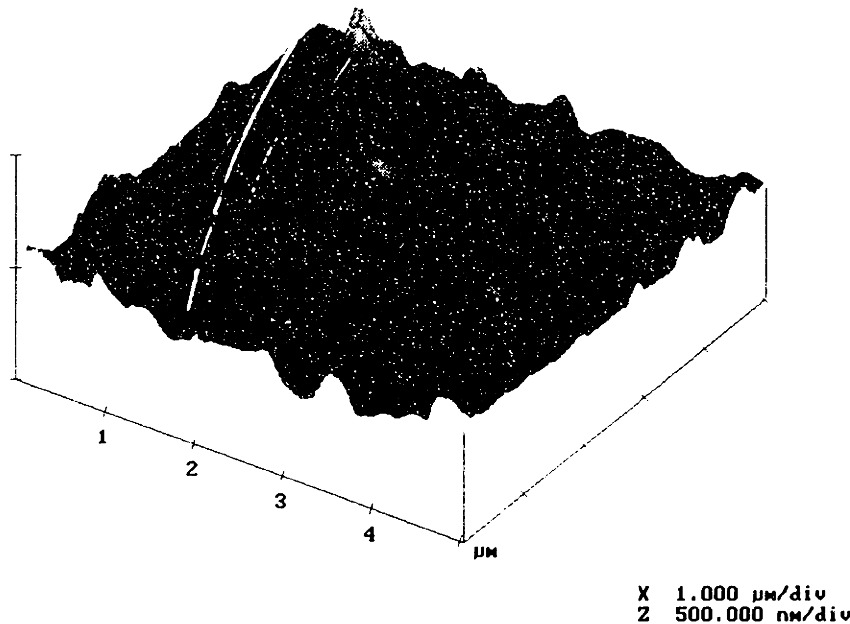

Figure 4.15: Three-dimensional AFM plot of doped polySi film, the large structural features are macroscopic voids, cracks, and disconnects.

4.5 Secondary Ion Mass Spectrometry

SIMS is used to acquire depth profiles of hydrogen in polySi before and after ECR passivation. All the hydrogenated samples are expected to display higher levels of hydrogen because in the ECR plasma, the ions penetrate the film surface and diffuse throughout the material. Figure 4.16 shows the profile of the 560 sample, which indicates a background hydrogen level of $6x10^{18}$ atoms/cm^3. It also shows the profile of the same sample after ECR hydrogenation; an enrichment of H to $3x10^{19}$ atoms/cm^3 is observed. H concentration is further increased to $1x10^{20}$ atoms/cm^3 for the 560ECR waveguides, which differ from the above passivated sample only in that they have a top SiO_2 layer. This oxide could have prevented hydrogen out-diffusion during ECR plasma cool-down, thereby maintaining a higher concentration in the polySi. Notice also that the levels of hydrogen are uniform across the thickness of the film; this is a good indication that ion diffusion was able to achieve steady state.

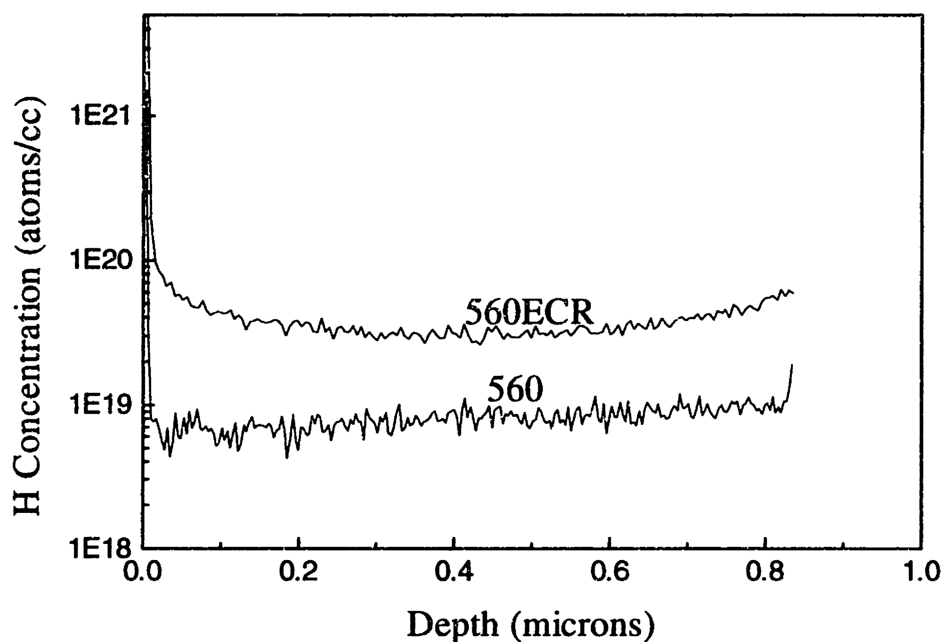

Figure 4.16: SIMS depth profiles of 560 and 560ECR. ECR passivation increased hydrogen concentration from $6x10^{18}$ to $3x10^{19}$ atoms/cm^3.

The 625 polySi has a higher background H level of $1x10^{19}$ atoms/cm^3, which surprisingly does not increase appreciably with ECR passivation (see Figure 4.17). The 625 sample is chemical-mechanically polished; as the SIMS data in Figure 4.18 indicates, this surface planarization technique actually reduces the H level to $4x10^{18}$ atoms/cm^3, similar to the 560 value. This 625CMP polySi is then hydrogenated in the ECR plasma; unlike the previous case, an H enrichment to $2x10^{19}$ atoms/cm^3 is measured. Table 4.9 summarizes the above SIMS results.

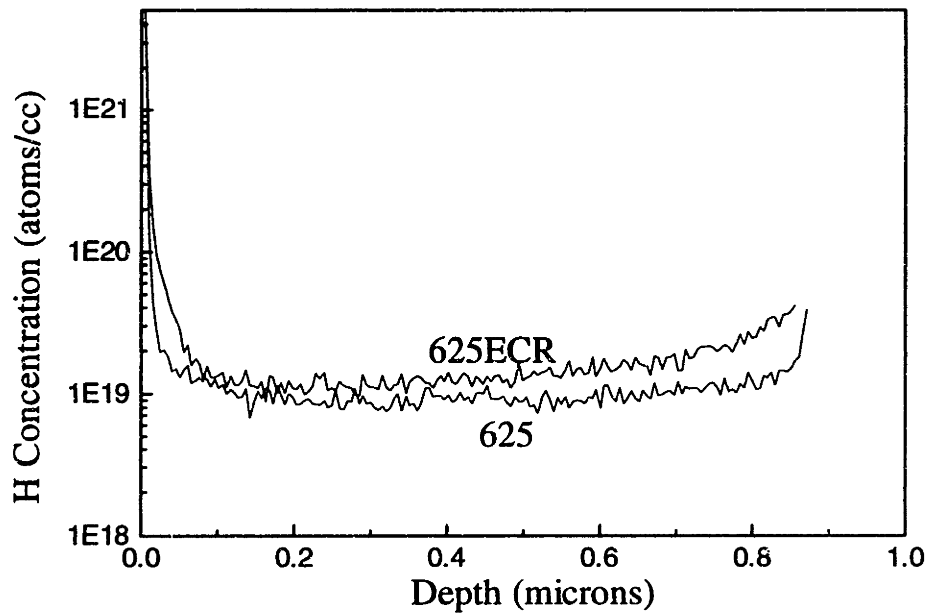

Figure 4.17: SIMS depth profiles of 625 and 625ECR. No appreciable increase in hydrogen level is observed.

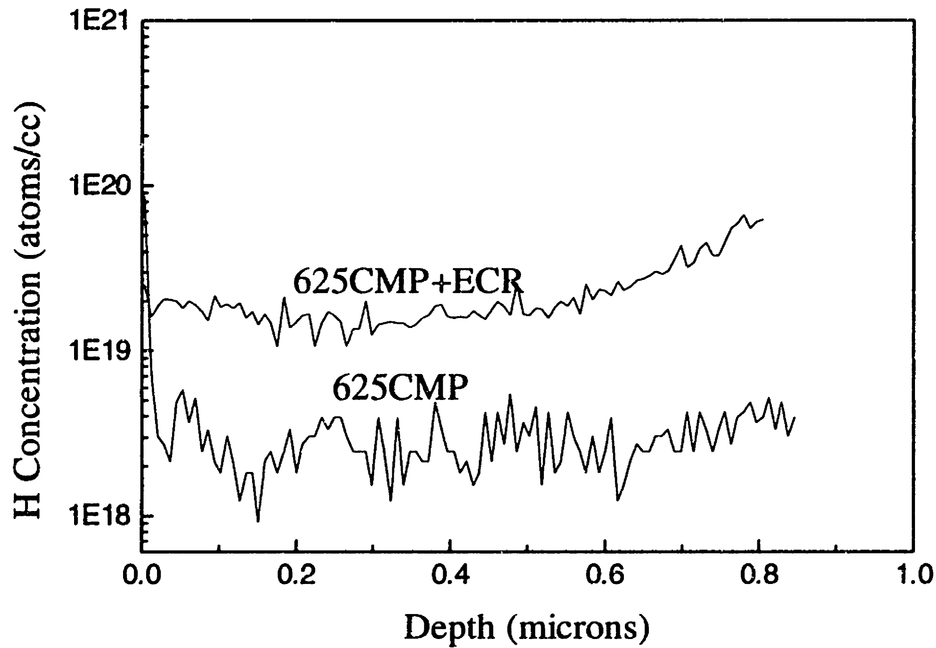

Figure 4.18: SIMS depth profiles of 625CMP and 625CMP+ECR. ECR passivation increased hydrogen concentration from 4×10^{18} to 2×10^{19} atoms/cm^3.

Material	atomic %	Material	atomic %
560	0.01	625	0.02
560ECR	0.06	625ECR	0.03
560ECR (W)	0.2	625CMP	0.01
...	...	625CMP+ECR	0.04

Table 4.9: Hydrogen concentration in polySi determined using SIMS.

4.6 Determination of Index of Refraction

The capabilities of spectrophotometry and ellipsometry are examined in this work in the hope of determining the refractive indices of the different polySi films. Because both of these approaches require knowledge of the extinction coefficients of the films, PDS is used to measure this material parameter. Unfortunately, the resulting data cannot be used due to flaws in the experiment. As a result, we have not been able to ascertain the refractive indices of the different polySi films fabricated.

4.7 Bending Loss Determination

Bending loss is determined for the 0.2μm-560 waveguides. First, cutback loss (dB/length) of these wavy structures is determined. By subtracting the loss of straight waveguides from this value, the contribution due to bends is obtained. This dB/length loss difference is then divided by the number of bends per length to obtain the loss per bend. The bend radii of these structures are estimated to be ~1μm, and loss per bend is found to be less than *1dB*. This remarkable result offers additional evidence that the polySi/SiO_2 material system is the preferred waveguide platform for on-chip applications.

Chapter 5

Discussion

This research effort has enabled a decrease in polySi waveguide transmission loss from 35dB/cm to 9dB/cm. Various process modifications contribute to this reduction, and even those that do not offer deeper understanding of the remaining challenges. In addition, important processing/material/performance inter-dependencies are uncovered from analysis of the experimental results. These issues and a detailed search for the mechanisms of the remaining 9dB/cm loss are discussed below.

5.1 Deposition Conditions

In the search for low-loss polySi as the waveguide core material, four film deposition temperatures are studied - 470°C, 560°C, 625°C, and 700°C. The resulting films vary in grain structure, grain size, surface topography, and transmission loss.

5.1.1 Grain structure and Grain Size

As XTEM images of the post-anneal samples show, the higher deposition temperatures of 625°C and 700°C result in columnar grain structure while the lower temperatures of 470°C and 560°C give more equi-axial structure. Since these columnar grains are the result of surface nucleation and equi-axial grains are the result of bulk nucleation, the 625°C and 700°C films are deposited as polySi while the 470°C and 560°C films are deposited as amorphous silicon. These findings agree with published results, which suggest that the transition deposition temperature between polySi and amorphous silicon is around 600°C.

The four types of polySi also differ with regards to the dimensions of their grains. Figure 5.1 shows that grain size increases with decreasing deposition temperature. It also illustrates the well-documented trend that recrystallized amorphous-to-polySi films generally have larger grains than films deposited as polySi.

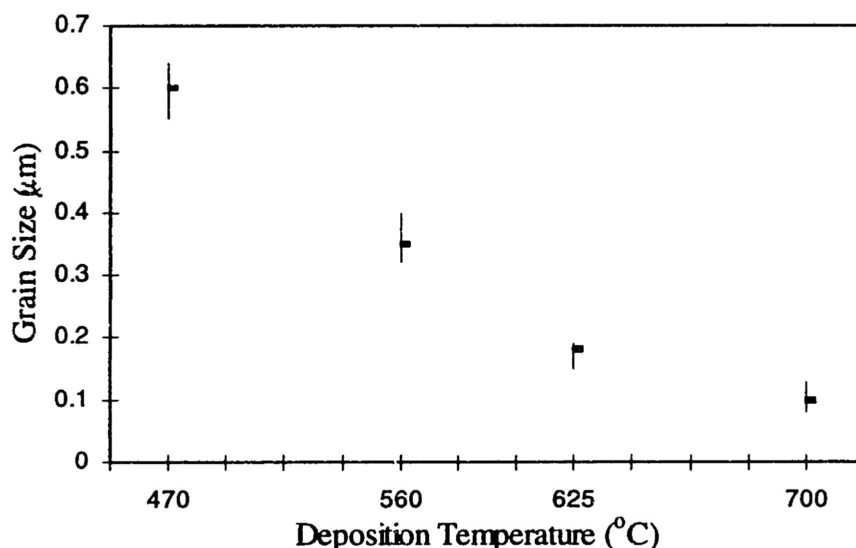

Figure 5.1: Temperature dependence of grain size.*

5.1.2 Surface Roughness and Transmission Loss

Out of the four materials, the 625 film has the highest rms roughness. As a result of tremendous surface scattering, this sample has a relatively high transmission loss of 77dB/cm. After CMP, its roughness is reduced to 4nm and its loss sees a corresponding decrease to 37dB/cm. The 560 structure also exhibits the same rms value of 4nm; and despite having different grain structure, it shows the same loss as well. According to Tien's analysis (Equation 2.11), the 4nm roughness of these films contributes only 2dB/cm to the total

* The grain sizes for 470 and 700 are determined from films with 0.2μm thickness.
The sizes for 560 and 625 are determined from films with 1μm thickness.

loss. Most of the residual 37dB/cm, therefore, is the result of sidewall scattering and/or bulk absorption and scattering.

The mechanism of surface scattering also cannot account for the high losses in the 700 fine-grain and 470 disilane polySi films because they both have very smooth surfaces. The fine-grain sample has a loss of 167dB/cm, higher than even that of amorphous silicon. This poor transmission is partly due to absorption by the film's numerous amorphous regions and large volume of grain boundaries (as a result of small grains). Also, the different refractive indices of amorphous silicon and crystalline silicon contribute to photon scattering, a process not present in the completely amorphous sample. This last loss mechanism, if significant, may explain why the fine-grain film has higher loss than the amorphous film. The sources of disilane polySi's high loss is more obscure. It is certain, however, that this material's low degree of crystallinity is not the only cause of loss since its transmission is worse than that of amorphous silicon. Visual examination and AFM analysis of this sample shows that the cladding layers are very rough, a possible indication of processing problems. Further investigation is necessary to identify the exact loss mechanisms.

Both 560 and 625CMP structures show promising waveguide performance. The 560 material is more favorable, however, because it does not require the additional process step of surface planarization. As a result, the majority of experiments are performed with the aim to improve this material's transmission.

5.2 Doped Polycrystalline Silicon

In an attempt to fabricate polySi waveguides with grain sizes on the order of micrometers, a patterned wafer with silicon film deposited at 560°C is doped with phosphorous. It has been reported that doping of silicon with phosphorous or arsenic increases the rate of grain growth by up to several orders of magnitude when compared with undoped silicon [42]. This growth enhancement is believed to stem from an increase in silicon self-diffusion and therefore atomic mobility of the grain boundaries. There is also evidence that grain size increases with dopant concentration, so the 560 film is degenerately doped to achieve the largest grains possible.

Unfortunately, the resulting polySi, instead of having the highest degree of crystallinity and grain size, is populated with voids, cracks, and disconnects. This failure to produce high quality material is traced to an inadequate processing sequence. The starting material for this experiment is a patterned wafer. The doping process with $POCl_3$ gas involves oxidation of the silicon surface. After grain growth, this oxide layer is removed with buffered oxide etch to allow dopant out-diffusion. Note that since the bottom oxide cladding is exposed during this wet etch step, some of it is removed along with the top, thermally grown oxide. Not surprisingly, delamination and lift-off of the silicon waveguides occur, resulting in the observed macroscopic defects.

For future experiments, an unpatterned polySi film should be used as the starting material for dopant incorporation. In this manner, removal of the top oxide layer after drive-in will not affect the bottom cladding. Since grain growth can produce material protrusion, the waveguides should be formed only after anneal and out-diffusion to avoid rough sidewalls. Furthermore, arsenic might be a better dopant than phosphorous because its higher vapor pressure allows more efficient out-diffusion.

5.3 Waveguide Thickness

To investigate how waveguide dimension affects transmission loss, 0.2µm-560 guides are fabricated and their loss is compared to that of their thicker 1µm counterparts. Even though the 4nm rms roughness of the 560 films does not contribute significant loss to the 1µm thick guides, it can cause more scattering in the thinner 0.2µm films by allowing a much stronger interaction between the optical fields and the waveguide surfaces. In addition, because the optical modes in thinner guides extend further outside of the core, one would expect additional loss of optical power. Nonetheless, because the SiO_2 cladding** into which the modes spread is much less lossy than polySi, this decline in confinement can actually improve transmission. In this case, less optical power is affected by the "lossy" core and consequently a higher fraction can propagate to the output. These two compet-

** Similar material as silica used for long-haul communication.

ing forces of surface scattering and field penetration, therefore, determine the change in transmission loss due to the decrease in waveguide thickness.

As shown in Table 4.2, the reduction in 560 waveguide thickness from 1μm to 0.2μm results in a decrease in loss from 37dB/cm to 27dB/cm. This finding immediately identifies field penetration as the dominant effect. To determine how much of the loss difference is due to change in confinement, a simulation is performed on polySi/SiO_2 planar waveguides of different thicknesses. The result shows that confinement is 99% for 1μm thick guides and only 78% for 0.2μm thick guides [43]. Since the 560 guides have a loss of 37dB/cm, this simulation predicts that the 0.2μm-560 guides have a loss of 29dB/cm, which is very close to the measured value of 27dB/cm. Figure 5.2 shows the simulated results of core loss as a function of waveguide thickness; the two measured values are included for comparison. Because of the close agreement between simulated and measured loss values, one can also conclude that the 4nm rms surface roughness of the 560 polySi does not contribute additional loss to the 0.2μm thick guides.

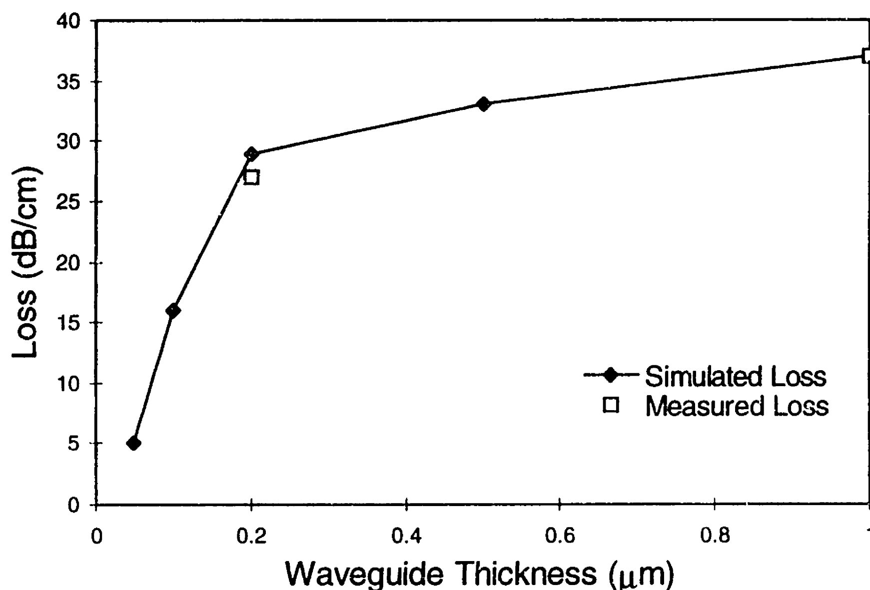

Figure 5.2: Simulated and measured core loss as a function of waveguide thickness[43].

5.4 Sidewall Scattering

To determine whether waveguide sidewall roughness is an important loss mechanism, two etch chemistries - $SF_6/O_2/He$ and HBr/Cl_2 - are used to fabricate 0.2μm-560 structures with different sidewall qualities. Unfortunately, quantitative analysis of roughness using AFM is unsuccessful due to complications associated with positioning the sample on its side to expose the sidewalls for measurement. Instead, SEM is used to qualitatively examine the resulting waveguides. The HBr/Cl_2 preferential etch is found to give much more vertical sidewalls and smoother features than the $SF_6/O_2/He$ isotropic etch. If sidewall roughness contributes to loss, then the HBr/Ci_2 sample should have better transmission. Loss measurement, however, shows no substantial difference between the two samples; both exhibit loss of approximately 27dB/cm.

To gain a better understanding of how the propagating modes interact with the sidewalls, simulation is performed to determine the field distribution within these 0.2μm × 4μm guides. It is found that only high order modes actually extend far enough to be scattered by the rough features on these vertical surfaces. Since these high-order modes satisfy the condition of total internal reflection at the waveguide output surface, they are reflected back into the waveguide even if they are able to propagate this far. As a result, their loss at the sidewalls do not contribute to additional power decrease.

Figure 5.3 offers further proof that sidewall roughness does not result in transmission loss for 4μm wide guides. It shows the loss contribution of sidewalls calculated and measured for waveguides of different widths. The calculated results are obtained by assuming a periodic 20nm rms roughness. The measured values are obtained by testing single-crystalline silicon waveguides etched with the $SF_6/O_2/He$ combination. Because bulk loss and surface roughness of these crystalline guides are negligible (~1dB/cm), the measured losses are entirely due to sidewall scattering. Notice the perfect agreement between the calculated and measured values. They both show that for waveguide widths of 3μm or longer, the effects of sidewall quality is negligible. Scattering loss is important only for shorter widths when the lower-order modes interact more strongly with these vertical surfaces.

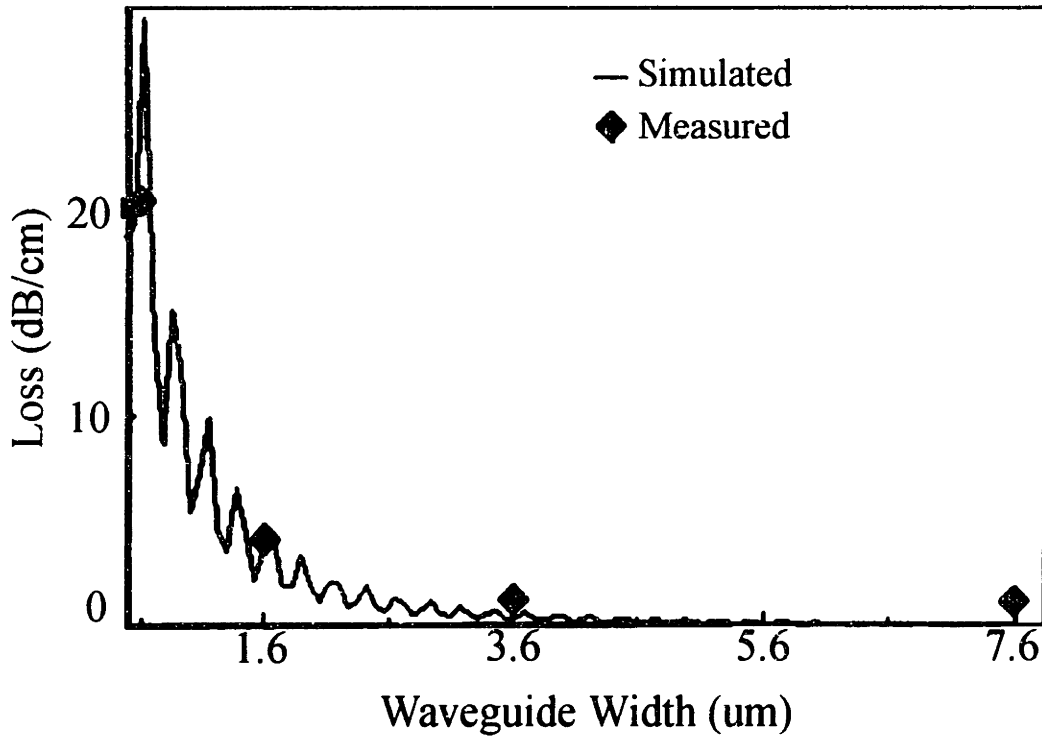

Figure 5.3: Simulated sidewall scattering loss as a function of waveguide widths [43].

5.5 Bulk Absorption and Scattering

Because optical scattering due to waveguide surface and sidewall roughness contributes only slightly to the total transmission loss of polySi waveguides, bulk absorption and scattering is likely responsible for nearly all of the 37dB/cm of 560 and 625CMP samples as well as the 27dB/cm of 0.2μm-560 samples. XTEM images presented in Section 4.2 identify amorphous regions and intragrain defects in these polySi films. Since these lattice irregularities can cause both absorption and scattering, they are likely an important source of bulk loss. Additionally, silicon dangling bonds, which exist as defect levels in the energy gap, can give rise to considerable sub-bandgap absorption.

5.5.1 Amorphous Silicon - Temperature Treatments

To reduce the amounts of amorphous silicon and intragrain defects, high temperature thermal treatments have proven very effective. Since these anneals can also supply the needed energy for further grain growth, they can reduce the volume of grain boundaries as well. In addition to the standard anneal of 16 hours at 600°C, both the 560 and 0.2μm-560 samples are annealed for 16 hours at 1100°C (in an oxygen contaminated ambient). As the XTEM image of Figure 4.4 shows, this high temperature treatment greatly improves material crystallinity and reduces the grain boundary width. As expected, grain growth is also observed as the average grain size increases from 0.35μm to 0.5μm for the 1μm thick film. Unfortunately, despite these impressive structural improvements, optical transmission in the 560/1100°C waveguide is poor. The output power is so low that it is undetectable even by the power meter. The most likely culprit is the oxygen atoms in the annealing ambient. At the high temperature of 1100°C, they diffuse deep inside the film through the grain boundaries and oxidize the silicon atoms they encounter. Since SiO_2 has a much lower refractive index than silicon, it can cause scattering of the optical modes. thereby resulting in the high measured loss.

The 560 waveguides crystallized with the standard anneal do not show this same detrimental result because the much lower annealing temperature of 600°C does not allow such significant oxygen diffusion. Nonetheless, even this lower O_2 presence in the waveguides contributes to transmission loss. A comparison of a 0.2μm-560 sample annealed in pure nitrogen with one that is annealed with the oxygen leak shows a loss difference of 7dB/cm. This smaller oxygen incorporation also affects the grain structure of the polySi film. As Figure 4.5 shows, the material annealed in pure nitrogen is much more crystalline. Notice that for both samples, the average grain size of 0.2μm is equal to the thickness of the film. It is believed that at the early stages of crystallization when the grain size is smaller than the layer thickness, grain growth is three dimensional. The average grain size increases to lower the energy of the material through elimination of the energy associated with grain boundaries. Once the grain size is equal to the film thickness, grain growth stops. This specimen thickness effect is what limits the grain size in these 0.2μm-

560 samples to 0.2μm. For secondary grain growth in the lateral direction, higher temperatures are needed to overcome the energy barrier.

Since the nitrogen anneal yields improvement in waveguide transmission, the high temperature treatment at 1100°C is repeated in a pure N_2 ambient for the 0.2μm-560 sample. As Figure 4.6 shows, the resulting film is completely crystalline with an average grain size of 0.28μm. Notice that this grain dimension exceeds the thickness of the film, suggesting that secondary grain growth occurred during anneal. As a result of these improvements in crystalline structure and the absence of SiO_2 formation, the measured loss is reduced to 11dB/cm.

5.5.2 Dangling Bonds - Hydrogenation

Dangling bonds are generally associated with grain boundaries, where structural irregularities give rise to under-coordinated bonding schemes. By the same token, they are also found in amorphous silicon and possibly intragrain defects. To eliminate this mechanism of optical loss, different hydrogenation techniques are used to passivate dangling bonds in 560, 625, 625CMP, and 0.2μm-560 films. Figure 5.4 summarizes the resulting changes in transmission loss.

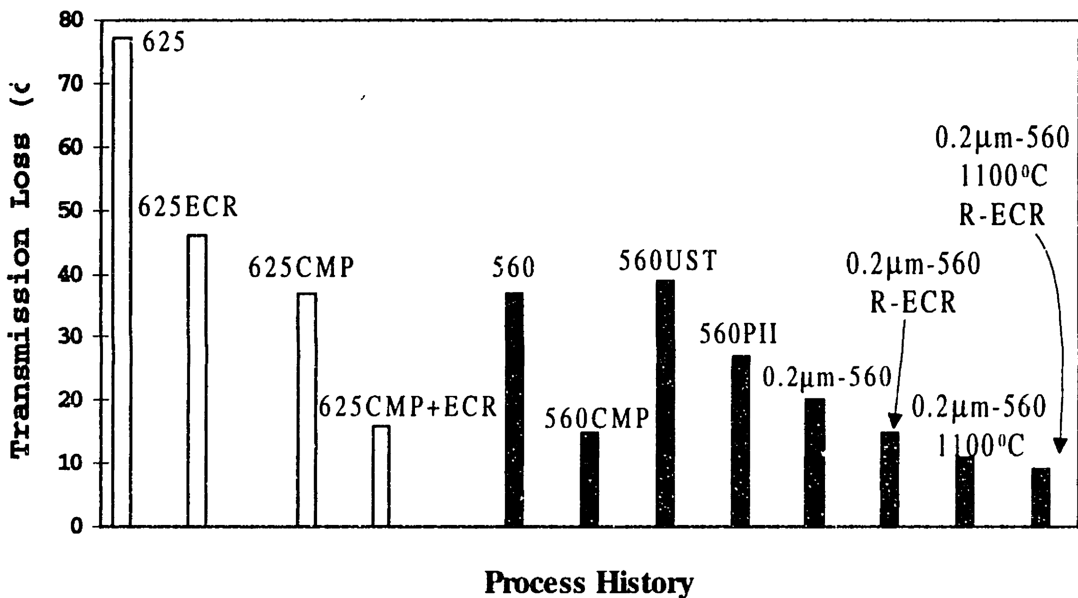

Figure 5.4: Histogram comparing the effectiveness of different hydrogenation techniques.

High-density ECR plasma hydrogenation appears to be the most effective method; it reduces loss in 560 and 625CMP waveguides from 37dB/cm to ~15dB/cm. Its impact on the 625 sample is even more impressive; it cuts loss from 77dB/cm to 46dB/cm, a 30dB/cm difference. To understand how loss reduction is affected by hydrogen incorporation, hydrogen depth profiles are obtained with SIMS. This analysis observes a less than 5×10^{18} atoms/cm^3 enhancement in hydrogen concentration for the passivated 625 film but shows an approximate 1.6×10^{19} atoms/cm^3 enhancement for the passivated 625CMP film. Since the two starting materials differ only with respect to their surface roughness, the SIMS data seems to suggest that plasma penetration is better for films with smoother surfaces. Unfortunately, these hydrogen incorporation results do not tell the whole story as ECR passivation gives a 30dB/cm loss reduction for the rough 625 sample but only a 20dB/cm reduction for the 625CMP sample. One possible explanation is that the excess hydrogen atoms in the 625CMP film are inactive. They reside in polySi but do not contribute to dangling bond passivation.

Another interesting result is observed when comparing the hydrogen concentrations of 560ECR and 560ECR waveguides - a difference of more than 6×10^{19} hydrogen atoms / cm^3 is detected. These two structures differ only in that the latter has an oxide layer on top of the polySi film. Because the ECR plasma is shut off near the end of the hydrogenation process, a possible explanation for the observed concentration difference is that the oxide layer prevented hydrogen out-diffusion during chamber cool-down from 350°C to 25°C. The measured result is of course a higher hydrogen concentration. For future passivation studies, the plasma should be kept running as long as the sample is above room temperature. In this manner, the top coat of SiO_2 is no longer needed to prevent out-diffusion. In fact, its absence can allow higher hydrogen incorporation because the ions do not have to first penetrate the oxide to reach the polySi. Nonetheless, care must be given to ensure that the sample surface is not damaged by the direct impact of high velocity plasma particles.

Large percentages of hydrogen introduced into polySi are inactive due to atom clustering; an energy of at least 1eV is required for their dissociation. UST experiments are performed on the 560ECR samples to supply this needed energy. As shown in Figure

5.4, the result is very disappointing. This technique not only fails to improve transmission, it actually takes waveguide loss back to 39dB/cm. Since the UST process involves high frequency vibration, it is possible that it creates micro-cracks in the polySi film, thereby reducing transmission. This vibration could also have dissociated some of the weak Si-H bonds, returning the dangling bonds to their unpassivated state.

The process of PII, with its high dose and energy plasma, promised to be a technique that offers higher hydrogen incorporation than the ECR method. While this may be true, the resulting 560PII waveguides exhibit a transmission loss of 27dB/cm, approximately 10dB/cm higher than the best ECR result of 15dB/cm. Since the sample used for this experiment does not contain a protective oxide layer, the lower than expected improvement in transmission is probably due to surface damage sustained during the impact of high velocity plasma constituents. To verify this hypothesis, a 560 sample with oxide should be subjected to the same process conditions and measured for comparison.

Concerned with the loss implications of surface damage, a remote-source ECR plasma technique is used to passivate 0.2μm-560 and 0.2μm-560(1100°C) waveguides annealed in pure nitrogen. The resulting losses are 15dB/cm and 9dB/cm, respectively. Even though these numbers are quite impressive, the fact that the loss of the 0.2μm-560(R-ECR) sample is equivalent to that of the 560ECR sample makes one suspect that this remote-source technique allows lower hydrogen incorporation. This conclusion is drawn because the 560ECR sample is 1μm thick and is annealed in the low oxygen partial pressure ambient, two attributes that lead to higher losses. As a result, the fact that the two very dissimilar samples are passivated to yield the same loss indicates that the remote-ECR technique is less effective. One way to verify this hypothesis is to measure hydrogen depth profiles of R-ECR samples and compare them to those of ECR samples. In any case, this remote-source technique, together with the high temperature crystallization treatment, gives the lowest reported polySi waveguide transmission loss of 9dB/cm.

5.6 Bending Loss

Due to the large refractive index contrast between polySi and SiO_2, bending loss in this waveguide system is simulated to be less than 1dB/cm for radii of curvature greater than

$3\mu m$. Since the true length of such bends is only on the order of micrometers, loss per bend is actually extremely trivial also for smaller curvatures. This result is confirmed in practice. Out-of-plane bends with approximately $1\mu m$ radii are found to have loss of only 1dB per bend. Because these bends are formed by fabricating two levels of waveguides, this experiment also demonstrates the functionality of multiple interconnects. These extraordinary results offer further proof that the polySi/SiO_2 system is an excellent choice for optical interconnection.

5.7 Loss vs. Wavelength

This research effort has focused on demonstrating the functionality of polySi waveguides at $\lambda=1.55\mu m$. There is no reason, however, to believe that this is the best wavelength of operation. Some of the waveguides are also tested at $\lambda=1.32\mu m$ because the SiGe relaxed buffer photodetector, currently the most promising silicon-based, VLSI compatible detector, operations efficiently only at this and shorter wavelengths. Figure 5.5 compares the transmission losses at $\lambda=1.32\mu m$ and $1.55\mu m$.

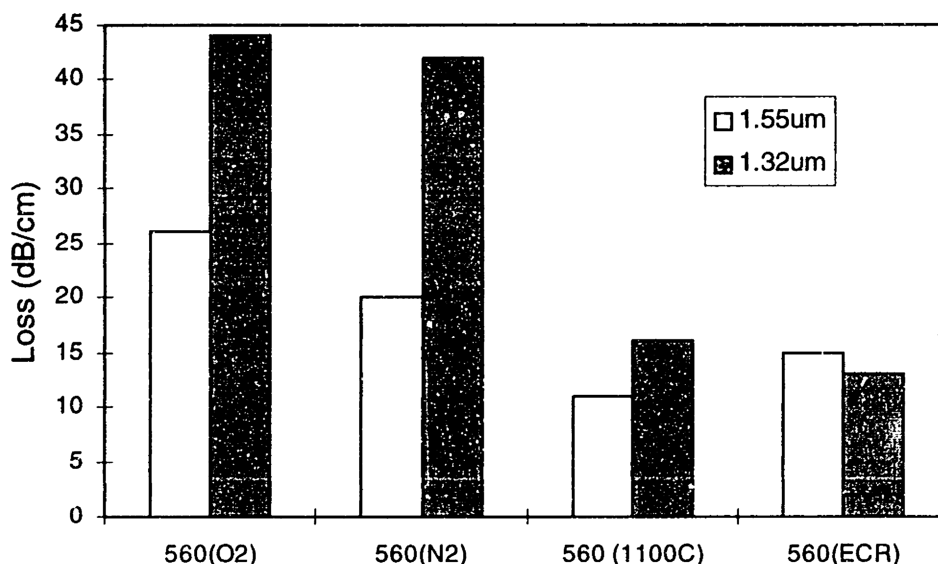

Figure 5.5: Transmission loss at $\lambda = 1.32\mu m$ and $1.55\mu m$.

For the standard annealed 0.2μm-560 (O_2) and 0.2μm-560 (N_2) samples, transmission losses at λ=1.32μm are 44dB/cm and 42dB/cm, respectively. They are each more than 20dB/cm higher than the losses at λ=1.55μm. When the 0.2μm-560 (N_2) sample is annealed for an additional 16 hours at 1100°C, the loss difference at the two wavelengths is reduced to only 5dB/cm. Since the only notable material changes resulting from the high temperature treatment are the degree of crystallinity and grain size, dangling bonds associated with amorphous silicon may be the cause of the higher losses at 1.32μm. It has been estimated that the energies of dangling bond sites are located near the center of the silicon bandgap. Crystalline silicon has an energy gap of 1.1eV; therefore, its dangling bonds can efficiently absorb both 1.55μm and 1.32μm radiation. Amorphous silicon has a wider energy gap between 1.6 and 1.8eV. Numerous defect levels are thus too far from either conduction or valence band to absorb the longer wavelength light; however, they can still allow efficient absorption at 1.32μm.

For the 560ECR sample, transmission losses are 15dB/cm for λ=1.55μm and 13dB/cm for λ=1.32μm. The observed difference is within experimental error. Since hydrogenation of this sample has effectively passivated its dangling bond sites, the insignificant change in loss as a function of wavelength confirms the hypothesis that these defects are the cause of the previously measured higher losses at the shorter wavelength. Because the amount of amorphous regions in this 560ECR sample is actually higher when compared with the 0.2μm-560 (N_2) sample, Raleigh scattering due to density fluctuations in amorphous silicon may not be a substantial contributor to any observed loss difference.

With regards to polySi waveguides in general, 1.55μm is perhaps the better wavelength of operation. However, if the amount of amorphous silicon or dangling bonds is minimized, transmission loss is similar at λ=1.32μm.

5.8 Residual Loss

Currently the lowest-loss polySi waveguide is the passivated 0.2μm-560 structure annealed in nitrogen at 1100°C for 16 hours. Its 9dB/cm loss, however, is still much higher than the 1dB/cm of single-crystalline silicon guides. It is unclear exactly what mechanisms

contribute to this observed loss difference , but some likely possibilities readily come to mind. The single most important difference between polySi and crystalline silicon is the presence of grain boundaries in the former material. These grain boundaries contain dangling bonds which can cause sub-gap absorption. The density and index differences between these amorphous boundaries and the crystalline grains can also give rise to Rayleigh scattering and back reflection. Furthermore, this high-temperature annealed polySi film most likely has a rough surface as a result of secondary grain growth, surface scattering therefore can also be a substantial source of loss. These loss mechanisms are discussed below.

5.8.1 Grain Boundary absorption

The 1100°C-annealed 0.2μm-560 polySi film is completely crystallized; its dangling bonds therefore resides mainly at the grain boundaries. In the unpassivated state, these defects are efficient optical absorption centers. Fortunately, the high temperature treatment has effectively reduced the width of the grain boundaries and thus the amount of dangling bonds.

For a rough estimate of the loss contribution of these defect states, several simplifying assumptions are made. The grain boundaries are treated as amorphous silicon with thicknesses between 1.5 and 2nm, typical values used in modeling of polySi [37]. Their contribution to loss in dB/volume is assumed to be equivalent to that measured for the amorphous silicon waveguides. In doing so, Rayleigh scattering due to density fluctuations in the amorphous material is also included. Since TEM analysis of the 0.2μm-560 (1100°C) sample shows columnar grains with an average in-plane grain size of 0.28μm, a 1cm-long waveguide with 0.2μm×4μm cross-sectional area contains approximately 510,000 grains. Assuming a grain boundary thickness of 1.5nm, these grains allow a total boundary volume of 200μm^3. The amorphous silicon waveguides have a loss of 143dB/cm. In terms of transmission loss per volume, it contributes 1.4×10^{-2}dB/μm^3. As a result, the grain boundaries in the 0.2μm-560 (1100°C) waveguides give rise to approximately 3dB/cm. This loss value, however, varies with the assumed boundary thick-

ness. For example, if a value of 2nm is used instead, the resulting loss contribution is 4dB/cm.

Remote-ECR hydrogenation of this 0.2μm-560(1100°C) sample yields a loss reduction of 2dB/cm. According to the above estimation, at least another 1 to 2dB/cm can be eliminated by optimizing the process of dangling bond passivation.

5.8.2 Grain Boundary Scattering

The presence of grain boundaries in the waveguide core can also give rise to optical back reflection and Rayleigh scattering. Back reflection is probably more significant, but it is difficult to model because knowledge of grain boundary positions with respect to the propagating modes is required. One can, however, easily determine the upper-limit of Rayleigh scattering because loss at two wavelengths is measured. For λ=1.32μm, loss of the 0.2μm-560(1100°C) sample is 16dB/cm. Since absorption by grain boundaries can account for 4dB/cm, a maximum of 12dB/cm can be the result of Rayleigh scattering. Using the Rayleigh law of $I \propto 1/\lambda^4$, it is found that at most 3dB/cm of the 11dB/cm loss at λ=1.55μm is due to scattering. Since hydrogen incorporation does not significantly change the refractive index of a material, this upper scattering limit of 3dB/cm is probably also valid for the passivated sample.

Assuming that the scattering centers are spherical particles with radius a, it is also possible to determine the number of such centers required to give a certain level of loss. The total scattered power from each center is

$$P_s = \frac{4\pi}{3}\left(\frac{\varepsilon_s - \varepsilon}{\varepsilon_s + 2\varepsilon}\left(\frac{2\pi}{\lambda}\right)^2 a^3\right)^2 \frac{P_i}{area}, \tag{5.1}$$

where ε_s is the dielectric constant of the particle, ε is the dielectric constant of the matrix, λ is the optical wavelength, and P_i is the input power. For a particle radius of 2nm, it is found that 6,390 scattering particles/grain or 4×10^{17} particles/cm^3 are needed to bring about a loss of 3dB/cm. These numbers are much too large to be realistic; therefore, transmission loss due to Rayleigh scattering is expected to be much less than 3dB/cm.

5.8.3 Surface Scattering

Because of the strong interaction between the optical modes and the polySi surface, scattering due to roughness can be an important source of loss for the thin waveguides of 0.2μm thickness. For the 0.2μm-560 waveguides, only a 4nm rms roughness is measured; it does not give rise to noticeable loss. The high temperature treatment at 1100°C, however, most likely roughens the film surface. Unfortunately, we are unable to quantitatively determine this roughness for the sample annealed in pure nitrogen. Nonetheless, because the high temperature sample annealed with the oxygen contamination has a roughness of 10nm and an oxidizing ambient can result in more rough films than a pure nitrogen ambient, we can confidently assume a roughness between 4 and 10nm for the sample annealed in pure nitrogen. Tien's analysis can not be used for these thin waveguides, but by performing the calculation for a 1μm-thick sample, it can give the lower limit of surface loss. By assuming a roughness of 7nm, it estimates that at least 5dB/cm is due to surface scattering. The best way to confirm this result is to planarize the polySi film with CMP and then measure the reduction in transmission loss.

Chapter 6

Conclusion

This study has investigated numerous fabrication processes to develop low-loss polySi/SiO_2 waveguides for silicon optoelectronic integrated circuits. By minimizing the bulk absorption and scattering mechanisms of polySi, transmission loss at λ=1.55μm has been reduced from 35dB/cm to 11dB/cm. The most effective method for reducing bulk loss is to passivate silicon dangling bonds with high-density ECR hydrogen plasma. For strip waveguides deposited at 560°C and annealed at 600°C for 16 hours, hydrogenation has enabled a loss decrease of 22dB/cm.

Optical transmission has also improved with high temperature heat treatments, where residual amorphous regions in the film are fully crystallized and the total grain boundary volume is reduced. Because amorphous silicon and grain boundaries are the two main sources of dangling bonds, high temperature anneals serve similar functions as hydrogenation in terms of minimizing optical absorption. A 16 hour anneal at 1100°C has demonstrated a 10dB/cm reduction in waveguide loss. In performing any heat treatment, it is crucial to maintain a non-oxidizing ambient. Because oxygen preferentially oxidizes the polySi grain boundaries, it can cause significant optical scattering as a result of the large index contrast between silicon and SiO_2 (Δn=2). Even slight oxygen incorporation has been found to add at least 5dB/cm to waveguide loss.

Reduction of waveguide cross-sectional dimensions from 1×8μm to 0.2×4μm has also led to an improvement in transmission; a loss difference of 10dB/cm is measured. Because the optical modes do not interact strongly with the sidewalls, this decrease in loss is believed to be the result of the change in thickness. Indeed, simulation shows that opti-

cal confinement is nearly 100% for 1μm-thick structures but is only 78% for 0.2μm-thick ones. Because the thinner waveguides allow less light to be affected by the lossy polySi core, they naturally show better transmission. Another effect of the reduction in thickness is the increased interaction between the polySi film surface and the propagating optical modes. For the smooth material under investigation, however, no noticeable increase in scattering is observed.

The polySi waveguides are also tested at λ=1.32μm. It is found that for samples with amorphous silicon and thick grain boundaries, loss is considerably higher at this shorter wavelength than at λ=1.55μm. On the other hand, for hydrogenated or fully crystallized samples, no significant loss difference is observed. The preliminary conclusion is that dangling bonds and other amorphous silicon defects cause more efficient absorption at λ=1.32μm.

The current best polySi/SiO_2 waveguide has a transmission loss of 9dB/cm at λ=1.55μm, a dramatic improvement over the 1700dB/cm value reported less than 15 years ago [16]. This low loss is the result of desirable material properties such as high degree of crystallinity, passivated dangling bonds, and smooth surfaces. Nonetheless, these parameters are yet to be optimized. For instance, ~5dB/cm of the residual loss may be contributed by the film's estimated 7nm rms surface roughness. To further improve transmission, it is therefore necessary to planarize the film surface. Another option is to re-investigate the disilane deposition process, which has been reported to yield smooth, large-grain polySi. The increase in grain size is of course an added advantage because it reduces the volume of grain boundaries and, in turn, the amount of dangling bonds. Although in our best waveguide material absorption at these defect sites is not as important as surface scattering, it is estimated to be the source of 1-2dB/cm. As a result, successful implementation of the above techniques is expected to allow an additional 4-5dB/cm reduction in loss. The remaining 4dB/cm (9dB/cm - 5dB/cm) is likely caused by bulk scattering, which may also decrease slightly with the growth of large grain material. Ultimately, loss in polySi/SiO_2 waveguides can be as low as 4dB/cm.

Chapter 7

Future Work

Before the polySi/SiO_2 waveguide system can be implemented for optoelectronic interconnection, a significant amount of additional development is required. Today's lowest loss of 9dB/cm is a great improvement on previous research efforts, but the achievement of even lower losses is tremendously desirable because it can relieve the stringent detection-limit requirement currently placed on the receiver electronics. Additionally, IC manufacturing maintains various thermal and throughput constraints, the current waveguide fabrication process must therefore be modified in order to fully realize monolithic integration. Recommended experiments for future polySi waveguide development are summarized below.

7.1 Dangling Bond Passivation

The process of hydrogenation has allowed tremendous improvement in waveguide transmission by passivating silicon dangling bonds. Its effect on the polySi film under investigation, however, is not fully understood. In particular, little is known about the interrelationship among hydrogenation time, dangling bond passivation, and transmission loss. The experiment to investigate this issue is already underway. It involves hydrogenating samples for different time durations (10, 20, 60, and 120 minutes) in a remote-source ECR plasma. The resulting hydrogen concentrations are being measured with SIMS, and the amounts of incorporated hydrogen that actually passivate dangling bonds will also be determined . The most direct measure of this parameter is a comparison of the spin densities of the samples before and after hydrogenation. A well-known technique for this purpose

is electron paramagnetic resonance (EPR) spectroscopy, which is based on the interaction between the electron spin and a magnetic field. In the silicon crystal, which has tetrahedral symmetry, every atom shares two electrons in covalent bond with each of its nearest neighbors. These electrons are paired and do not give an EPR signal. At a dangling bond site, however, the electron has no partner in the same orbital; for this reason it does give an EPR signal. EPR spectroscopy and loss measurement will allow correlation of dangling bond passivation with transmission loss. Any observed trends may also be helpful in identifying the optimal hydrogenation time for future experiments.

In passivated polySi films, significant amounts of hydrogen do not contribute to passivation because they form weakly bound clusters or are accommodated by strained Si-Si bonds [29]. It has been found that when these samples are subjected to a low-temperature anneal, some of the excess hydrogen are released and can passivate additional dangling bond defects. An approximate 5 times reduction in spin density has been reported with this technique [44]. As a result, the ECR hydrogenated waveguides should be subjected to a similar anneal in order to further reduce their transmission loss.

Some concerns with using hydrogen passivation are possible material side-effects and instability of Si-H bonds. So far our investigation offers no evidence of any such problems, but unrelated studies have shown light-induced instability and even defect generation [44, 45, 46]. These phenomena are most extensively documented for hydrogenated amorphous silicon, in which the hydrogen is only loosely bonded to silicon and have relatively high mobility even at low temperatures. It has been proposed that hydrogen migration is the cause of the observed increases in defect concentration [47]. Hydrogen motion induces structural changes in the silicon network such as broken Si-Si bonds. The resulting dangling bonds are stabilized against reformation when the hydrogen passivates some, but not all, of these defects. Hydrogen mobility in silicon is controlled by the concentration of electronic carriers [47]; therefore, it is substantially enhanced when the carrier population is increased by optical absorption. Recently light-induced creation of dangling bonds is also demonstrated in hydrogenated polySi, whose spin density doubled after prolonged illumination [44]. Even though this effect is observed for high energy light above the absorption edge of silicon, 1.55μm operation may also induce absorption (sub-bandgap) to allow enhancement of hydrogen mobility. As a result, this issue

must be investigated to ensure the long-term stability of hydrogen passivation under various operating conditions.

7.2 Surface Planarization

For the 1100°C annealed 0.2μm-560 sample, preliminary calculation has found that approximately 4dB/cm of its 11dB/cm loss is the result of surface scattering. The most obvious solution is to planarize the film surface to reduce its ~7nm* rms roughness. CMP has proven to be a very fast and effective method for this purpose; it lowered the roughness of the 625 polySi film from 20nm to 4nm in a matter of seconds. This method will certainly allow quick verification of the above calculated results. Unfortunately, CMP may not be the optimal resolution in the long run because many layers of smooth surfaces are difficult and expensive to achieve with this technique. In light of this challenge, it may be desirable to re-investigate the disilane deposition process, which has been reported to yield very smooth surfaces as well as large grain sizes [24].

7.3 Performance Characterization

Transmission loss is the only measure of waveguide performance examined in this study, but dispersion is perhaps just as important especially for high speed applications. Dispersion measures the temporal spread of the light pulse traveling through the waveguide, it therefore determines the speed of data transfer. For the current multi-mode structures, there are three sources of such pulse broadening: modal, material, and waveguide. To further investigate the functionality of the polySi/SiO_2 system for optical interconnection, it is essential to identify these dispersion quantities.

The initial study of out-of-plane waveguide bends has yielded excellent result of less than 1dB loss per bend for radii of ~1μm. For data distribution, low loss in-plane bends and efficient couplers and splitters are also needed. After transmission is satisfactorily optimized, the next task is to study these passive waveguide devices.

---

* An estimated value.

7.4 Process Integration

Monolithic integration of optical devices with electronics raises numerous reliability and processing compatibility concerns, important among which are the possible out-diffusion of hydrogen atoms and the high temperature steps used in waveguide fabrication. As established previously, Si-H bonds are weak; the hydrogen atoms also have relatively high mobility in silicon and SiO_2 even at low temperatures. It is conceivable, therefore, that some of the incorporated hydrogen can diffuse beyond the oxide cladding during post-passivation process steps. This out-diffusion of hydrogen can be detrimental to the stability of electronic devices. To confine hydrogen atoms within the waveguides, a simple solution is to use a Si_3N_4 diffusion barrier, a material in which hydrogen has a considerably lower mobility. Si_3N_4 can be deposited to isolate the SiO_2/polySi/SiO_2 structures from the other devices.

The use of high processing temperatures is another important concern because in conventional integrated circuits, electrical interconnects and various contacts are made of aluminum, which has a relatively low melting point of 660°C. Obviously, these devices cannot withstand the 1100°C anneal used to fully crystallize the polySi film. As a matter of fact, they may not retain structural integrity even at the deposition temperature of 560°C and the standard annealing temperature of 600°C. At these lower temperatures, aluminum structures do not undergo melting, but their high thermal expansion may give rise to excessive material stress and cause void formation or other microstructural defects.

To avoid these problems, one possible integration scheme is to separate the processing of optical devices from that of electronics. Two wafers are thus required. After the fabrication of the individual devices, the active surfaces of these wafers are bonded together to link their operations. This method of integration is advantageous in that it allows the use of the existing waveguide processing recipe without any modifications, but alignment issues may be a big limitation to its wide-spread implementation.

Integration can also be achieved by either suppressing all process temperatures below 500°C or designing the fabrication sequence such that the aluminum structures are not affected by any high temperature steps. The former alternative is explored below because it offers a higher degree of processing flexibility.

Most studies involving polySi thin films work with material deposited with silane gas at 550°C or 560°C, but the use of disilane gas has enabled deposition temperatures as low as 450°C [24]. In addition to allowing low processing temperatures, disilane deposition has the significant added advantage of high deposition rates, which can improve throughput. Furthermore, it yields high quality films with ultra-smooth surfaces and large crystallized grain sizes. For instance, the 470°C disilane process investigated in this study was reported to give much larger post-anneal grains compared to higher temperature methods. All of these advantages make silicon deposition with disilane gas an attractive option for polySi waveguide fabrication.

Silicon films deposited below ~580°C are in the amorphous phase. To obtain crystalline structure, they must be subjected to some type of post-deposition thermal treatment. The most common method for this purpose is solid-phase crystallization, during which the high temperatures transform the metastable amorphous phase to the stable crystalline phase. This process is typically carried out via simple furnace annealing of the film at around 600°C. The overall transformation rates are slow, complete crystallization requires several tens of hours.

Recently, low-temperature crystalline-silicon TFT technology has prompted further development of excimer-laser crystallization of thin amorphous silicon films. In this technique, a pulse laser imparts high energy radiation (~900mJ/cm^2 for 200nm thickness) to the silicon film, rapidly melting the illuminated areas. The high temperatures involved in this melting process are confined to the near-surface region by using short laser pulse durations (tens of nanoseconds), optical wavelengths that are highly coupled to silicon (UV wavelengths), and thick isolation layers of SiO_2 (2-3μm) [48]. It is found that these spatial and temporal localization of the heat-affected region allows the substrate temperature to remain relatively low. The laser crystallized microstructure consists of elongated and laterally columnar grains that originate from the unmelted portions of the film and terminate as they meet in the center of the melted region [49]. The grain size is dependent on the incident energy density, which determines the degree of melting and the number of solid seeds at the bottom oxide interface. It is found that near-complete melting of the silicon film yields the largest grain sizes after solidification. The resulting film also exhibits high degree of crystallinity only achievable with high temperature furnace anneals. Furthermore, arbitrarily large single-crystalline regions can be obtained by carefully controlling the width of the incident beamlet on the film and the total translation dis-

tance. In summary, disilane-based silicon deposition and laser crystallization are ideal for future waveguide development because they not only allow low processing temperatures, but also can yield high quality, low defect silicon films.

Bibliography

1 M. R. Black, Master Thesis, Massachusetts Institute of Technology, 1995.

2 L. C. Kimerling, D. M. Koker, B. Zheng, F. Y. Ren, and J. Michel, *Semiconductor Silicon Electrochemical Society Proceedings*, 1994.

3 J. S. Foresi, M. R. Black, A. M. Agarwal, and L. C. Kimerling. *Appl. Phys. Lett.*, **68**(15):2052-2054, April 1996.

4 C. Z. Zhao, G. Z. Li, E. K. Liu, Y. Gao, and X. D. Liu, *Appl. Phys. Lett.*, **67**(17):2448-2449, October 1995.

5 N. Yamauchi and R. Reif, *J. Appl. Phys.*, **75**(7):3235-3257, April 1994

6 D. Tsoukalas and D. Kouvatsos, *Appl. Phys. Lett.*, **68**(11):1549-1551, March 1996.

7 B. E. A. Saleh and M. C. Teich, *Fundamentals of Photonics* (John Wiley & Sons, Inc., New York, 1991) p.277.

8 K. J. Ebeling, Integrated Optoelectronics (Springer-Verlag, New York, 1989) p. 38.

9 F. Y. G. Ren, J. Michel, Q. Sun-Paduano, B. Zheng, H. Kitagawa, D. C. Jacobson, J. M. Poate, and L. C. Kimerling, MRS Spring Meeting, San Francisco, 1993.

10 L. M. Giovane, L. Liao, D. R. Lim, A. M. Agarwal, E. A. Fitzgerald, and L. C. Kimerling, *SPIE Photonics West*, February 1997.

11 D. R. Lim, Bachelor Thesis, Massachusetts Institute of Technology, 1994.

12 U. Fischer, T. Zinke, B. Schuppert, and K. Petermann, *Electronic Letters*, **30**(5):406-408, 1993.

13 Y. Liu, E. Liu, G. Li, S. Zhang, J. Luo, F. Zhou, M. Cheng, B. Li, and H. Ge, *Appl. Phys. Lett.*, **64**(16):2079-2080, April 1994.

14 J. H. Yap, Master Thesis, Massachusetts Institute of Technology, 1994.

15 S. J. Krause, B. L. Chen, and M. K. El-Ghor, *IEEE Proc. - International SOI Conference*, 1991.

16 R. E. Jones, Jr. And S. P. Wesolowski, *J. Appl. Phys.* **56**: 1701-1706, 1984.

17 W. B. Jackson, N. M. Johnson, and D. K. Biegelsen, *Appl. Phys. Lett.*, **43**(2): 195-197, July 1983.

18 D. Adler, in *Physical Properties of Amorphous Materials*, edited by D. Adler *et al.* (Plenum Press, New York, 1985) p.46-47.

19 G. Harbeke, L. Drausbauer, E. F. Steigmeier, A. E. Widmer, H. F. Kappert, and G. Neugebauer, *J. Electrochem. Soc.: Solid-State Science and Technology*, **131**: 657-682, 1984.

20 K. Morigaki, in *Amorphous Silicon and Related Materials*, edited by H. Fritzsche (World Scientific, New Jersey, 1989) p.600-601.

21 L. Haji, P. Joubert, J. Stoemenos, and N. A. Economou, *J. Appl. Phys.* **75**(8):3944-3952, April 1994.

22 N. H. Nickel and W. B. Jackson, *The American Physical Society*, **51**(8): 4872-4881, February 1995.

23 D. Foster, A. Learn, and T. Kamins, *Solid State Technol.*, 227, 1984.

24 A. T. Voutsas and M. D. Hatalis, *J. Electrochem. Soc.*, **140**: 282, (1993).

25 K. E. Violette, M. C. Ozturk, K. N. Christensen, and D. M. Maher., *J. Electrochem. Soc.*, **143**: 649-657, February 1996.

26 T. I. Kamins and J. E. Turner, *Solid State Technol.*, 80, 1990.

27 A. T. Voutsas, M. K. Hatalis, J. Boyce, and A. Chiang, *J. Appl. Phys.*, **78**(12):6999-7006, December 1995.

28 N. H. Nickel, W. B. Jackson, I. W. Wu, C. C. Tsai, and A. Chiang, *The American Physical Society*, **52**(11): 7791-7794, September 1995.

29 N. H. Nickel, N. M. Johnson, and W. B. Jackson, *Appl. Phys. Lett.*, **62**(25): 3285-3287, June 1993.

30 R. Pandya and B. A. Kahn, *J. Appl. Phys.*, **62**:3244, 1987.

31 D. Jousse, S. L. Delage, and S. S. Iyer, *Philos. Mag. B.*, **63**:443, 1989.

32 G. A. Northrop and G. S. Oehrlein, in *Defects in Semiconductors*, edited by H. J. von Bardeleben (Materials Science Forum, Paris, 1986), Vol.10-12, p.1253.

33 E. S. Cielaszyk, K. H. R. Kirmse, R. A. Stewart, and A. E. Wendt, *Appl. Phys. Lett*, **67**(21):3099-3101, November 1995.

34 S. Ostapenko, L. Jastrzebski, and J. Lagowski, *Appl. Phys. Lett.*, **68**(20):2873-2875, May 1996.

35 J. D. Bernstein, S. Qin, C. Chan, and T. J. King, *IEEE Electronic Device Letters*, **16**(10):421-423, October 1995.

36 T. Kamins, *Polycrystalline Silicon for Integrated Circuit Applications, Second edition*, (Kluwer Academic Publishers, New York, 1991) p. 78.

37 T. Kamins, *Polycrystalline Silicon for Integrated Circuit Applications, Second edition*, (Kluwer Academic Publishers, New York, 1991) p. 54-56.

38 D. Bisero, *Materials Letters*, **18**(4):215-217, 1994.

39 B. D. Cullity, *Elements of X-ray Diffraction, Second Edition*, (Addison-Wesley Publishing Company, Inc., Reading, Massachusetts, 1978), p.287.

40 B. D. Cullity, *Elements of X-ray Diffraction, Second Edition*, (Addison-Wesley Publishing Company, Inc., Reading, Massachusetts, 1978), p.105.

41 G. Lubberts, B. C. Burkey, F. Moser, and E. A. Trabka, *J. Appl. Phys.*, **52**(11):6870-6878, November 1981.

42 H. J. Kim and C. V. Thompson, *MRS Symposium Proceedings: Polysilicon Films and Interfaces, Volume 106*, (MRS, Pittsburgh, 1988), p. 143.

43 J. S. Foresi, private communication.

44 N. H. Nickel, W. B. Jackson, and N. M. Johnson, *Physical Review Letters*, **71**(17):2733-2736, October 1993.

45 D. L. Staebler and C. R. Wronski, *Appl. Phys. Lett*, **31**:292, 1977.

46 N. H. Nickel, N. M. Johnson, and J. Walker, *Physical Review Letter*, **75**(20): 3720-3723, November 1995.

47 P. V. Santos, N. M. Johnson, and R. A. Street, *MRS Symposium Proceedings*, **258**: 353-358, 1992.

48 J. S. Im and R. S. Sposili, *MRS Bulletin*, p. 39-48, March 1996.

49 H. J. Kim and J. S. Im, *Appl. Phys. Lett.*, **68**(11): 1513-1515, March 1996.